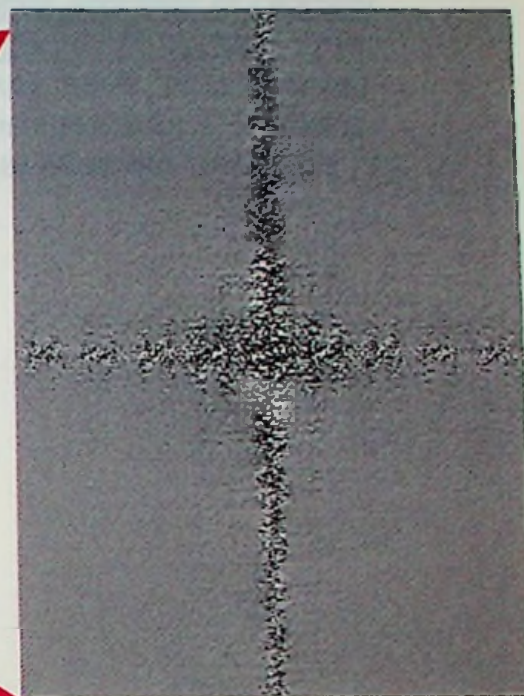
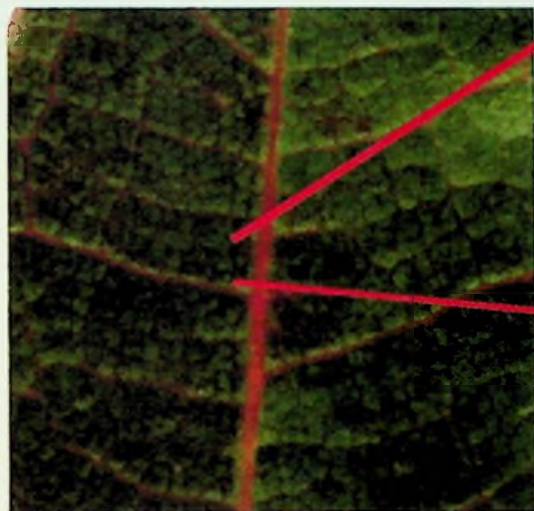


PHYSICS  
MARSHALL UNIVERSITY

# The Acquisition and Quantitative Analysis of Digitally Generated Fourier Transforms Resulting from the Physiognomy of Various Tree and Shrub Species



A Thesis submitted to the Marshall University Graduate College and the  
Department of Physics and Physical Sciences in partial fulfillment of the  
requirements for Master's Degree in Physical Science  
with an emphasis in Physics

By

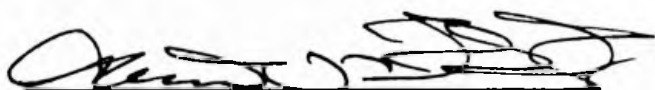
Alicia Eldridge-Spears

Department of Physics and Physical Science  
Marshall University, Huntington, WV  
June, 1999

Marshall University  
Department of Physics and Physical Science

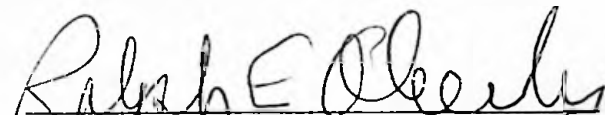
The following thesis, The Acquisition and Quantitative Analysis of Digitally Generated Fourier Transforms Resulting from the Physiognomy of Various Tree and Shrub Species, was accepted on the 10<sup>th</sup> day of July, 1999, as presented by Alicia Eldridge-Spears, in partial fulfillment of the requirements for a Master's degree in Physical Science with an emphasis in Physics at Marshall University.

Review Committee Members



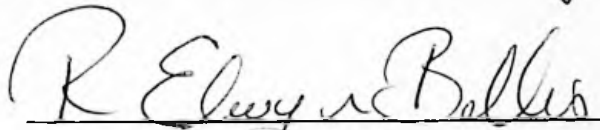
Dr. James O. Brumfield, Thesis Advisor  
Graduate Faculties of Biological Sciences  
and of Physics and Physical Sciences

July 7, 1999  
Date



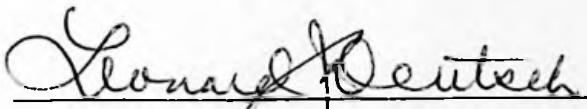
Dr. Ralph E. Oberly, Thesis Advisor  
Professor, Department of Physics and Physical Sciences

July 7, 1999  
Date



Dr. R. Elwyn Bellis, Academic Graduate Advisor  
Professor, Department of Physics and Physical Sciences

July 7, 1999  
Date



Dr. Leonard J. Deutsch  
Dean, Graduate College

7/7/99  
Date

## Acknowledgements

The author would like to thank Dr. Brumfield, Dr. Oberly, and Dr. Bellis for their time toward and devotion to my completion of this research and thesis project. Without their countless hours, support, instruction, and guidance this research project could not have reached this magnitude. I also owe a debt of gratitude to Dr. James Joy, Dr. Dewey Sanderson and my immediate family for their unique contributions as well.

## Table of Contents

Approval Page.....	ii
Acknowledgements.....	iii
List of Illustrations and Figures.....	v
List of Tables.....	vi
Abstract.....	1
Introduction.....	2
Project Methodology.....	10
Research Techniques.....	27
Results and Analysis.....	34
Conclusion.....	41
Resources.....	47
Appendix A – Phase 1 data.....	50
Appendix B – Phase 2 data.....	60
Appendix C – Phase 3 data.....	72
About the Author.....	92

## List of Illustrations and Figures

Double Slit Diffraction, .....2 constructive and destructive inference	2
Fourier Transform, .....3 continuous mathematical function	3
Cellular Structure .....7	7
Leaf Cross-section .....7	7
Scanned Leaf Samples ..... 14	14
Leaf Samples with Algorithm Applied ..... 15	15
Fast Fourier Transforms .....16	16
Filtered Fourier Transform.....17	17
Veinlet Study Area..... 17, 19	17, 19
Ordered Fourier Transform .....17, 19	17, 19
Altered Fourier Transform.....18	18
Reverse Fourier Transform.....18	18
Zeroth Order and First Order Separation.....20	20
Scanner's Light Path.....21	21
Sample Calculations.....22	22

## List of Tables

Fourier Transform Measurements, Green Sweet Gum leaf .....	20
Calculated Cellular Dimensions, Fall 1998 .....	22
Calculated Cellular Dimensions, Spring 1999 .....	23
Comparison of Calculated and Measured Cellular Dimensions .....	24
Calculated Cellular Dimensions Correlated to Paradermal Layers at 400X ...	25

## Abstract

An optical Fourier transform represents the interference of wavefronts produced as light passes through multiple slits. Theoretically, any image containing periodic structure causes diffraction. The cellular arrangement of a plant leaf and the regularity in venation are ideal conditions for diffracting light. As light passes through columns of cells, its path is altered according to the distance and orientation present.

A photograph or slide of a leaf or the leaf itself may be used to produce a diffraction pattern by either optical or digital means. Optically, a laser beam directed through a slide is refracted by a converging lens and focused onto a piece of film at the transform plane. Digitally, software such as ER Mapper processes a scanned image using the Fast Fourier Transform (FFT) algorithm that closely approximates the mathematical analysis by summing the sine and cosine functions, referred to as the real and imaginary bands, respectively. Due to the flexibility and resolving capabilities, the digital method was utilized to acquire and to analyze transforms.

The Fourier transforms were analyzed qualitatively according to venation. High spatial frequency in the veins and veinlets did not determine the amount of detail in the transform. The transforms from the top surface of a leaf had very high order information, but the bottom of the leaf exhibited only a central maximum, characterized by low frequency. Veins are apparent on both sides of the leaf; however, cells are ordered on the top of the leaf and more random underneath. Fourier transforms are produced by even higher spatial frequency resulting from the cellular arrangement at the top of the leaf, independent of the venation.

To quantitatively analyze the Fourier transforms, the patterns were measured to determine the spacing between successive maximum orders. Using the "cell values" and "cell coordinates" features of ER Mapper, the maximum interference values were located and the distance between the central maximum and each order were measured. The calculated cell dimensions ranged from 15 to 45 microns.

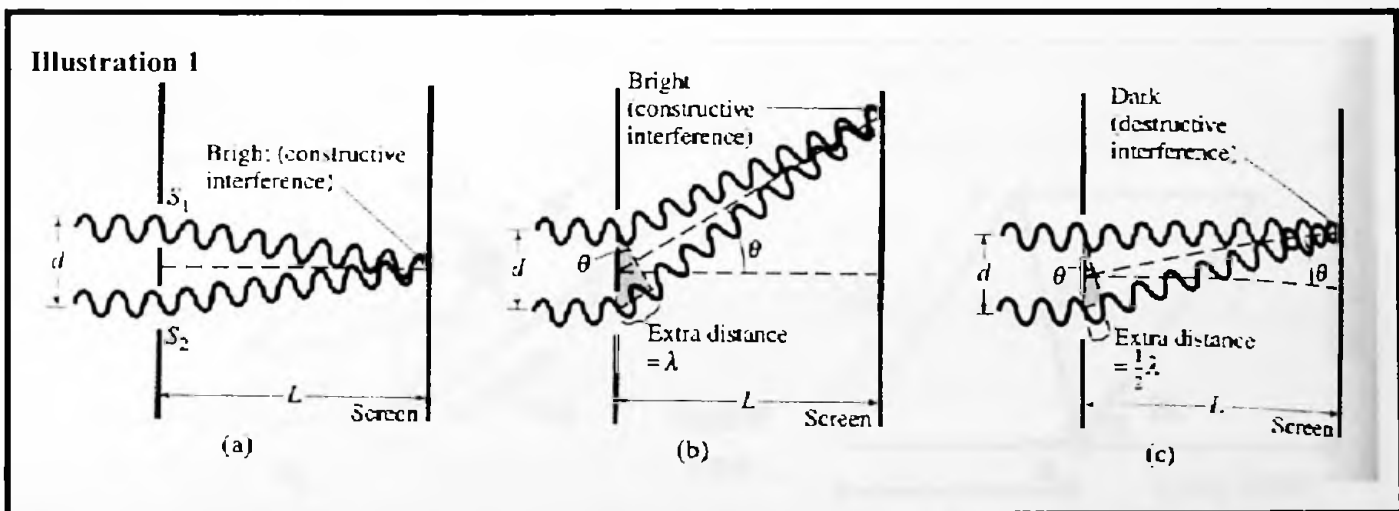
Transforms from leaf layers photographed at 400X magnification suggest that the palisade cells and the cell walls both diffract light. Cellular dimensions predicted by the Fourier transform appear to result from the sum of the palisade diameter and the cell wall thickness for a total width of 14.5 to 16.5 microns. A correlation between Fourier transforms produced by individual leaves may be compared quantitatively to those arising from an entire tree to accurately represent patterns of plant physiognomy and cellular dimensions.

**Keywords for library reference: Optics, Fourier transform, diffraction, interference, digital image processing, mathematical modeling, plant physiognomy**

# Chapter One

## Introduction

By definition, light exhibits the property of diffraction when it bends as a result of passing through or around a barrier, such as a pair of slits. The light's amount of coherence determines in part if the waves will interfere to create a maximum or a minimum. When waves of light pass through slits, a spherical wavefront develops on the other side of the slits. As the wavefronts propagate radially from the openings, the energies begin overlapping. If the waves are in phase, the crests interfere constructively to produce a maximum; conversely, waves that meet crest to trough interfere destructively to make a minima or area of darkness. See illustration 1. Due to constructive and destructive interference, a specific arrangement of dots will appear which is called a diffraction pattern. See illustration 1(Giancoli, 1998).



Double slit diffraction refers to the interference patterns from two slits; however, multiple slits or periodicity also produce diffraction patterns. A slide or a photograph can function as a type of diffraction grating if the image contains a



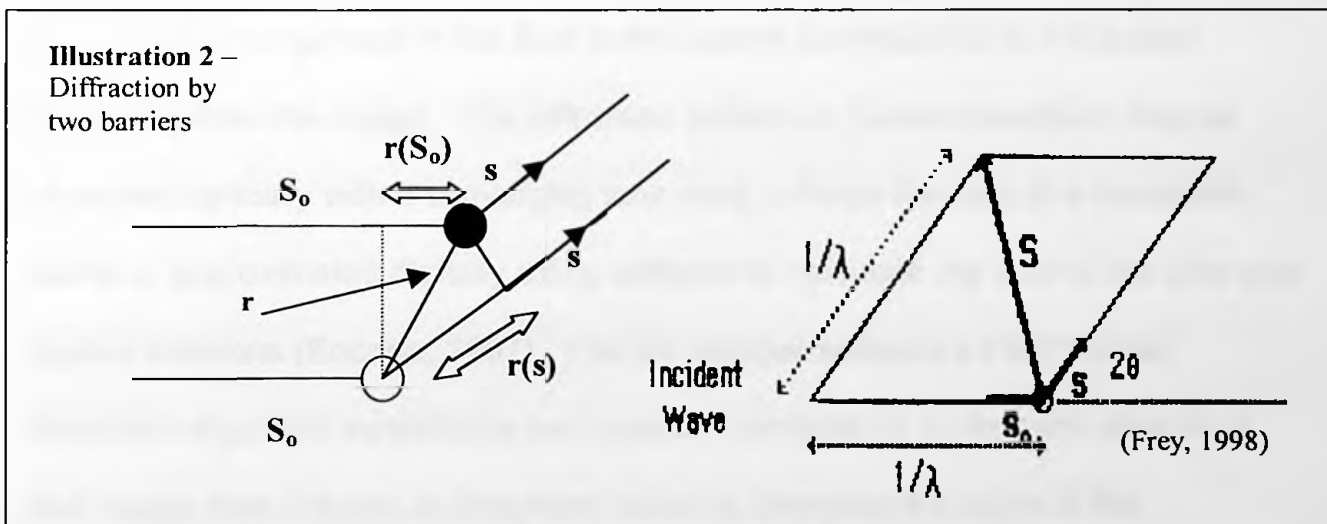
periodic structure, such as a series of vertical lines, to bend the light and produce a regular pattern of constructive and destructive interference. The orientation of and spacing between the dots in the array will be unique to the wavelength of light and the structures in the image.

The interference pattern, known as a Fourier transform, was named after the French mathematician, Baron Jean Baptiste Fourier, who developed the theory explaining how continuous and discontinuous mathematical functions can be represented (Encarta, 1997). The mathematical Fourier transform or “Fourier integral” is represented by

$$F(S) = \int_{-\infty}^{\infty} \rho(r) e^{2\pi i r S} dr \quad (\text{see illustration 2})$$

where  $r$  represents the spacing between the objects and where  $S$ , coordinant of the diffraction pattern, is

$$|S| = \frac{2 |\sin \theta|}{\lambda} \quad (\text{see illustration 2})$$



The product of the spacing and the pattern coordinant yields an inverse relationship between spatial frequency in the image and the Fourier transform

(Frey, 1998). Consequently, the tighter the spacing in the image, the greater the separation in the transform. Vertical orientation in the image results in a horizontal arrangement in the Fourier transform pattern (Frey, 1998). In addition, low spatial frequency in the image will produce closely spaced dots, and, conversely, high spatial frequencies will be represented by wide spacing (Reynolds, 1989). The spacing in a diffraction pattern corresponds directly to the dimensions of the slits by the following equation:

$$d \sin\theta = n\lambda$$

For angles less than 10 degrees, an approximation can be made in which theta,  $\theta$ , equals the angular separation between the orders,  $x$ , divided by the distance to the screen,  $L$ . The formula for determining slit widths,  $d$ , becomes

$$d = n\lambda L/x$$

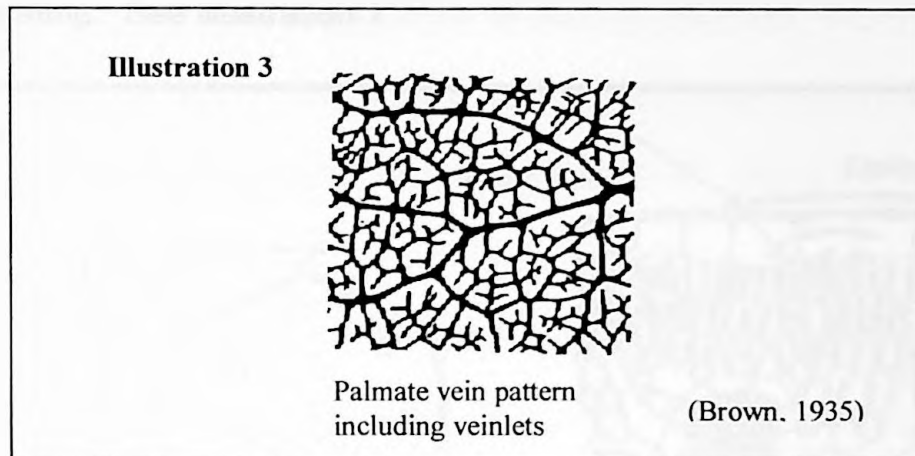
where  $n$  represents the order number and  $\lambda$  is the wavelength of light used. See illustration 1 (Giancoli, 1998).

The arrangement of the dots in the pattern corresponds to the spatial frequency from the image. The diffraction pattern or Fourier transform may be observed optically with a converging lens used to focus the rays at a transform plane or approximated digitally using software to calculate the sum of the sine and cosine functions (Encarta, 1997). The ER Mapper software's Fast Fourier transform algorithm establishes two complex numbers ( $x$ ,  $y$ ) for each pixel for a real image then creates an imaginary band by changing the signs of the coordinate pair (ER Mapper 6.0 Applications, 1998). Because a Fourier transform is an infinitely continuous wave pattern, the computer must make certain

assumptions in order to complete the calculation. The program performs a function called "padding" (ER Mapper 5.0 Reference, 1995) whereby it extends the image along the horizontal and vertical axes with "synthetic data extrapolated from the actual values" in a process referred to as "tiling" (ER Mapper 5.0 Applications, 1995). By "padding" the image, edge effects are limited because the boundaries of the image do not dramatically drop to zero (ER Mapper 6.0 Applications). After "padding" the image, the addition of the sine and cosine functions is performed under the condition of "wrapping" during which the continuous wave function is simulated by extending the "Fast Fourier Transformation" algorithm to connect the left and right edges as well as the top and bottom edges. "Wrapping" creates a loop through which the computer cycles several million times. By padding and wrapping the dataset, the edges should match smoothly thus emulating a continuous function. Without these assumptions, discontinuities may appear and be exaggerated when frequencies reverberate between the image's edges, creating an anomaly indicated by the presence of a St. George's cross along the x and y axes (ER Mapper 6.0 Applications, 1998).

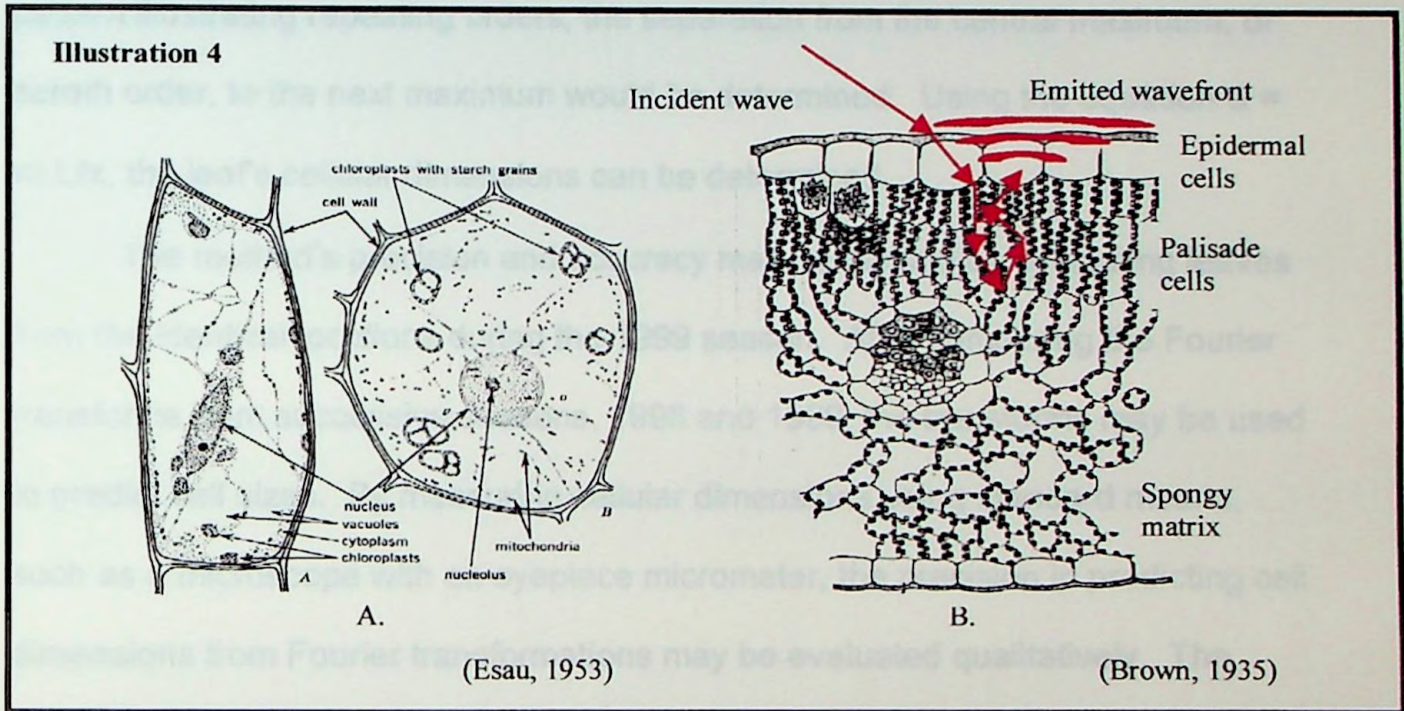
Theoretically, a Fourier transform may be acquired, analyzed, or altered to obtain information about any image that contains periodicity. Filtering Fourier transforms allows low or high frequency information to be removed, such as unwanted periodicities caused by raster patterns resulting from the image's pixel array (Oberly, 1993). Uses of Fourier transforms have been researched in the biomedical field concerning periodic structures in macromolecules like proteins (AOL, 1998). Similarly, plant species exhibit regular spacing, or periodicity, in both

venation and cellular arrangement as parameters of their physiognomy (Brumfield, 1997). Plant physiognomy refers to the apparent physical characteristics of a life form and its structure in a natural setting such as a community (Whittaker, 1970; Dansereau, 1957).



Veins may be classified into three categories: pinnates, palmates, and a combination of the two. The distinctive characterization of pinnates is a central vein with regularly spaced branching veins. Palmates have more than one main vein extending from the stem (Esau, 1953) and random branching that becomes smaller and smaller veinlets. See illustration 3 (Brown, 1935). The veins correspond to low spatial frequency and the roughly rectangular cells constitute high spatial frequency. See illustration 4A. Just below the waxy cuticle, under the leaf's surface, or epidermis, a series of roughly rectangular cells comprise the space between ends of the veinlets. See illustration 4 (Esau, 1953). According to theory, as incident light waves penetrate the cuticle of the leaf they are refracted, and internally reflected, refracted, and diffracted through both the epidermis cells and the vertically arranged palisade cell layers (Bickford and Dunn, 1972). When the light rays reach the more randomly arranged spongy matrix along the bottom of the leaf, they will reflect and diffract upward, eventually emerging from the leaf's

surface. See illustration 4B (Brumfield, 1997 and 1998). The required wavefronts develop in order to create a detectable diffraction pattern. A Fourier transform with sufficient detail to produce successive orders may be used to calculate the cell dimensions because the cell infrastructure would correspond to the slits in a diffraction grating. See illustration 1.



By developing a method for obtaining, displaying, and analyzing diffraction patterns generated from photographs of various leaves, the Fourier transform optical and mathematical theories may be put into practice. The limitations of such a proposal lie in the ability to resolve the diffraction pattern into separate components. The transform pattern created by waves diffracted through the cells, fifteen microns in diameter, and the spacing between cells, two microns apart, would be difficult to detect. The sample must be on the correct order of magnitude to achieve wide spacing and the detection devices must be sensitive enough to resolve the pattern spatially and spectrally. Although the Fourier transform may be

obtained by either optical or digital means, the hardware and software used in the digital techniques offer increased precision and flexibility. After establishing an algorithm for producing Fourier transforms from tree leaves collected in 1997, 1998 samples with known dimensions and identical resolutions would create a transform pattern from which measurements may be collected. From a transform pattern illustrating repeating orders, the separation from the central maximum, or zeroth order, to the next maximum would be determined. Using the equation  $d = n\lambda L/x$ , the leaf's cellular dimensions can be determined.

The method's precision and accuracy may be verified by evaluating leaves from the identical locations during the 1999 season. After comparing the Fourier transforms from successive seasons, 1998 and 1999, the transforms may be used to predict cell sizes. By measuring cellular dimensions using standard means, such as a microscope with an eyepiece micrometer, the precision in predicting cell dimensions from Fourier transformations may be evaluated qualitatively. The limitation of such a comparison lies in the lack of precision of the eyepiece micrometer. Due to the crude equipment available, the measurements are only precise to one micron whereas the Fourier transform predictions were precise to one hundredth of a micron.

In addition to recording actual average cell widths, a microscope equipped with a camera may be used to photograph selected interior layers of the 1999 leaves in order to generate Fourier transforms. See appendix C. These transforms may be qualitatively compared to the transforms from the scanned leaf

in order to validate which portions of the transform may be attributed to specific leaf cells or layers. See illustration 4.

## Chapter Two

### Project Methodology

Research proceeded in three separate phases from theory to acquisition and quantitative analysis. In phase one, twenty-four photographic slides of leaves were used to test the theory that any periodically arranged physiognomic structure would yield a Fourier transform. See appendix A. The images were processed in a variety of ways in order to create the desired transform. After production of transforms was possible, it was qualitatively verified that the transforms arose largely from the cell walls rather than the vein patterns. During phase two, new leaf samples were scanned directly and the algorithm, established in phase one, was used to create transforms. To generate transforms, from which measurements could be made, small sections of the leaves were scanned digitally and processed. See appendix B. The resulting transforms were measured to determine the separation between the central maximum and the successive orders from which the cell widths and heights were calculated. The third and final stage required verification of the technique's precision for predicting cellular dimensions. Because cell sizes differ according to the amount of water and sunlight available, leaves were collected from the same tree or shrub at roughly equal distances from the ground. Samples from the 1999 season were collected, scanned, processed and quantitatively compared to the original samples. See appendix C. Paradermal views of each of five leaves were photographed at 200 to 400 times magnification then Fourier transforms generated from the images. The resulting



patterns were qualitatively compared to the Fourier transforms produced by the scanned leaf physiognomy in order to determine the internal leaf structure responsible for each aspect of the diffraction pattern. Finally, the samples were measured using a microscope with an eyepiece micrometer and compared to the Fourier transform predictions.

Initially, in phase one of the research, 1 to 1 ratio photographic slides of leaves from a water maple and of a lilac bush were exposed to collimated light from a Helium-Neon laser. The light transmitted through the slide was refracted by a Fourier lens and focused onto photographic film. The two leaves produced a bright spot that appeared to have diagonal flares unique to the slide.

Unfortunately, no exposure time yielded a pattern from which individual dots or orders could be seen. By calculating the separation between dots from measurements of individual cell widths using

$$\theta = \sin^{-1} \lambda/d \quad \text{and} \quad \Delta x = f \tan \theta$$

(Oberly, 1993), the resolution required was on the order of 50 to 450 microns from leaves whose cells ranged from 4.5 mm to .5 mm. Optically, this resolution was not reasonable so the specimens were photographed from farther away, resulting in a small-scale image. The increased spatial frequency would produce a wider diffraction pattern. Because the Fourier transform patterns were not readily discernable with the optical equipment, the focus of the research then shifted to digital analysis of scanned slides using ER Mapper.

Four of the original 1 to 1 ratio slides and all of the small-scale slides were digitally scanned as transparencies at 1200 pixels per inch resolution. See

appendix A figures 1a-17a, 19a-24a. After the image brightness, size, and contrast were adjusted in Adobe Photoshop 3.0, each file was saved in TIFF format and imported into ER Mapper (ER Mapper, 1995). Image by image, algorithms that best enhanced the leaf were determined, created, saved, and processed using the "Fast Fourier Transformations" function in ER Mapper. See appendix A (ER Mapper 5.0, 1995). A Fourier transform with discrete discernable values illustrated by distinguishable individual dots on a black background was the desired result, and the research primarily focused on developing algorithms that produced distinct, resolute, and useful transforms. See appendix A figures 1c-4c, 5f, 7c-17c, 18b, 21c-24c.

At the onset, adjusting the intensity distribution or contrast enhanced the quality of the leaf photo by detailing the subtle venation before the Fourier transform was performed on the entire file. Using a 200 megahertz Intel Pentium processor, the resulting transform required thirty to forty minutes and 100 to 200 megabytes of memory for storage. Unfortunately, the Fourier transforms were saturated with high frequency data detail making the central maximum the only distinguishable feature. To decrease the process time, only one band was used based on the resolution available. Finally, the red band was chosen because it produces the most interspecies differentiation (Brumfield, 1996) and has the highest degree of penetration into the leaf (Bickford and Dunn, 1972). Displaying the images in "greyscale" yielded the best optical feature display. See appendix A figures 1b-17b, 18a, 19b-24b. The "pseudocolor surface palette" of the red band

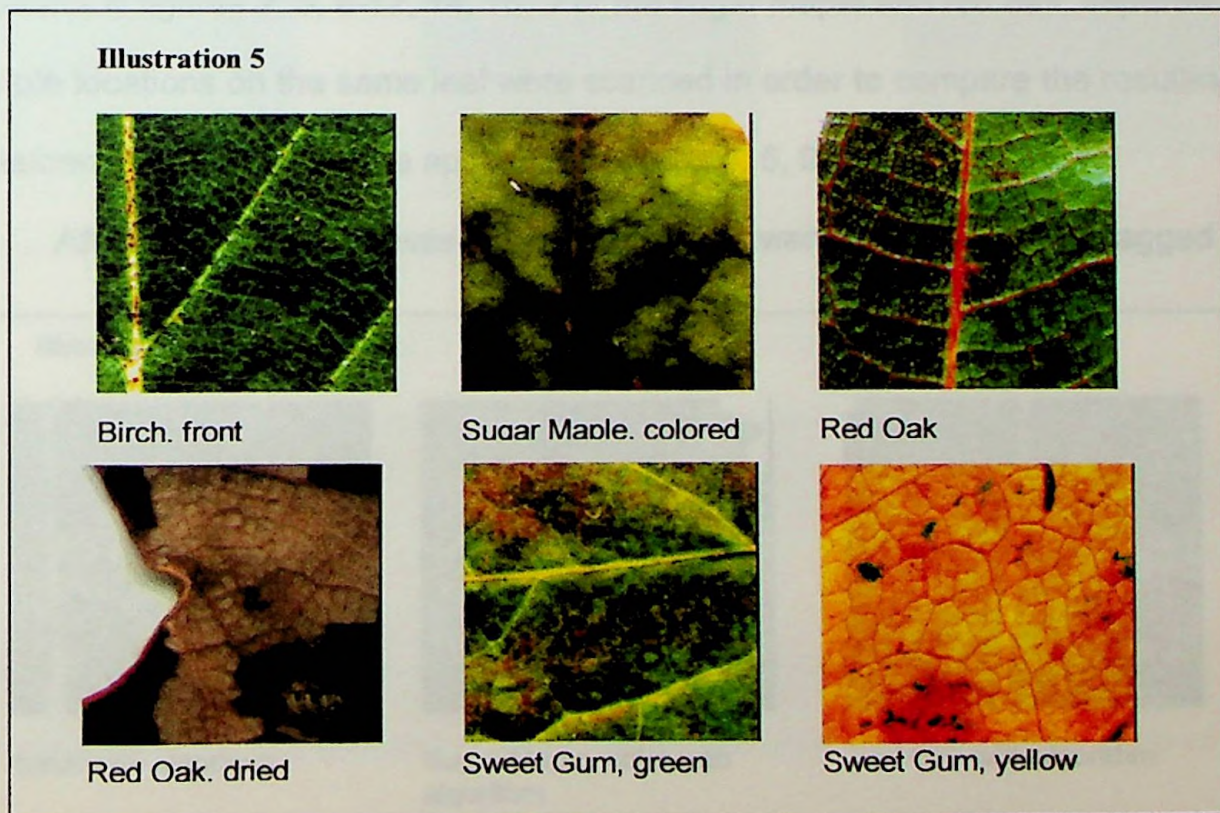
was saved as a "dataset" then analyzed digitally for diffraction patterns (ER Mapper 5.0, 1995).

The Fourier transform process was completed in a few seconds as a result of the changes. Using the 1 to 1 ratio Water Maple image, the first distinguishable Fourier transform was produced. See appendix A figures 18a and 18b. By carefully zooming in with ER Mapper, very high frequency detail appears, especially along the horizontal axis. The algorithms were saved for the small-scale images and for the 1 to 1 ratio slides of the lilac, wild cherry, and cherry leaves. See appendix A figures 7b, 22b, and 1b. However, the files that gave the most consistent transform patterns were the small-scale images. From this point, all small-scale slides were scanned and assigned the "pseudo layer," red band, "greyscale" algorithm then processed by the Fourier transform function. See appendix A figures 1b-24b and 1c-24c. Minor adjustments in the "histogram," which is a graph of the spectral intensity distribution, were made as needed to decrease or increase the brightness and contrast on an image by image basis.

The algorithms for all twenty-four slides were saved as datasets, but not all of them produced clear transforms. See appendix A figures 5c, 6c, 19c, and 20c. The first lilac, the grape, and the mock apple leaf samples contained excessive background noise despite changes in the algorithm. If a leaf did not produce a Fourier transform with the first algorithm displayed, the degree of zooming, the color palette, and/or the histogram distribution were altered using ER Mapper. The new algorithm was saved as a "dataset" and the image processed again. After all slides were processed, the patterns were to be analyzed for similarities in

orientation and spacing from one species to the next, within a species, from the top of the leaf to the bottom, or from one sample to another of the same species. Because the Fourier transforms yielded high order information from the top surface of the leaves, but not from the more randomly arranged leaf bottom, it was observed that the diffraction patterns were caused by the cell walls on the surface or within the palisade layer of the leaf. To quantitatively analyze the Fourier transform pattern, the images would have to be collected again by using a uniform scale, i.e. no "zooming," and by supplying measured parameters of 1.2 by 1.2 centimeters.

In phase two, the quantitative analysis of Fourier transform patterns, the project goals included generation of patterns that exhibited orders, analysis of transforms to determine physiognomic similarities between species, measurement of the separation between successive orders, and calculation of cell widths. On



November 4 and 5, 1998 leaf samples were collected on Piedmont Road in West Huntington from birch, holly, red oak, elderberry, sugar maple, sweet gum, and water maple trees. Leaves were selected from a height of approximately six feet from the ground and generally from the westward facing side of the tree. Within twenty-four hours, the leaves were digitally scanned parallel to the epidermis by a color flatbed Memorex scanner at 1200 dots per inch resolution. Because the files were excessively large at such a high resolution, the scanning area was reduced to a 1.2 by 1.2 centimeters square for all of the samples. The regions of the leaves scanned were chosen according to the area that appeared to have the best resolution after completing the scan preview. For later analysis, scanned areas included tops, bottoms, green, colored, and dried leaf portions. See illustration 5 and appendix B figures 1a-15a. In addition, two to three different leaves from elderberry, holly, sweet gum, sugar maple, and water maple were scanned. See appendix B figures 2, 3, 6-12, 14, 15. For the sugar maple and red oak, separate sample locations on the same leaf were scanned in order to compare the resulting transforms for similarity. See appendix B figures 4, 5, 9, and 10.

After scanning the leaves, all of the samples were saved as TIFF, Tagged

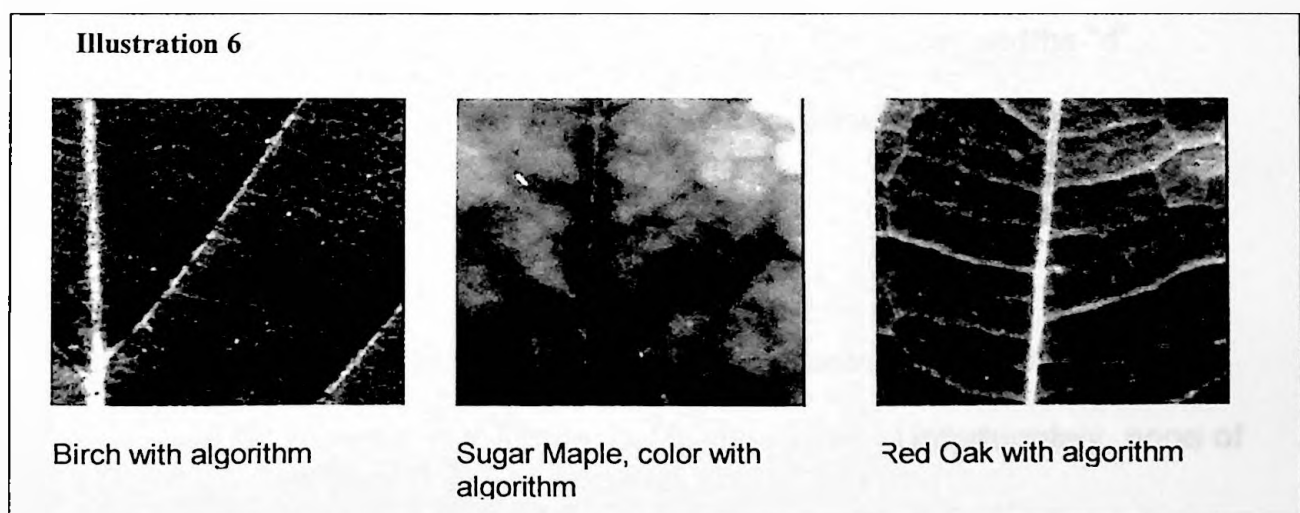
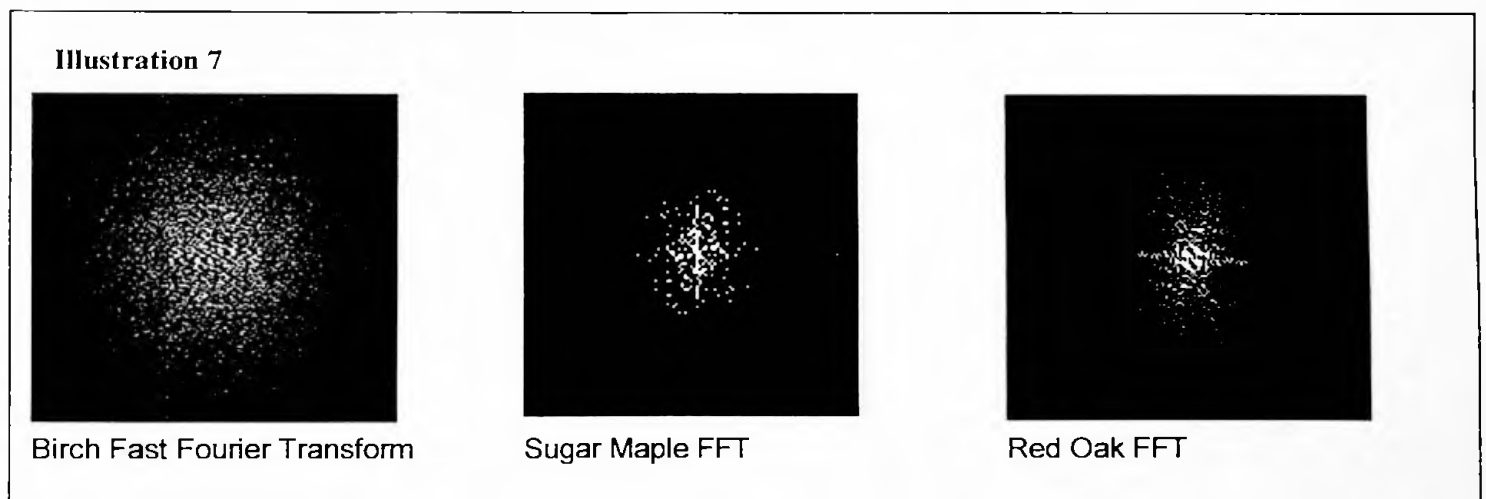


Image File Format, files and imported into ER Mapper 5.5 format so that an algorithm could be applied and fast Fourier transforms generated. In accordance with the previously established algorithm, the green and blue layers or bands were turned off and the red layer was changed into a pseudo layer for which the greyscale color palette had been selected. After turning off the “smoothing” feature, the algorithm was applied to the image and the product saved as a dataset. See illustration 6 and appendix B figures 1b-15b. From the “Processes” pull down menu the “Fourier Transformation” function was selected and performed at full spectrum on each of the images. See illustration 7 and appendix B figures 1c-15c.



To quantitatively analyze the samples by calculating cell widths “d”, separations within the transform pattern had to be measured and applied to the formula

$$d = n\lambda L/x$$

The value “x” corresponds to the distance from the central maximum to another maximum, and “n” represents the order being measured. Unfortunately, none of

the transform patterns illustrated any repetition and, consequently, no orders. In addition, the values of "L," which is the distance to the screen, and " $\lambda$ " were also unknowns.

To determine the data needed to make calculations, several approaches were taken. Initially, high and low pass filters were applied to the images and to the transforms. The results were as expected: low pass filters removed the dots, or image values, on the outer portion of the transform and high pass filters revealed additional dots. Using the "cell value" and "coordinate value" windows, the intensities of the dots in the image and their separations from the central maximum were recorded by moving the cursor to the brightest regions. However, without specific order numbers this information was quantitatively useless. See illustration 1.

The second approach involved the development of a formula mask to apply to the transform that would indicate the precise order of magnitude represented in the leaf. A formula was developed to remove outside dots in the hope that a repetitive pattern revealed itself (ER Mapper, 1995). The formula was written in the formula region of the algorithm window as

If INPUT 1 > 1 then 1 else null

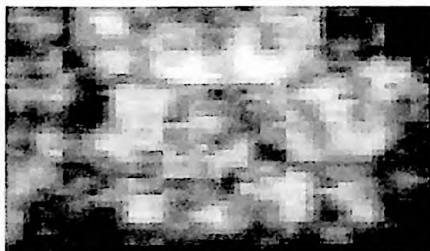


Fig. 1a Sugar maple color veinlet

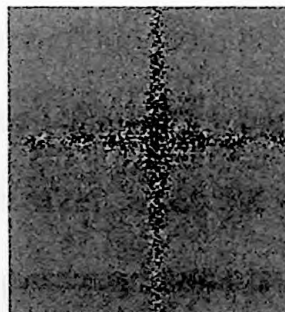


Fig. 1b Sugar maple veinlet FFT



Fig. 1c Sugar maple color FFT with formula

The input 1 value was determined by clicking on the majority of the dots in the transform and establishing a range of intensity values, specifically from the outer most dots. See figure 1b. The result was a simplified transform that was devoid of any information outside of the central maximum. See figure 1c. Such a transform would reveal only the lowest orders of periodicity, like the veins, but contain no information about the individual cells.

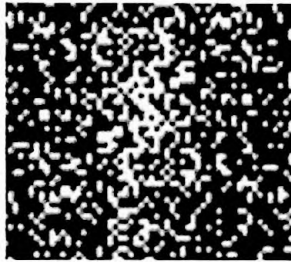


Fig. 2a Elderberry  
central max zoomed

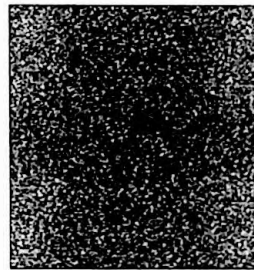


Fig. 2b Reverse FFT from  
zoomed central max

Filters were applied to the transform, and the new image was saved as a dataset. Theoretically, capturing the central maximum should result in a reverse transform containing only low order information such as the vein pattern in a leaf. Upon trying to regenerate the image by performing a “reverse Fourier transform” function, the program returned an error message indicating “input data has odd number of bands 1.” A fast Fourier transform created digitally arises from the summation of the sine and cosine functions. In the ER Mapper program, these functions are referred to as the real and imaginary bands, respectively. Using different filters and using only the “zoom” function, no “reverse” transform could be produced from a pattern that had been altered because the imaginary band was not included in the new dataset. However, when the new image was saved as an algorithm, a reverse transform was produced because both bands remained in the algorithm (ER Mapper, 1997). When the zoomed central maximum of the



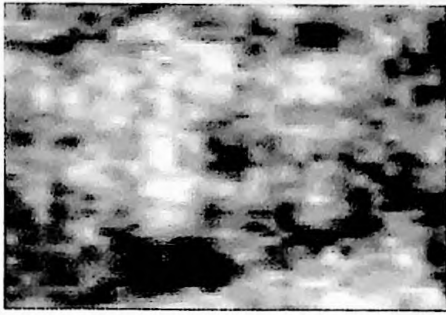


Fig. 3a Sweet gum green veinlet

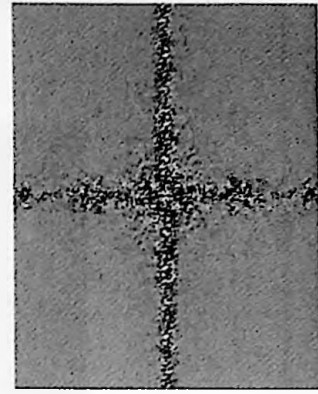
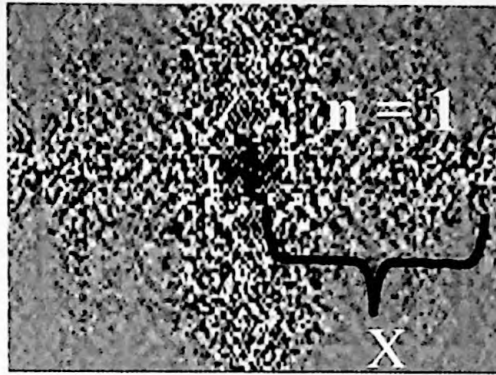


Fig. 3b Sweet gum green veinlet FFT with orders

elderberry leaf was saved as an algorithm, the reverse transform was produced and illustrated only very low spatial frequencies. See figure 2a-b.

The final approach toward making transform patterns with repeating orders stemmed from a suggestion by James Booth, Marshall University physics graduate and Computer Information Technologist. Extremely small sections of the leaves, within a series of veinlets, were selected with the zooming function then saved as new datasets. See figures 1a and 3a. See also appendix B, figures 1d, 1f, 1h, 3e, 3g, 4d, 4f-6f, 5d, 7d-11d, 12b, 13d, 14b, and 15b. Fast Fourier transforms were run on these selections with varying results. Excluding the two holly leaves, all of the samples produced Fourier transforms similar to figures 1b and 3b. See appendix B, figures 1i, 4e, 4g, 5e, 5g, 6g, 7e-11e, 12c, 13e, 14c, 15d. The new Fourier transform appeared to contain repetitions along both the vertical and horizontal axis. See fig. 1b, 3b. The ER Mapper features, cell value and cell coordinate, were used to find the central maximum value, the location of the successive orders, and the separation between the central maximum and each of the other maxima. See table 1 and illustration 8.

Illustration 8



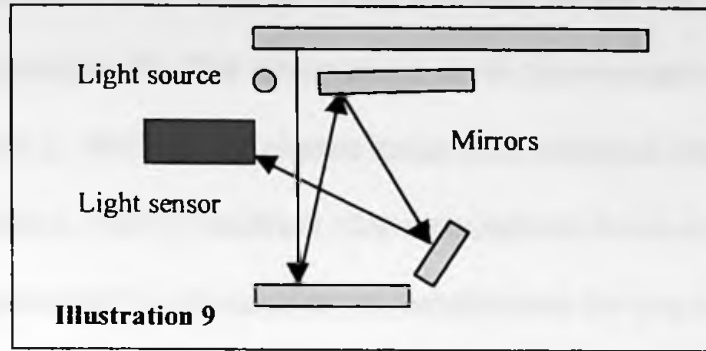
Sugar Maple veinlet FFT zoom, indicating recorded values for orders

Table 1: Green Sweet Gum Fourier Transform Measurements

Order number	Cell value	X coordinate	Y coordinate	Separation from central max (cm)
Zeroth	37.4744	283.16	283.77	n/a
First horizontal	.021186	416.01	282.57	.55236
Second horizontal	.008418	556.32	284.16	1.13928
First Vertical	.021839	284.96	184.93	.55604
Second Vertical	.010428	284.96	83.60	1.12029

Similar data tables were completed for each leaf sample, and, where possible, the third through the fifth orders were also measured. After collecting these data, the multiple slit diffraction equation only contained two unknown values, the wavelength and the screen distance.

Because the transforms were generated digitally, a few distance assumptions had to be made. Rather than measuring the "screen distance", the distance traveled from the image to the light sensor in the scanner was substituted. The scanner was disassembled, the light's path was diagrammed, and the path distance recorded as 5.25 inches or 13.3cm. See illustration 9.



The wavelength band chosen was the red; therefore, the value for lambda was set as a range from 700 nanometers to 650 nanometers for all calculations.

Finally, quantitative analysis could be done because all of the values for the equation,  $d = n\lambda L/x$ , were known. The calculated value for “d” represents the width of the cellular aperture from a paradermal view of the leaf as determined from the corresponding transform separations. The distance between the sensor and the leaves, “L,” was a constant value of 13.3 centimeters. The separation between orders in the frequency domain, the Fourier transform, was utilized to estimate two-dimensional distance values in the spatial domain, the image. The vertical orders were used to calculate the corresponding cell dimension in the “x” axis and the horizontal orders were used to estimate the “y” component of the cell’s dimensions. The cellular apertures, or slit widths, determined by each order were averaged to get a final experimental value for the wavelengths of 700 and 650 nanometers. See illustration 10.

For example, using the “cell values” window, the green Sweet Gum leaf yielded separations of .552 cm and 1.139 cm from the horizontal first and second orders as well as .556 cm and 1.120 cm from the vertical orders. See table 1. The average for these values ranges from 16.75 microns to 15.55 microns for the

cell's horizontal diameter and 16.65 to 15.45 microns for the cell's vertical diameter. See illustration 10. The dimensions were determined for all of the leaf samples. See table 2. Similar transforms arise from samples collected from whole trees (Brumfield, 1997); however, the calculations have not been performed and, thus, the agreement to cell sizes is not established for the two studies.

**Illustration 10 – Sample Calculation**  
 Green Sweet Gum, see tables 1 & 2

$$d = n\lambda L/x \quad \lambda = 7.00E-7m \text{ to } 6.50E-7m \quad L = .133m$$

<p><i>1<sup>st</sup> Order Horizontal, n = 1</i>  <math>x=5.5236E-3m</math>  <math>d = \frac{1(7.00E-7m)(.1333m)}{5.5236E-3m}</math>  <math>d = 1.69E-5m</math></p> <p><math>d = \frac{1(6.50E-7m)(.1333m)}{5.5236E-3m}</math>  <math>d = 1.57E-7m</math></p>	<p><i>2<sup>nd</sup> Order Horizontal, n = 2</i>  <math>x=1.1393E-2m</math>  <math>d = \frac{2(7.00E-7m)(.1333m)}{1.1393E-2m}</math>  <math>d = 1.64E-5m</math></p> <p><math>d = \frac{2(6.50E-7m)(.1333m)}{1.1393E-2m}</math>  <math>d = 1.52E-7m</math></p>
---	---

*Average diameter along "y" axis at 700nm = 1.665E-5m or 16.65 microns*

*Average diameter along "y" axis at 650nm = 1.545E-5m or 15.45 microns*

**Table 2: Calculated Cell Dimensions, Fall 1998**

Tree Species	Average cell "x" diameter: 700nm (microns)	Average cell "x" diameter: 650nm (microns)	Average cell "y" diameter: 700nm (microns)	Average cell "y" diameter: 650nm (microns)
Birch	37.50	34.80	38.04	35.30
Red Oak dried 1	36.98	34.33	38.00	35.30
Red Oak dried 2	37.40	34.79		
Elderberry 1	36.05	33.45	39.48	36.64
Elderberry 2	36.22	33.61	40.11	37.23
Elderberry 2, Trial 2	35.64	33.08	36.99	34.33
Elderberry 3	38.07	35.34	36.16	33.57
Sugar Maple green	36.88	34.23	55.79	39.24
Sugar Maple color	36.56	33.93	37.68	34.97
Sweet Gum green	16.75	15.55	16.65	15.45
Sweet Gum yellow	16.25	15.05	16.45	15.25
Sycamore	16.65	15.45	16.37	15.19
Water Maple A	49.30	45.77	16.85	15.15
Water Maple B	16.28	15.11	17.46	16.21

To verify the accuracy of the procedural methods from phase two, additional leaf samples from each tree studied were collected in June, 1999 from the newly developed foliage, thus beginning phase three. The leaves were collected six feet above the ground from the same trees used previously on Piedmont Road in West Huntington, West Virginia. Care was taken to select mature leaves and scan each within three hours of collection. The aforementioned procedures were applied in order to determine the cell diameters for each leaf. See table 3 and appendix C figures 1a-f, 2a-f, 7a-d, 8a-d, 10a-f, 13a-i, 20a-f, and 24a-f. The resulting cellular dimensions were compared to the original values in order to develop a season to season correlation. See table 3.

**Table 3 – Calculated Cellular Dimensions, Spring 1999**

Tree Species	Average Cell "x" diameter: 700 nm (microns)	Average Cell "x" diameter: 650 nm (microns)	Average Cell "y" diameter: 700 nm (microns)	Average Cell "y" diameter: 650 nm (microns)
Birch	16.12	14.96	16.59	15.40
Elderberry	17.52	16.26	18.14	16.83
Holly	16.39	15.22	16.51	15.33
Red Oak	16.25	15.08	17.53	16.27
Sugar Maple	18.78	17.43	18.65	17.31
Sweet Gum	19.81	18.39	18.12	16.82
Sycamore	18.72	17.37	18.41	17.09
Water Maple	18.91	17.56	18.34	17.03

In addition to determining a comparison between leaves of successive seasons, the calculated cell dimensions were evaluated by comparing the Fourier transform experimental values to standards obtained conventionally, using a microscope with a micrometer attachment. See table 4. The transforms were analyzed in order to develop a correlation between the internal leaf structure and the previously obtained transforms from leaf surfaces. The leaves, from which transforms were generated, were crudely sectioned paradermally with a scalpel

and observed under 100, 200 and 400 times magnification. The differing leaf layers of five species were photographed onto 35 millimeter film. The photos were subsequently scanned and digitally processed using ER Mapper. See appendix C figures 3a-6c, 8e, 8f, 9a-i, 11a-c, 12a-c, 14a-19c, and 25a-27c.

**Table 4: Comparison of Cell Dimensions**

Tree Species	Cell "x" diameter 1998 FFT (microns)	Cell "y" diameter 1998 FFT (microns)	Cell "x" diameter 1999 FFT (microns)	Cell "y" diameter 1999 FFT (microns)	Ave. Palisade Cell diameter with microscope (microns)
Elder-berry	36.05-33.45	39.48-36.64	17.52-16.26	18.14-16.83	12.5
Red Oak	36.98-34.33	38.00-35.30	16.25-15.08	17.53-16.27	12.5
Sugar Maple	36.88-34.23	55.79-39.24	18.78-17.43	18.65-17.31	12.5
Sweet Gum	16.75-15.55	16.65-15.45	19.81-18.39	18.12-16.82	12.7
Water Maple	16.28-15.11	17.46-16.21	18.91-17.56	18.34-17.03	12.5

Distinctive transforms were produced from photographs of paradermal views of the epidermis, epidermis/palisade layers, palisade cells, stomata, striated veins, and the spongy matrix all at 200 or 400 magnification. See appendix C figures 3a-6c, 8e, 8f, 9a-i, 11a-c, 12a-c, 14a-19c, and 25a-27c. The Red Oak, Sugar Maple, Water Maple, and Sweet Gum transforms exhibited periodicities from which calculations were made. See table 4 and appendix C figures 8f, 9c, 9i, 11c, 12c, 16c, 17c, 25-27c. The transforms arose from leaf sections that contained the striated vein, the palisade layers, or the stomata in the Elderberry. See appendix C figure 4c. Each ordered transform was measured and the slit widths calculated in order to ascertain what feature produced the Fourier transformation. See table 5. At 400X magnification, the photograph dimensions can be converted to actual cell sizes in microns by multiplying by a 1:500 ratio.

**Table 5: Predicted Leaf Dimensions Correlated to Layers at 400X**

Tree Species	Fourier Transform Predicted Diameters (for spatial domain) (millimeters)	Corresponding Region of Photograph at 400X
Elderberry	8.63 - 8.02	Palisade cell and the adjacent cell wall
Red Oak	2.81 - 2.61 6.20 - 5.76	Cell wall thickness and palisade cell diameter
Sugar Maple	3.15 - 2.92 4.51 - 4.19	Palisade cell diameter and cell walls
Sweet Gum	4.91 - 5.29	Palisade cell diameter
Water Maple	1.93 - 2.08	Cell wall thickness or spacing between palisade cells

The last puzzling aspect of the transforms was the distinct periodicity in the "x" and "y" axes that can be produced only by very regularly spaced horizontal and vertical lines. Such lines must be characteristics of the image or some feature added by the processing techniques. The techniques in question were the scanning process, during which analog data is converted to digital data, and the calculations done by the ER Mapper software when performing the Fourier transform algorithm. The photograph of a Sweet Gum viewing the palisade layer paradermally was scanned at 45 degrees and 90 degrees from the original orientation, then the new images were processed to obtain their respective Fourier transforms. See appendix C figures 18a, 18c, 19a, and 19b. In addition, the Sycamore leaf was scanned at 0, 20, 50, and 90 degrees. See appendix C figures 20a, 20b, 21-23a. The Fourier transforms produced by the four Sycamore images and the three Sweet Gum images were analyzed for any recurring periodicity attributable to the scanning process, referred to as "scan lines." See appendix C figures 18b, 19c, 20c-d, 21b-23c. No such periodic structure was present.

To evaluate the impact of digital calculation anomalies, the fast Fourier transform algorithms were performed by enabling the "prevent wrapping" feature.

As mentioned in chapter one, wrapping is a technique to artificially simulate a continuous mathematical function. Without wrapping, the effect of the image edges should become pronounced. The "prevent wrapping" option was engaged when producing transforms for the Sweet Gum veinlet 3, the new Sycamore scans, the Water Maple and Sweet Gum palisade layers, and the Water Maple veinlets 1 and 2. As expected, all of the images contained the St. George's cross in the vertical and horizontal planes. See appendix C figures 13j, 13k, 17d, 17e, 20c, 21-23b27d, 27e. The Fourier transform algorithms with and without prevent wrapping were compared to establish what portion of the original image was merely a calculation error rather than a periodicity arising from the internal leaf structure. The portions of the transforms that had been interpreted as orders were not associated with the periodicities of the St. George's cross.



## Chapter Three

### Research Techniques

A Nikon flat bed scanner with a special light source for use with transparencies was used to scan each of the slides into Adobe Photoshop 3.0. A black mask was placed around the slides, the resolution was set at 1200 pixels per inch (non-interpolated), and the brightness at a value of two before a preview was done of the photograph. The resulting preview was "zoomed in" so that the area containing the leaf was highlighted. After "zooming out," the image was previewed again. Finally, the image was scanned and saved into Photoshop 3.0. In Photoshop, the image was cropped to contain only the leaf, and the brightness was increased so the detail of the leaf was apparent. Each file contained between .5 megabytes and 2 megabytes of data.

Due to the size of the files, each was saved as TIFF images onto a "Zip" diskette. The twenty-eight slides comprised nearly 50 megabytes of data that had to be copied onto MURSAC 008, a workstation in the MURSAC/ISAT/Physics networked computer laboratories that uses a 200 megahertz Pentium processor and Microsoft NT operating system. The workstation contained the ER Mapper program necessary for further analysis of the images. Initially, Iomega Zip drive software downloaded from the Internet was used to add the external Zip drive MURSAC 008. Unfortunately, the computer would not recognize the new hardware and data could not be copied. The second option was transferring the files via the MURSAC network from the Zip drive on "ODIN", a twin Pentium

workstation using Microsoft NT and operating as the MURSAC Network Server, into MURSAC 008's hard drive.

A pathway from MURSAC 008 to "ODIN" was established using the "Network Neighborhood File." Finally, from the icon, "My Computer", the data files stored on the Zip drive of "ODIN" were copied into ER Mapper in the tutorial file located in the datasets directory. When "ODIN" was no longer available due to its architecture undergoing changes, the pathway was established on the MURSAC Network from Dr. D. Sanderson's computer, "Sanderso," to MURSAC 008 and used for the remainder of the phase one research. Using the "Utilities" pull down menu, the TIFF graphics files were imported into ER Mapper and converted into "dataset" files. One slide at a time was loaded into an image window so its algorithm could be altered.

By opening the ER Mapper algorithm window, alterations in the bands, layers, filters, histogram, and formulas can be made for any image (ER Mapper 5.0 Workbook, 1995). For each image, the "blue and green layers" were turned off using the tool bar, and the "red layer" changed into a "pseudo surface layer" from the "Edit" pull down menu. The "color palette" was changed to "greyscale" before applying the algorithm. Additional adjustments were made depending on the clarity of the leaf. Typical changes included darkening the image by manually altering the histogram or applying linear, autoclip, or Gaussian transforms (ER Mapper 5.0 Workbook, 1995). The Horseweed, Sycamores 1 and 2, and the bottom of the Indian Flame tree leaves all required such alterations. See appendix A figures 4b, 15b, 16b, 5d. On rarer occasions, the red band was used in place of

the pseudo layer in an effort to preserve image resolution as with the Snowball Bush, Lilacs 1 and 2, the walnut, and the "jumbo leaf front." See appendix A figures 13b, 6b, 7b, 17b, 23b. Generally, the poor quality of the original slide fostered the need for band changes. The "Zoom" function enhanced the image only when the smoothing feature was deactivated; however, later, zooming was not practiced because larger features in the image led to minimal high pass resolution in the resulting transform. After the visibility of the image was maximized, the algorithm was saved as a dataset.

The Fourier Transform algorithm, located in the "Processes" pull down menu, analyzes the mathematical sine and cosine functions of each image to digitally develop a diffraction pattern for the specified wavelength bands. The input dataset originated in the saved algorithm and the output dataset name had the ending "red" to indicate the wavelength used. The program passes over the rows of pixels during the 10 to 20 seconds for analysis of the dataset. Finally, the pattern, containing roughly 5 megabytes of information, can be observed by opening a new window. If the transform was good, the background was black (see appendix A figures 1c-4c) indicating no noisy interference (appendix A figures 5c and 6c). However, to display the transform, the ER Mapper program must rescale the image to fit within 255 intensity values which may cause some percentage of the data to be lost. The cluster of dots was a tiny portion of the window that had to be zoomed several times to achieve maximum visibility. See appendix A figures 23c-d.

Pattern analysis followed the acquisition of acceptable Fourier transform patterns. All of the usable files from MURSAC 008 were saved to the Zip drive in Dr. Sanderson's computer because the volume of data surpassed 100 megabytes. An internal Iomega Zip drive was installed onto a Toshiba Infinia 2130 which uses a 233 megahertz Pentium processor and Microsoft Windows 95 operating system. The files were printed as hard copies from a high resolution, photo quality Hewlett Packard DeskJet 722C printer, model C5871A. The images were left in ER Mapper format because they could not be converted back to TIFF files and exported to Adobe Photoshop 4.0 or into Microsoft Word. In this phase of research, the analysis remained qualitative based on similarities in the leaves compared to their corresponding diffraction pattern from the hard copies. High and low pass filters were applied to the images and the resulting transform lacked spatial or spectral data due to diminished clarity and the return of noise. The next step in the analysis required that the spacing in the dot array be measured and referenced to the original image. The width of the slide set the initial perimeters for the TIFF files; however, the small-scale images were not scanned to the slide extents in an effort to obtain the highest resolution of the region containing the leaf.

In stage two, each of the leaf samples was scanned directly onto a Memorex SCF 6120P color flatbed scanner using the MrScan Easy software that accompanied the scanning device. Because the files were in excess of 5 megabytes each, the scan area was limited to a 1.44 square centimeter area at 1200 dots per inch. Higher resolution or a larger sample area resulted in data files

that were unmanageably large. The scanned images were saved on the hard drive of Toshiba Infinia 2130 then imported into ER Mapper 5.5 using the "import graphics formats" file. The samples were adjusted according to the previously established algorithm. The Fast Fourier Transform, or FFT, process generated patterns from all of the leaf samples by summing the sine and cosine functions in one Cartesian coordinate plane quadrant and duplicating the result into the opposing quadrant. The files were saved onto the hard drive and backed up onto zip diskettes. The Microsoft NT workstation/servers labeled as "ODIN" and "Headhoncho" on the MURSAC network were used alternatively with the Toshiba model while a series of manipulations were performed on the images and their Fourier transforms, using the ER Mapper 5.5 and Adobe Photoshop 4.0 software.

Because the original Fourier transforms contained only a central maximum, small veinlet sections of each image's algorithm were selected by dragging a box around the desired region. The new selections yielded transforms with successive orders; unfortunately, such orders had been misinterpreted as background noise in phase one. Using the "cell value" and "cell coordinates" features located in the "View" pull-down menu, the maxima were determined and the separations between them measured by clicking on one dot then dragging the mouse to the central maximum. See illustration 8. Many orders appeared to have an associated bandwidth, or secondary peak corresponding to +/-1.5 to 2 microns variations in the slit widths.

In Phase three, a leaf from each physiognomic type analyzed in phase two was collected. The epidermal and palisade cells were measured from a

paradermal view with a microscope equipped with an eyepiece micrometer. With a 40-power objective lens and a 10-power eyepiece, each marking on the micrometer represented 2.45 microns. Five to ten palisade cells were selected randomly from crude paradermal sections of the leaf from which the cuticle and epidermis were removed with a scalpel. For the five chosen species, the measured values, averaged from all of the trials, were between 12 microns and 13 microns. See table 4. The leaf sections containing epidermal cells produced average values between 30 and 40 microns for all species.

The specimens were prepared by removing a paradermal section of the leaf, slicing thin layers of the leaf at an angle with a sharp scalpel, placing the leaf on a slide, applying a droplet of water, and attaching a glass cover slip to the top of the leaf. After the leaves were observed and measured at 400X with a standard transmission microscope containing a special fiberoptic specimen-reflective light source, images were captured for additional analysis. Using 400-speed Fuji 35 millimeter film for color prints, various paradermal layers of leaves from the epidermis to the spongy matrix of the mesophyll were photographed. See appendix C figures 3a-6c, 8e, 8f, 9a-i, 11a-c, 12a-c, 14a-19c, and 25a-27c. The apparatus used was a Zeiss microscope equipped with Nikon lenses and the MC63 automatic light meter. The photographs were processed at Kramer's Photography in Huntington, WV. For each photograph, an area of one hundred square centimeters was scanned at 300 dots per inch and processed using the aforementioned Memorex scanner, Adobe Photoshop 4.0, and ER Mapper 5.5. The Fourier transforms exhibiting periodicity were measured using the "cell

coordinate” and the “cell value” windows of ER Mapper. The photographs were measured with a stainless steel C-Thru ruler with a millimeter scale in order to compare the transform-predicted values to the actual periodicities.

The “prevent wrapping” feature and the scanning techniques were altered to assess the effects of digital image processing on the resulting Fourier transform. The Sweet Gum palisade layer photograph and a Sycamore leaf were physically rotated prior to separate scans in order to detect a recurring periodicity. See appendix C figures 18a-19c and 20a-23c. To enable “prevent wrapping,” the option was selected in the “Forward Fourier Transformations” window. “Prevent wrapping” was performed on the Sycamore leaves scanned at four different orientations to highlight processing periodicities. The Sweet Gum leaf and the Water Maple veinlet that did not produce obvious orders originally were processed to detect the presence of orders. See appendix C figure 13c. Finally, the Sweet Gum veinlet 3, the Sweet Gum palisade layer and Water Maple palisade/spongy matrix were processed to determine the portion of their ordered transforms that may be produced erroneously by the software. See appendix C figures 13j, 13k, 17d, 17e, 27d, 27e. All transforms were qualitatively compared to the transforms produced using the wrapping technique.

## Chapter Four

### Results and Analysis

Fourier transformations from tree leaves are produced when an algorithm is applied in which the red layer is converted to a pseudo layer and the color palette changed to greyscale. During phase one, the analysis of the leaves' Fourier transforms lies in the qualitative observation of similarities that emerged from one leaf to the next based on both their images and their corresponding diffraction patterns. When comparing the Red, Sugar, and Water Maples. See appendix A figures 11a-c, 14a-c, 18a-b, 21 a-c, all three leaves exhibit the major venation pattern of a palmate with smaller branching veins. The Fourier transforms of all three contain a unique starburst quality and high degree of detail not found in many other species. The sugar and water maples studied in phase two did not produce identical transforms, but do demonstrate the same six-sided array, when "zoomed in," as those generated in phase one. See appendix B figures 10a-f, 14a-c, 15a-d.

In addition to the maples, the Snowball Bush, the Rose of Sharon, the Horseweed, the walnut, and the front of the "Jumbo Leaf," were all species exhibiting a large degree of high frequency detail. See appendix A figures 13a-c, 12a-c, 4a-c, 17a-c, and 23a-d. The walnut and the Snowball Bush share a spiral effect in their respective transform pattern that was not present in any of the other samples from either phase one or two. To the naked eye, none of these leaves have comparable features. The walnut is distinctly pinnate in structure while the jumbo leaf, the maples, and the Snowball Bush are combinations of



palmate/pinnate, at best. Further comparison between palmates and pinnates (Brumfield, 1998) did not yield any common arrangements in the transform patterns. In fact in phase two, all of the samples produced transforms with distinctly vertical and horizontal patterns regardless of the venation type. See appendix B-C.

A lack of comparable venation suggests that the transforms must arise from another periodicity within the leaf. Since a correlation between the appearance of the leaf and its resulting transform could not be established, the focus shifted to Fourier transforms exhibiting similarities. The mature Pin Oak, the Sycamore II, and the small-scale Water Maple all had an extended diagonal line passing through a rectangular arrangement in the lower frequencies. See appendix A figures 9c, 16c, 21c. All of the leaves have significant branching venation to explain similarities in the central maxima; however, other slides of the Sycamore and the Water Maple had shown remarkably more information than these transforms contained. See appendix A figures 15c and 18b, 19c, and 20c. Immediately, the common factor was determined; each of these slides had been “zoomed in” more than most. The original datasets were accessed and changed to encompass a much larger portion of the leaf. The Sycamore produced a detailed transform so the new algorithms were applied to the other two slides. The mature Pin Oak also showed high frequency information; however, the Fourier transform produced from the Water Maple had the most high frequency detail because the pattern never yielded a black background. See appendix A figure 19c. The zooming was also reduced on the bottom surface of the “jumbo leaf”

slide and, again, a higher order of single dots emerged. See appendix A figures 24c and 24e.

The "jumbo leaf" and the Indian Flame tree leaf were photographed on both sides. See appendix A figures 5a, 5d, 23b, 24b. The detailed photos of the bottom of the leaves created transforms with no high frequency data and very simplified, low pass information. See appendix A figures 5f, 24c, and 24e. Conversely, the "jumbo leaf" top contained one of the highest numbers of individual dots and the Indian Flame tree leaf transform was overwhelmed with high pass data that was assumed to be background noise. See appendix A figures 5c and 23d. In a cross-sectional view, the major structural change from the top to the bottom of the leaf arises from the periodic palisade layer giving way to the less organized spongy matrix. See illustration 4. Because the overall venation remained the same, the cellular structure must be an integral part of the diffraction barrier.

The final qualitative, physiognomic comparison of Fourier transforms was between leaves collected at different developmental stages. The young Pin Oak's transform showed a concentration of dots around the central maximum. The mature Pin Oak illustrated a much more open center and dots extending diagonally away from the center. The overall shape of both transforms was a slightly skewed rectangle. The increased detail in the higher spatial frequencies is to be expected as the cells become better defined, more numerous, smaller and more closely packed. No such comparisons could be made in phase two because all of the leaves were collected in the late autumn as the colors were changing.

In phase two, quantitative analysis required that a Fourier transform be created so that measurements could be made and applied to the formula  $d \sin \theta = n \lambda$ . To create a transform pattern with orders, a small section within a set of veinlets or an entire tree from a far distance must be selected (Brumfield, Bloemer, and Oberly, 1997). The transform pattern consists of a series of dots at varying intensity values that can be evaluated using the "cell values" window of ER Mapper. After pinpointing the dots with the largest values, the "cell coordinates" window is used to determine the separation between each maxima and the central max. See illustration 9. Each of the orders, when applied to the formula  $d = n \lambda L / x$ , produced slit width values with general agreement. See illustration 10. The resulting values, when averaged, represent either the cell "x" or "y" spatial components. The experimental cell widths ranged from 15 microns to 45 microns. See table 2. All calculated values are on the correct order of magnitude for actual cell diameters according to experimental measurement and the work by Bickford and Dunn in 1972.

Comparisons from one leaf sample's dimensions to another also indicate agreement. The dried Red Oak samples were collected from the same section of the leaf; in fact, Red Oak 2 was an inner portion of the study area for Red Oak 1. The agreement between the values as seen in table 2 indicates that the transform pattern from the larger section containing four veinlets is providing the same information as found in a single veinlet. The samples from the elderberry and the sweet gum were completely different leaves even exhibiting a seasonal color change; however, the experimental cell diameters agreed to within one micron.

The Sugar Maples, also separate leaves, agreed from less than one micron to twelve microns. The only samples with significant differences were the Water Maples. The horizontal diameters differed by as much as thirty microns, but the vertical values differed by less than one micron. See table 2. The similarities between calculated values from separate leaves imply a predictable regularity within a species, at least among leaves on the same developmental level and similar physiognomies.

In phase three, leaves were collected from the same trees one season later. Again, small veinlet portions were selected, the appropriate algorithm applied, the transform generated, and the cell dimensions calculated. The new Fourier transforms predicted cell "x" diameters from 14.96 to 19.81 microns and "y" diameters of 15.33 to 18.65 microns. The dimensions from 1999 were approximately 20 microns smaller than the typical values collected in 1998. The dimensions from 1999 were dramatically affected by drought conditions present during the formation of the foliage. Conversely, the samples collected in 1998 had formed during wetter than normal conditions.

Using a microscope with an eyepiece micrometer and a 35 millimeter camera attachment, five species were measured under 400X magnification. The average epidermal cells were approximately 30 to 40 microns, palisade cells averaged 12.5 microns in diameter, and cell walls were 1 to 2 microns thick. The photographs of various leaf layers were used to generate Fourier transforms from which calculations were made and correlated to the original image. The dimensions obtained from the Water Maple at 400X magnification were from 1.93

to 2.08 millimeters which corresponded to the distances between the palisade cells in the photograph. See appendix C figure 26a. However, the Sweet Gum palisade layer at 400X magnification predicted slit widths of 4.91 to 5.29 millimeters which roughly compare to the 6.5 millimeters average cell diameter in the photograph. See appendix C figure 16a. Similarly, the Red Oak predicted diameters ranging from 6.2 to 5.8 millimeters, closely agreed to the photograph's average 5.7 millimeters. See appendix C figure 8e. The Fourier transforms for all five species contained physiognomic components arising from the palisade cells or the cell wall. See table 5. For each leaf, the most fundamental periodicity arises from the tightly packed palisade cells, the cell's walls, and any intercellular medium between it and the adjacent cell. The Fourier transformation appears to be a combination of these spatial frequencies and the spectral frequencies of visible light acting upon those physiognomic parameters.

All of the leaf species produced an ordered transform with distinctive patterns along the vertical and horizontal axes. Investigations performed to assess the effects of processing techniques on the resulting transform patterns included the disabling and enabling of the "prevent wrapping" feature as well as rotation of the images prior to scanning. The transforms generated without "wrapping" produced exaggerated orders along the "x" and "y" axes. Close inspection of the transforms produced by the identical image did not reveal significant patterns associated with edge effects. See appendix C figures 20a-23c. The "prevent wrapping" results did not appear to affect the portions of the transforms used to make calculations. However, to precisely determine the

quantity of the transform containing edge effects, the transform would have to be masked to remove the St. George's cross pattern. The transforms produced by rotating the image prior to scan showed no signs of recurring periodicities that would be associated with the scanning or digitizing processes. See appendix C figures 20a-23c.

## Chapter Five

### Conclusion

The research's goal involved developing a method for digitally acquiring Fourier transform patterns from various tree and shrub leaves, qualitatively establishing physiognomic similarities, and quantitatively predicting the cellular dimensions. According to the theories of diffraction and interference, any image with periodic structure, such as veins or cellular arrangement, will produce a Fourier transform corresponding to the spatial frequency. A digital technique for acquiring such physiognomic patterns was established by the research. The method includes scanning photographs and slides of leaves or leaf samples at high resolution. After reducing the quantity of spectral information to only the red band, the image detail is enhanced by applying an algorithm with no smoothing, a pseudo layer palette in greyscale, and minimal zooming. Three of the Fourier transform patterns collected were enhancements of the original transform because a new algorithm with less magnification, or zooming, allowed the pattern to be spread apart. Due to this result, images should be reprocessed with minor alterations to either obtain a clear transform or a more informative one. The established algorithm produced thirty-nine separate, detailed dot patterns, each of which were unique to the leaf sample. Additional patterns may have emerged if all of the original 1:1 ratio slides had been analyzed while having all of the features of the algorithm in place.

Several results indicate that the Fourier transforms emerge from periodic structures within the leaf that exhibit high spatial frequencies. Initially, palmates

and pinnates were compared due to the obvious, large-scaled structural differences. Although several leaves appear to be similar to the naked eye, their transform patterns bear little relationship to one another other than the central maximum. For example, all of the maples, which were classified as palmates, exhibited a relatively empty central maximum, indicative of low spatial frequency, when compared to the detailed outer edges. High frequency transforms were similar to both the palmate, demonstrated in the Snowball Bush, and the distinctly pinnate-structured walnut. Since the primary vein arrangement in the two species is vastly different, the only reasonable conclusion is that diffraction patterns are produced by even smaller structures, such as organized cells. For the Snowball Bush and the walnut to have similar transforms, the internal cellular arrangement must be comparable between the two. As light passes through the spaces between the cells, it would be diffracted as necessary to create a Fourier transform. Below the well-arranged palisade cells is a more random matrix of spongy material incapable of producing a regular diffraction pattern.

To verify that the epidermis and palisade cells reflect light to produce a Fourier transform, patterns were generated and compared from the top and bottom sides of the same two leaves. The images from the top and bottom of the "jumbo leaf" produced Fourier transforms that one could explain based on the leaf's internal cellular structure. The top of the leaf yielded a pattern rich in numerous high frequency dots; however, the bottom of the leaf produced a simple, low spatial frequency pattern. Visual comparison of the images shows equally distinct veins in both sides yet the transform from the bottom of the leaf contained



no high frequency information. One obvious conclusion is that the detailed diffraction pattern is a result of the internal cellular structure, which is defined on the top of a leaf due to the palisade cells, but basically random in the spongy matrix underneath. If the Fourier transforms were merely the result of the venation, the top and the bottom would produce identical patterns. Cellular development from the young to mature Pin Oak indicate that the high frequency information increases as the cells become more numerous, compacted, and well-defined.

Based on observations of Fourier transform patterns produced by the Red Maple, Sugar Maple, Water Maple, Sycamore, Birch and Elderberry, the individual species appear to exhibit similar orientations in the separate dot arrays produced. All species produced unique transform patterns with varying degrees of spatial frequency. Selecting only the red band typically produced a diffraction pattern with a black background; however, the original patterns mistaken as background noise actually exhibited the presence of orders. The original ordered transforms could not be analyzed quantitatively because they were scanned with an unestablished zooming or magnification factor. The slides taken from the top and the bottom of the leaf suggest that the diffraction patterns result from the internal cellular arrangement of the leaf rather than the venation. After reviewing the reverse Fourier transform of the elderberry leaf in phase two, the central maximum appears to be the only portion of the pattern that represents the venation. Transforms with orders produced by veinlets and cell walls may be produced using

the red, green, and blue bands at a distance or by selecting a veinlet of the leaf and analyzing only the red wavelengths.

In order to utilize the Fourier transform technique quantitatively for species identification, physiognomy, or cellular development, in phase two, additional leaves were collected and scanned using specific distance perimeters. By scanning the same amount of area for each leaf and by eliminating zooming, accurate measurements were collected so qualitative analysis could be developed into less subjective quantitative conclusions.

By selecting portions of the leaves containing only veinlets, Fourier transforms emerge containing successive orders from which measurements were made and used to accurately predict the dimensions of the original sample. Qualitatively, the transform patterns depict unique spatial frequencies that may be used to delineate species and physiognomic patterns. Quantitatively, the calculated cell diameters agree to within a micron from one leaf to another within the Sugar maple, Sweet Gum, and Elderberry species, indicating uniform spatial frequencies among the cells within the leaves. Such periodicities may be used to delineate one species from another based on physiognomy and to differentiate among developmental stages. In phase three of the research, leaf samples collected from the spring, 1999 were compared to the fall, 1998 leaves.

The dimensions calculated by the Fourier transform of the original leaf are in close agreement to the values collected under microscopic, optical magnification. As stated in table 4, the separation between orders predicted a cell width of 15 to 19 microns. Although the epidermal cells are much larger, ranging

from 30 to 40 microns, under magnification, the palisade cells measured 12.5 microns in diameter with cell walls up to 2 microns thick. The Fourier transforms collected from magnified leaf layers all indicated diffraction produced by the palisade cells in conjunction with the cell walls yielding a total slit width of 14.5 to 16.5 microns. Because the cellular dimensions predicted from the transform range from 15 to 19 microns, it is reasonable to conclude that a leaf's Fourier transform is a viable method for measuring the diameter of palisade cells, including the cell wall. The ER Mapper Fast Fourier Transformation program, due to "padding", enlarges the Fourier transformation by roughly 10 percent (ER Mapper 6.0 Applications, 1998), which, after adjustment, would bring the predicted dimensions even closer into alignment. The predicted values are in close agreement to the palisade cellular dimensions and the "prevent wrapping" and scan orientation did not appear to affect the transform and its interpretation. Therefore, it is also reasonable to conclude that the digital processing techniques have minimal negative effects on the qualitative or quantitative analysis of Fourier transforms.

In the future, measuring cell dimensions from Fourier transform of physiognomic patterns may be extended to images acquired aerially from whole trees. The transforms may be measured in order to determine whether a measurable correlation exists between the physiognomy of the leaf and tree transforms. Fourier theory proposes that a transform extends from negative infinity to positive infinity suggesting that a diffraction pattern obtained at high elevations would include spatial information about both the tree and its constituent leaves. Due to the dramatic changes in cell size as a result of drought leaf,

Fourier transforms may also be utilized to evaluate the hydrology of a study site and possibly aid in defining ecosystems. Eventually, an amassed database may be used for species and physiognomy delineation and for developmental stage differentiation among the leaves collected by various sources of remotely sensed imagery.

## Resources

- Adobe Photoshop. Vers. 3.0. Computer software. Adobe Systems, Inc., 1994.
- Adobe Photoshop. Vers. 4.0. Computer software. Adobe Systems, Inc., 1996.
- American Online Search Engine. Topic: Optics Fourier Transforms. April, 1998.
- Bickford, Elwood D. and Stuart Dunn. Lighting for Plant Growth. The Kent State University Press: Kent, Ohio, 1972.
- Brown, William H. The Plant Kingdom. Boston: Ginn and Company, 1935.
- Brumfield, James O. and Ralph Oberly. Physics 511: Digital Image Processing. Huntington, WV: Marshall University, Spring 1996.
- Brumfield, James O., H.H. L. Bloemer, R. Oberly, and D. Sanderson. "Digital Evaluation of Optical Fourier Transforms of the Physiognomy for Vegetation Associations in Mountainous Terrain." Marshall University: Huntington, WV, 1997.
- Brumfield, James, Dr. Interview. Huntington, WV: Marshall University, Summer 1997, Spring 1998.
- Dansereau, Pierre. Biogeography: An Ecological Perspective. New York: Ronald, 1957.
- DeskJet 722C. Printer. Hewlett Packard, purchased at Office Max, 1997.
- ER Mapper. Vers. 5.5. Computer software. Earth Resource Mapping, 1997.
- Earth Resource Mapping. ER Mapper About Release 5.5. San Diego, CA, 1997.
- Earth Resource Mapping. ER Mapper 5.0: Applications. San Diego, CA, 1995.
- Earth Resource Mapping. ER Mapper 6.0: Applications. San Diego, CA, 1998.

- Earth Resources Mapping. ER Mapper 5.0, Level One Training Workbook. San Diego, CA August, 1995.
- Earth Resource Mapping. ER Mapper 5.5 Level One Training Workbook for Land Information Applications. San Diego, CA , 1997.
- Earth Resource Mapping. ER Mapper 5.0 Resource Manual. San Diego, CA June 1995.
- Earth Resource Mapping. ER Mapper 5.0 Tutorial. San Diego, CA, 1995.
- Earth Resource Mapping. ER Mapper 6.0 User Guide. San Diego, CA, 1998.
- Esau, Katherine. Plant Anatomy. John Wiley & Sons, Inc.: New York, 1953.
- Frey, T. Biology 750: Fourier Transforms Internet Lab Theory.  
Sci.sdsu.edu/Tfrey/Bio750/Fourier Transforms.html/ April, 1998.
- Giancoli, Douglas. Physics: Principles with Applications, 5<sup>th</sup> edition. Prentice Hall: New Jersey, 1998.
- Hecht, Eugene. Optic, 2<sup>nd</sup> ed. Reading, Massachusetts: Addison-Wesley Publishing Company, May, 1990.
- Lanzara, Paola and Mariella Pizzetti. Simon and Schuster's Guide to Trees. Simon and Schuster, Inc.: New York, 1978.
- Memorex SCF 6120P. Computer hardware, color flatbed scanner. Memtek Corporation, 1998.
- Microsoft Encarta '97 Encyclopedia. "Baron Jean Baptiste Joseph Fourier"  
Microsoft Corporation, 1996.
- Microsoft Encarta '97 Encyclopedia. "Optics - Interference and Diffraction"  
Microsoft Corporation, 1996.
- Microsoft Word. Office'97 version. Computer software. Microsoft, 1997.
- MrScan Easy. Vers. 4.04. Computer software. Memtek Corporation, 1998.
- Niklas, Karl J. Plant Biomechanics. Chicago: The University of Chicago Press, 1992.
- Nikon. Computer hardware, color flatbed scanner. Nikon, 1996.

Oberly, Ralph. Physics 304: Optics. Huntington, WV: Marshall University, Spring 1993.

Reynolds, George O., John DeVelis, and George Parrent. The New Physical Optics Notebook: Tutorials in Fourier Optics. Optical Engineering Press: New York, 1989.

Whittaker, R.H. Communities and Ecosystems. New York: McMillian Co., 1970.

Windows '95. Computer operating system. Microsoft, 1995.

Windows NT. Computer operating system. Microsoft, 1997.

Zim, Herbert S. and Alexander C. Martin. Trees: A Guide to Familiar American Trees. Golden Press: New York, 1956.

Zip 100. Computer hardware, internal zip drive. Iomega, purchased at Software City, Huntington, WV, 1998.

**Appendix A**  
**Phase One – Acquisition and Qualitative Analysis of Fourier Transforms**



Fig. 1a Cherry slide



Fig. 1b Cherry leaf with algorithm

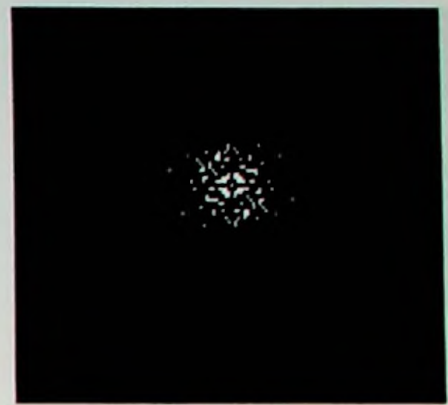


Fig. 1c Cherry FFT



Fig. 2a Green Ash slide

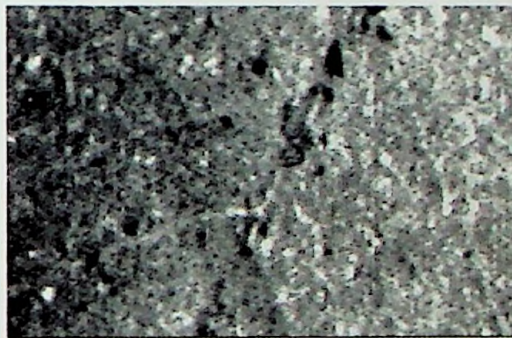


Fig. 2b Green Ash leaf, zoomed with algorithm



Fig. 2c Green Ash FFT

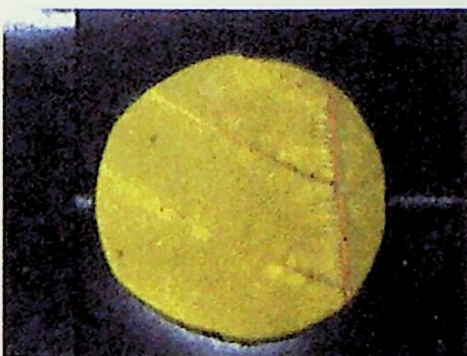


Fig. 3a Horse Chestnut slide



Fig. 3b Horse Chestnut, zoomed with algorithm



Fig. 3c Horse Chestnut FFT



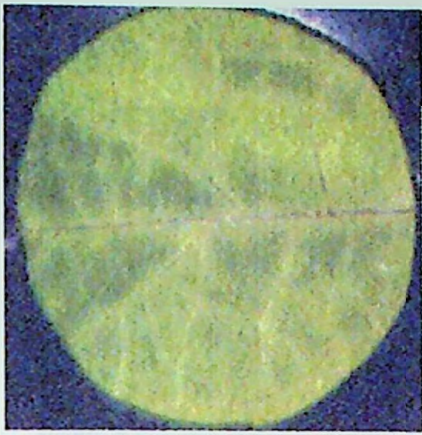


Fig. 4a Horse Weed slide

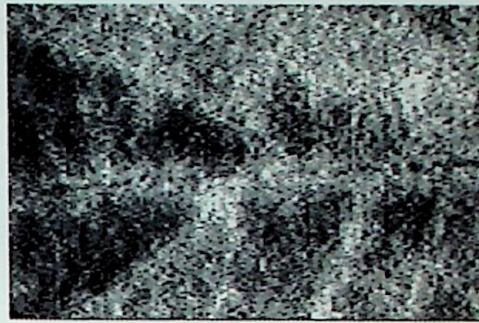


Fig. 4b Horse Weed, zoomed with algorithm



Fig. 4c Horse Weed FFT



Fig. 5a Indian Flame Tree slide

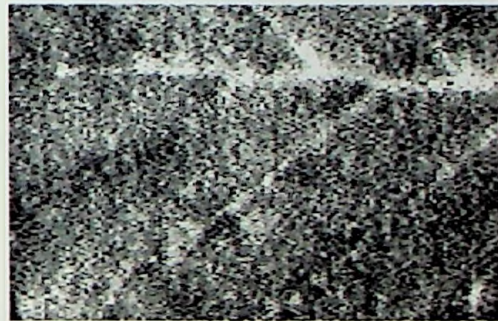


Fig. 5b Indian Flame Tree zoomed, with algorithm



Fig. 5c Indian Flame Tree FFT



Fig. 5d Indian Flame tree leaf back slide



Fig. 5e Indian Flame tree back, zoomed with algorithm



Fig. 5f Indian Flame Tree back FFT

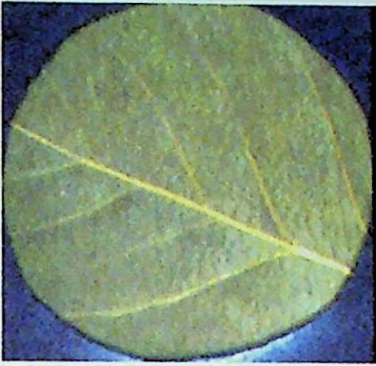


Fig. 6a Lilac slide I



Fig. 6b Lilac I, zoomed with algorithm



Fig. 6c Lilac I FFT

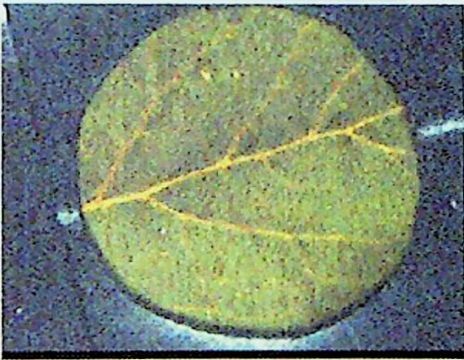


Fig. 7a Lilac leaf slide II



Fig. 7b Lilac II, zoomed with algorithm



Fig. 7c Lilac II FFT



Fig. 8a Mock Orange slide



Fig. 8b Mock Orange, zoomed with algorithm

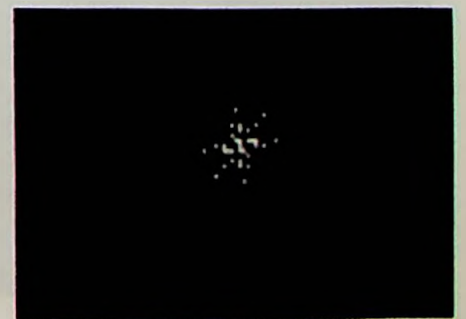


Fig. 8c Mock Orange FFT

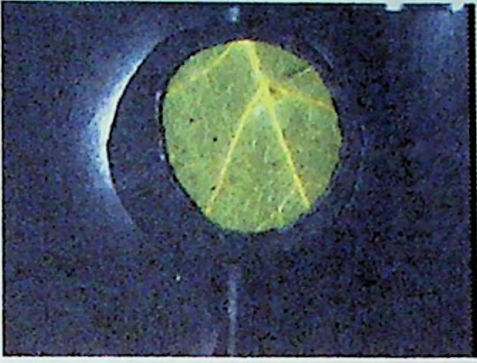


Fig. 9a Mature Pin Oak slide

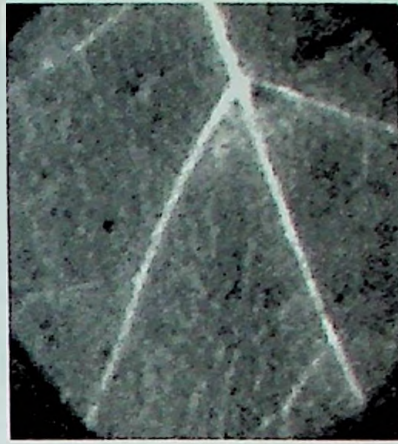


Fig. 9b Mature Pin Oak, zoomed with algorithm

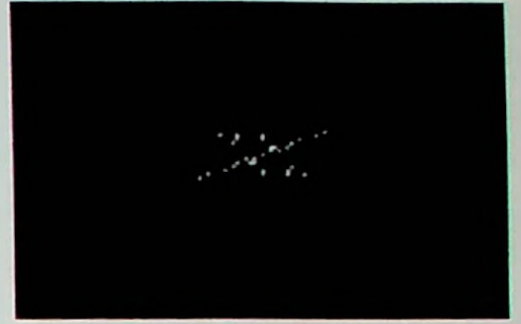


Fig. 9c Mature Pin Oak FFT



Fig. 10a Young Pin Oak slide

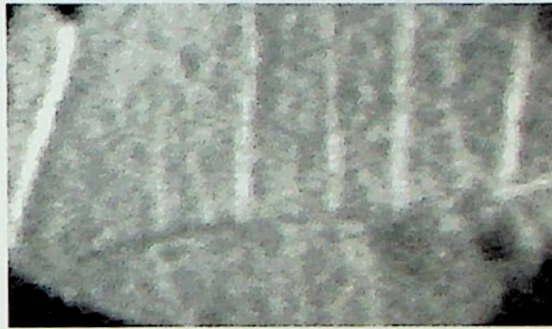


Fig. 10b Young Pin Oak, zoomed with algorithm



Fig. 10c Young Pin Oak FFT

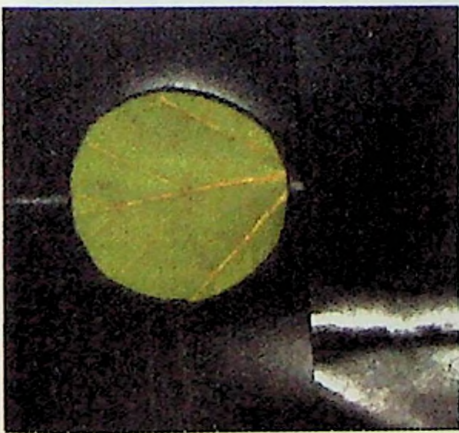


Fig. 11a Red Maple slide



Fig. 11b Red Maple, zoomed with algorithm



Fig. 11c Red Maple FFT

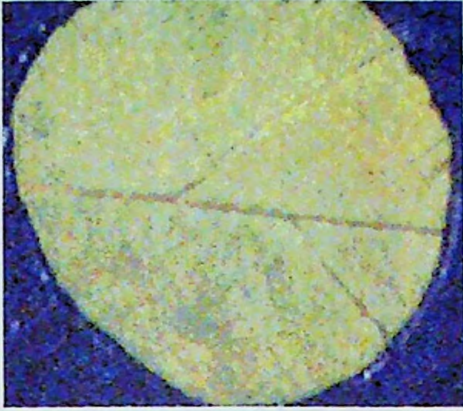


Fig. 12a Rose of Sharon slide



Fig. 12b Rose of Sharon, zoomed with algorithm

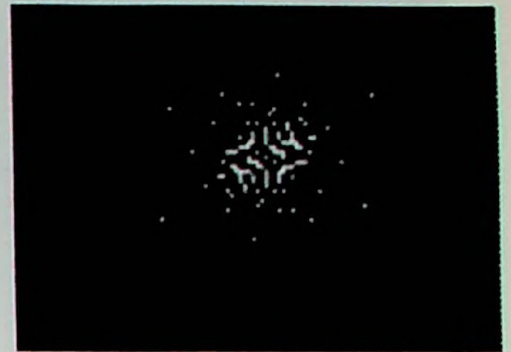


Fig. 12c Rose of Sharon FFT

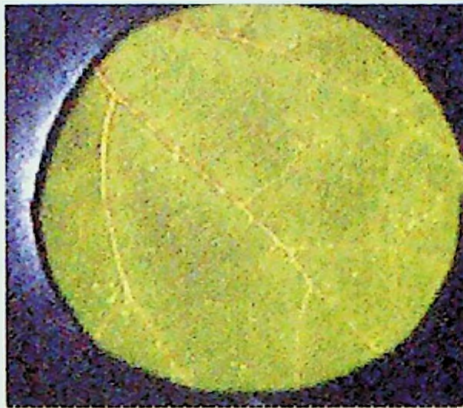


Fig. 13a Snowball Bush slide

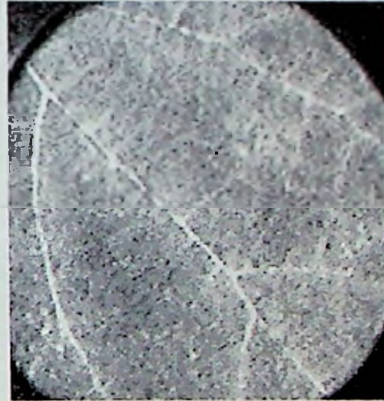


Fig. 13b Snowball Bush, zoomed with algorithm



Fig. 13c Snowball Bush FFT

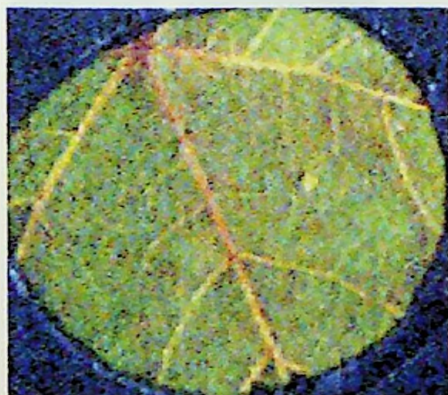


Fig. 14a Sugar Maple slide



Fig. 14b Sugar Maple, zoomed with algorithm



Fig. 14c Sugar Maple FFT

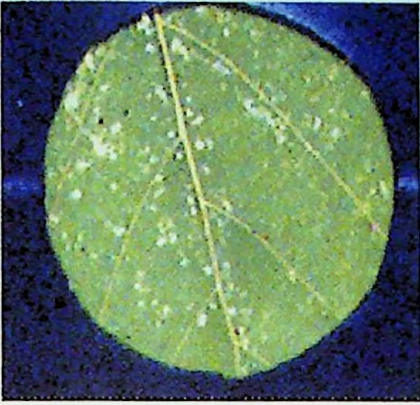


Fig. 15a Sycamore leaf I slide



Fig. 15b Sycamore I, with algorithm

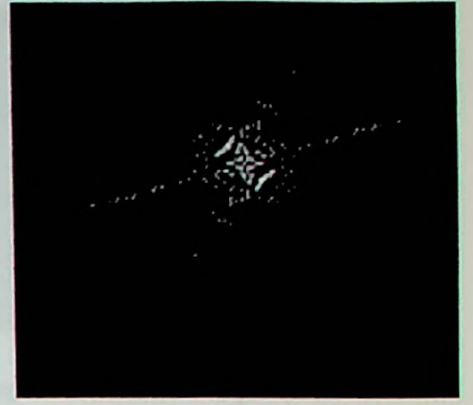


Fig. 15c Sycamore I FFT



Fig. 16a Sycamore leaf II slide



Fig. 16b Sycamore II, zoomed with algorithm

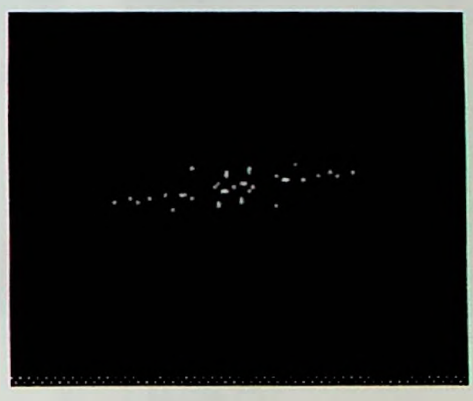


Fig. 16c Sycamore II FFT

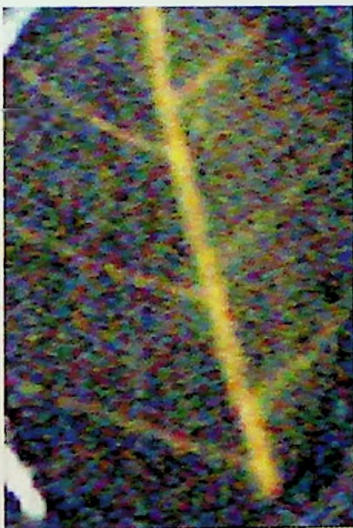


Fig. 17a Walnut slide



Fig. 17b Walnut with algorithm



Fig. 17c Walnut FFT

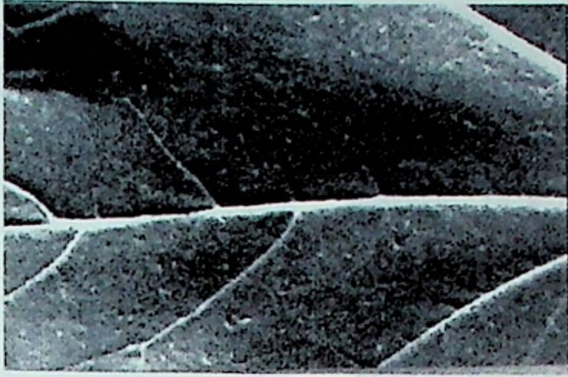


Fig. 18a Water Maple slide at 1:1 ratio, with algorithm and zooming



Fig. 18b Water Maple at 1:1 ratio FFT

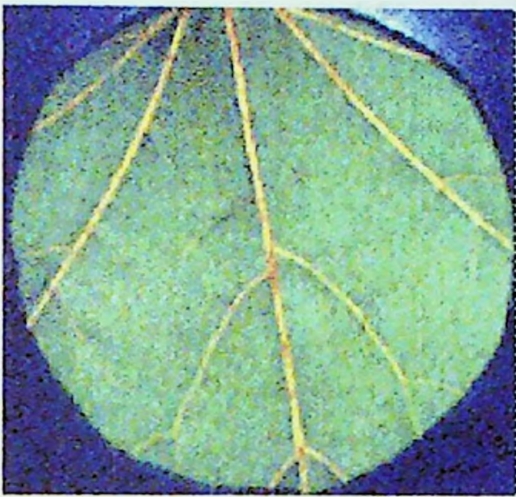


Fig. 19a Original Water Maple slide scan

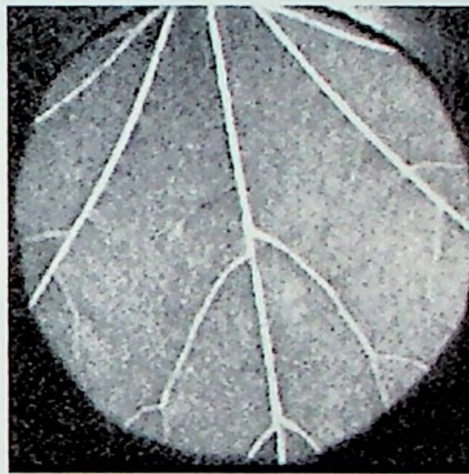


Fig. 19b Original Water Maple with algorithm



Fig. 19c Original Water Maple FFT

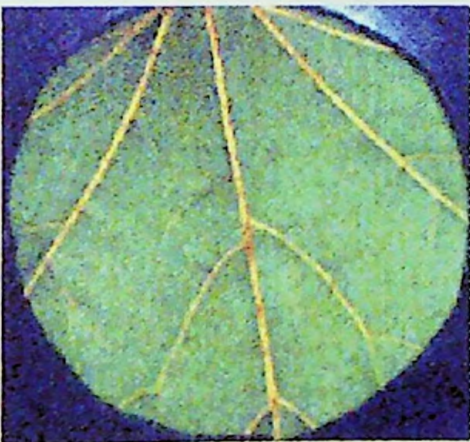


Fig. 20a Original Water Maple scan



Fig. 20b Original Water Maple, zoomed with algorithm



Fig. 20c Original Water Maple, with zooming



Fig. 21a Water Maple slide second scan

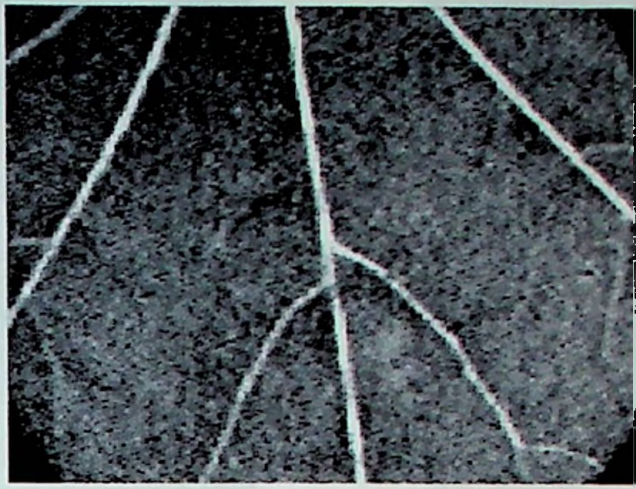


Fig. 21b Water Maple second scan, zoomed with algorithm



Fig. 21c Water Maple second scan FFT

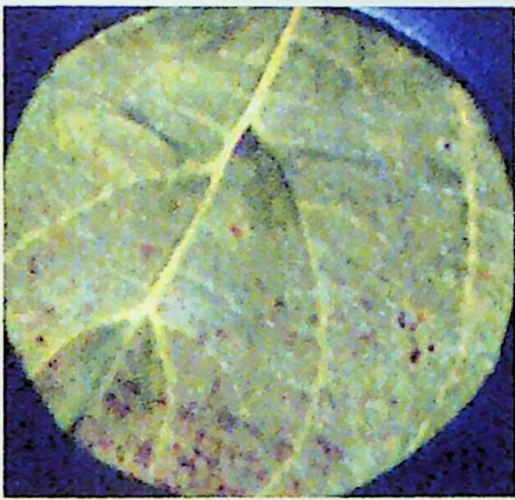


Fig. 22a Wild Cherry slide

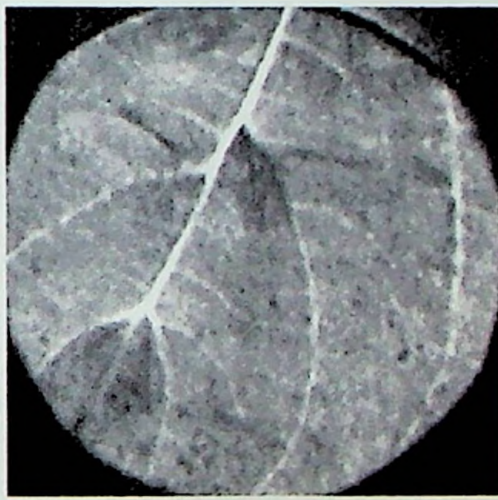


Fig. 22b Wild Cherry with algorithm



Fig. 22c Wild Cherry FFT



Fig. 23a Jumbo Leaf front, species unknown



Fig. 23b Jumbo Leaf front, zoomed with algorithm



Fig. 23c Jumbo leaf front FFT



Fig. 23d Jumbo leaf front FFT, zoomed central region



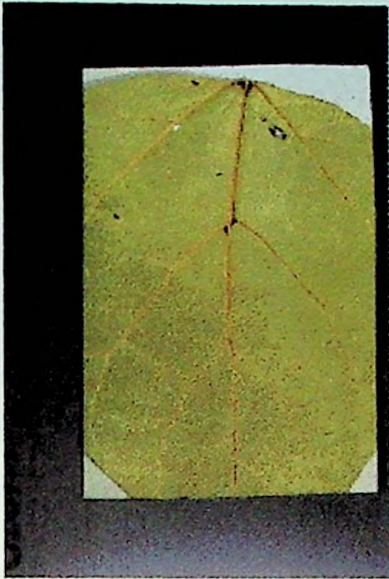


Fig. 24a Jumbo leaf, species unknown. back



Fig. 24b Jumbo leaf back, zoomed with algorithm

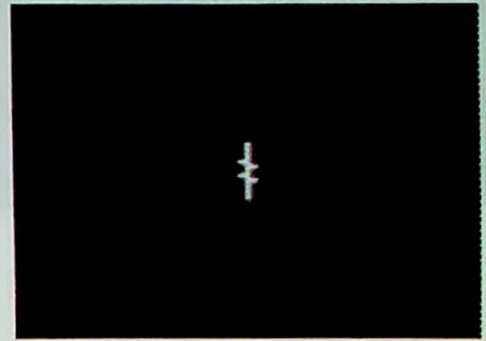


Fig. 24c Jumbo leaf back FFT



Fig. 24d Jumbo leaf back, zoomed with algorithm and linear transform

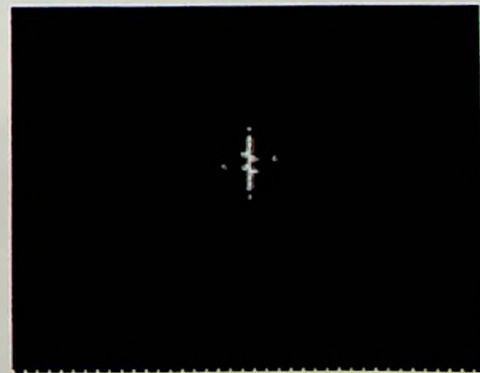


Fig. 24e Jumbo leaf back FFT

# Appendix B

## Phase Two - Quantitative Analysis of Fourier Transforms

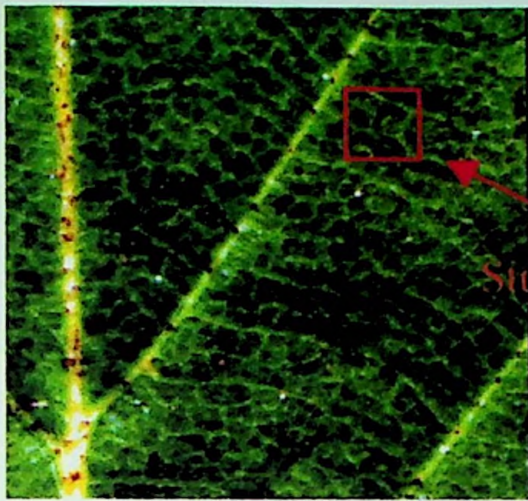


Fig. 1a Birch original image

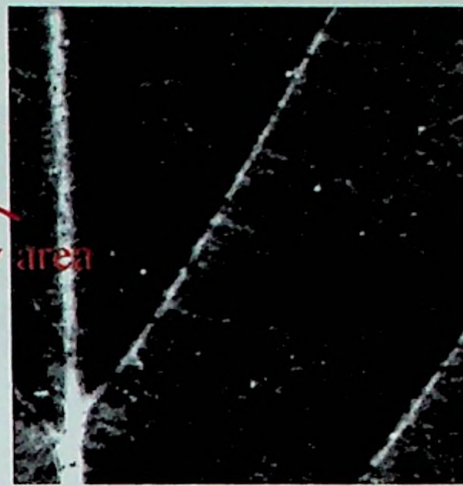


Fig. 1b Birch with algorithm

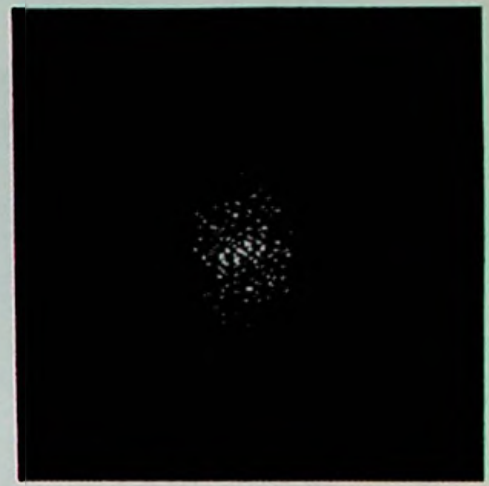


Fig. 1c Birch FFT

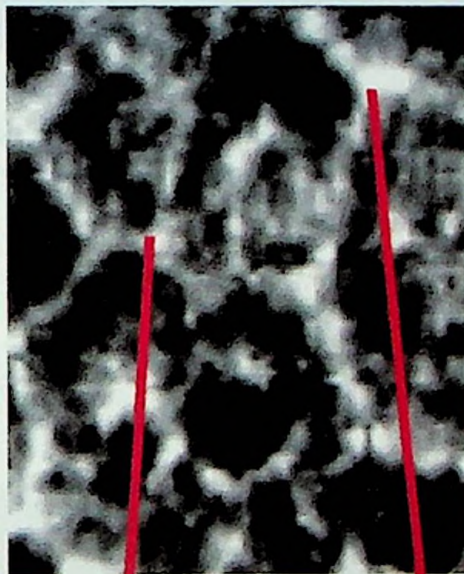


Fig. 1d Birch veinlet study area and zoomed region

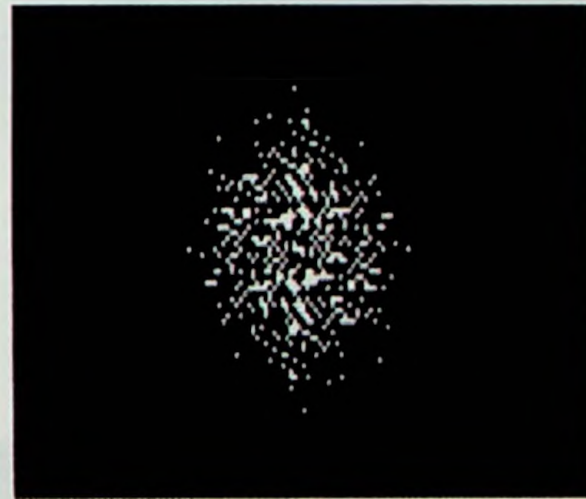


Fig. 1e Birch veinlet study area transform



Fig. 1f Birch Study area zoomed right section



Fig. 1g Birch veinlet study area zoomed region FFT

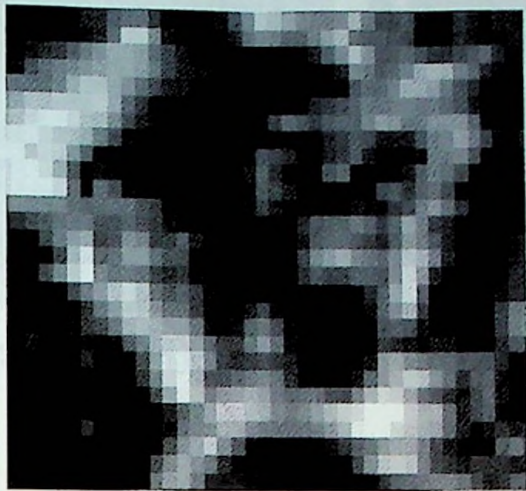


Fig. 1h Birch veinlet study area zoomed left portion

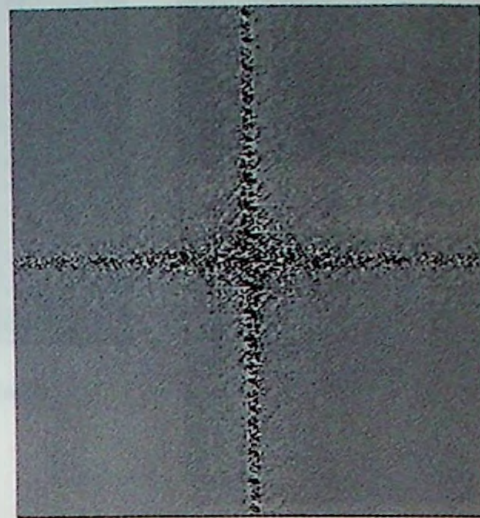


Fig. 1i Birch veinlet left portion FFT



Fig. 2a Holly A original scan



Fig. 2b Holly A with algorithm



Fig. 2c Holly A FFT

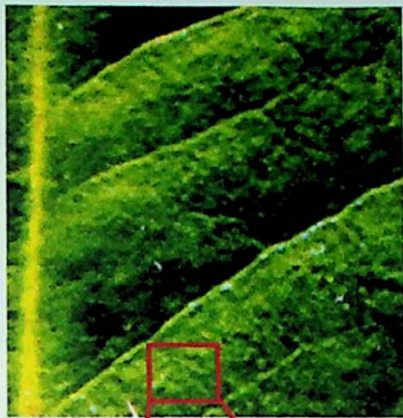


Fig. 3a Holly B original scan

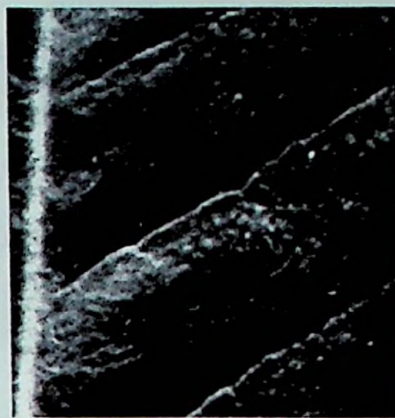


Fig. 3b Holly B with algorithm



Fig. 3c Holly B FFT

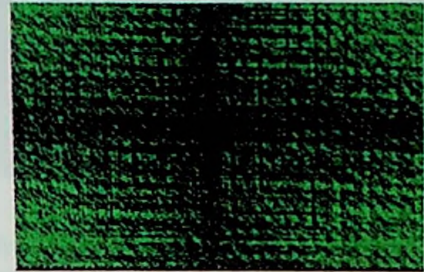


Fig. 3d Holly B FFT with color drapage at 99% autoclip

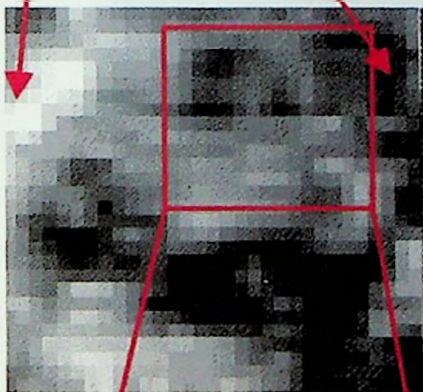


Fig. 3e Holly B veinlet study area



Fig. 3f Holly B veinlet FFT

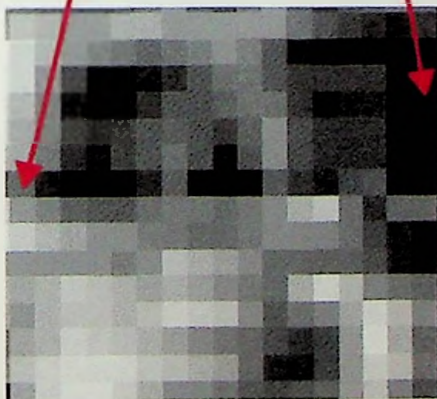


Fig. 3g Holly B veinlet study area zoomed



Fig. 3h Holly B zoomed veinlet FFT



Fig. 4a Red Oak 1 original scan

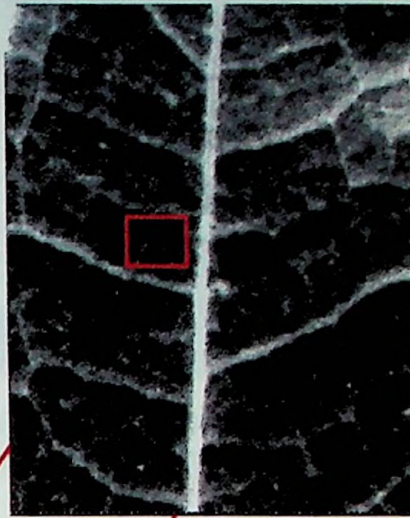


Fig. 4 b Red Oak with algorithm



Fig. 4c Red Oak FFT

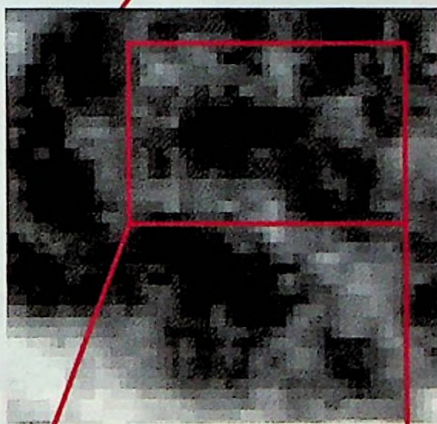


Fig. 4d Red Oak veinlet study area with algorithm

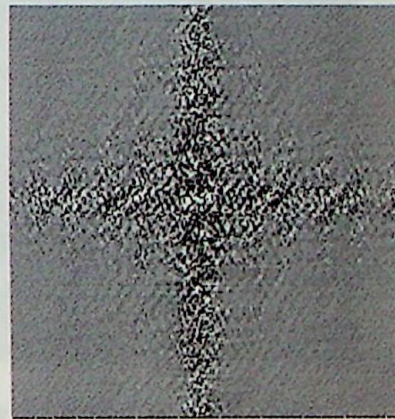


Fig. 4e Red Oak veinlet FFT



Fig. 4f Red Oak veinlet zoomed with algorithm



Fig. 4g Red Oak veinlet FFT



Fig. 5a Red Oak dried section original scan

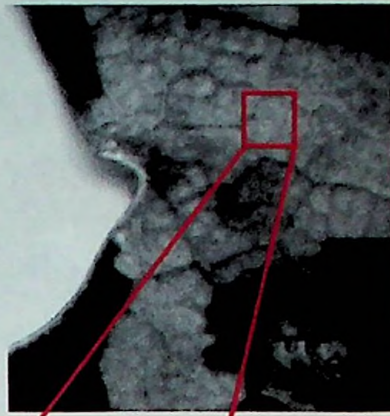


Fig. 5b Red Oak dried section with algorithm



Fig. 5c Red Oak dried section FFT

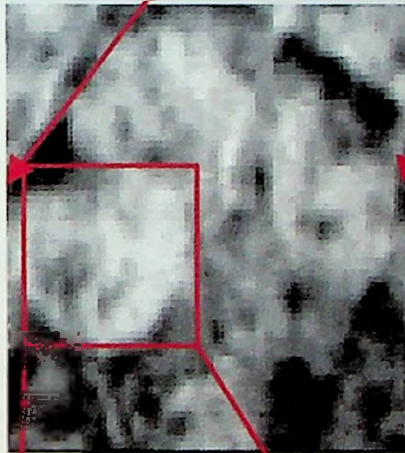


Fig. 5d Red Oak dried veinlet study area, zoomed



Fig. 5e Red Oak dried study area FFT

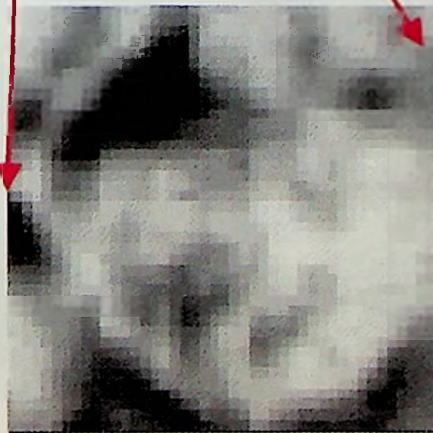


Fig. 5f Red Oak dried veinlet study area II

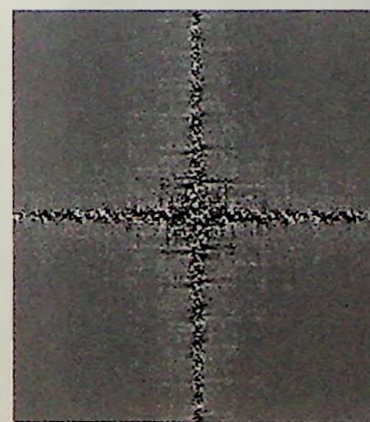


Fig. 5g Red Oak dried veinlet study area II FFT

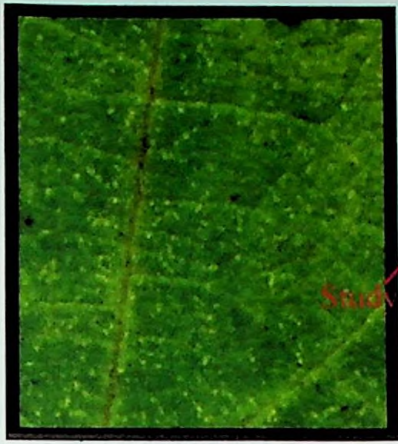


Fig. 6a Elderberry 1 original scan

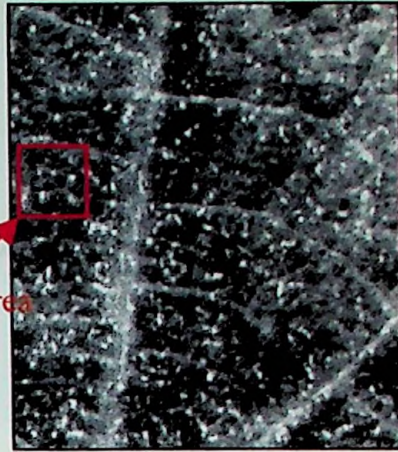


Fig. 6b Elderberry 1 with algorithm



Fig. 6c Elderberry 1 FFT

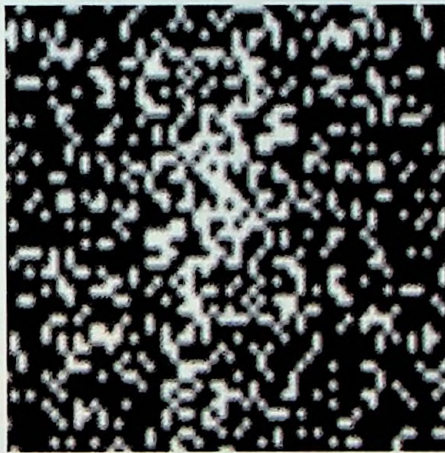


Fig. 6d Elderberry 1 FFT central region zoomed



Fig. 6e Elderberry 1 Reversed Fourier Transform from zoomed central maximum

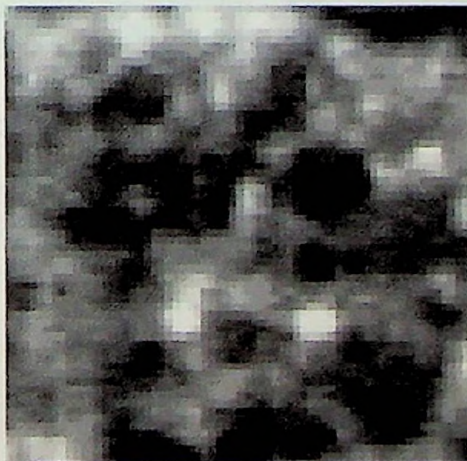


Fig. 6f Elderberry 1 veinlet

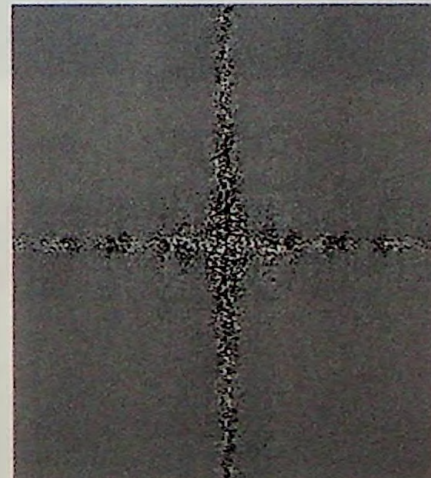


Fig. 6g Elderberry 1 veinlet FFT

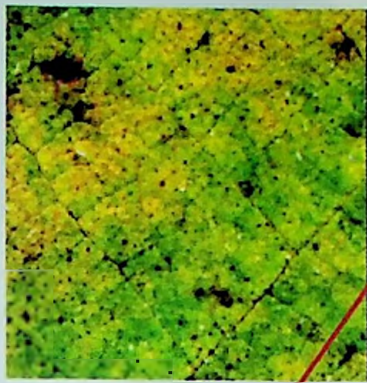


Fig. 7a Elderberry 2

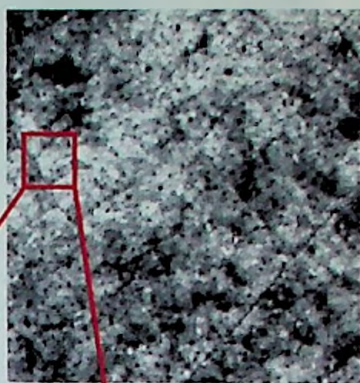


Fig. 7b Elderberry 2 with algorithm

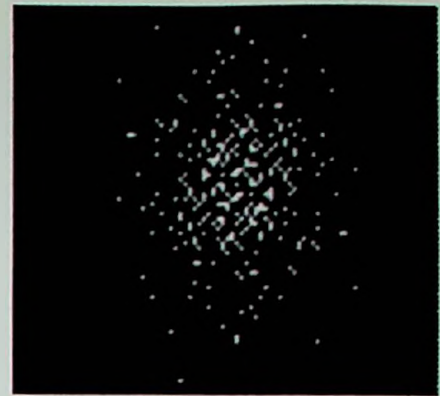


Fig. 7c Elderberry 2 FFT



Fig. 7d Elderberry 2 veinlet

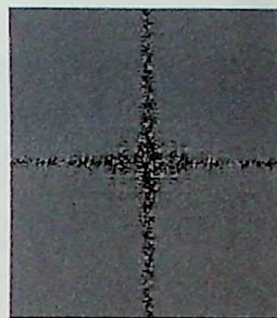


Fig. 7e Elderberry 2 veinlet FFT



Fig. 8a Elderberry 3 original scan



Fig. 8b Elderberry 3 with algorithm



Fig. 8c Elderberry 3 FFT



Fig. 8d Elderberry 3 veinlet



Fig. 8e Elderberry 3 veinlet FFT





Fig. 9a Sugar Maple, color original scan



Fig. 9b Sugar Maple color, with algorithm

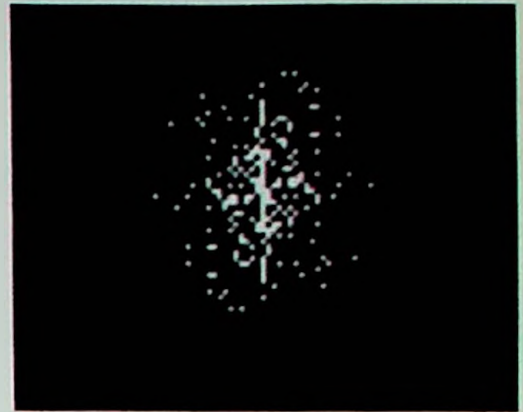


Fig. 9c Sugar Maple color FFT

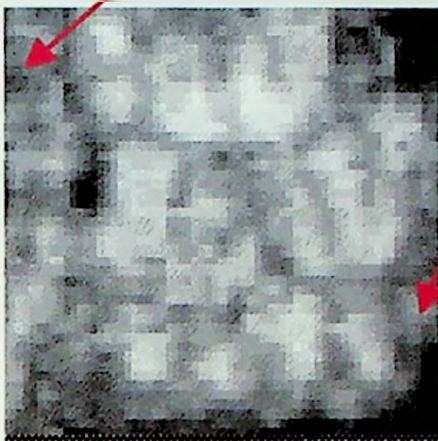


Fig. 9d Sugar Maple color veinlet study area



Fig. 9e Sugar Maple color veinlet FFT

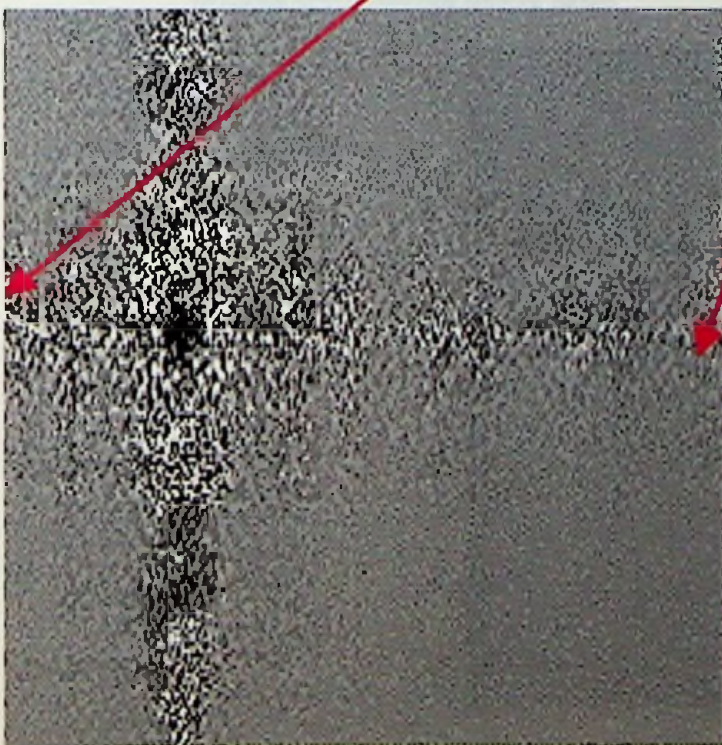


Fig. 9f Sugar Maple, color veinlet FFT zoomed

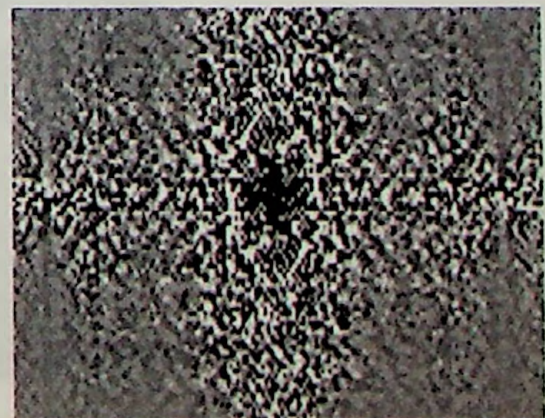


Fig. 9g Sugar Maple color veinlet FFT central max and first order zoomed

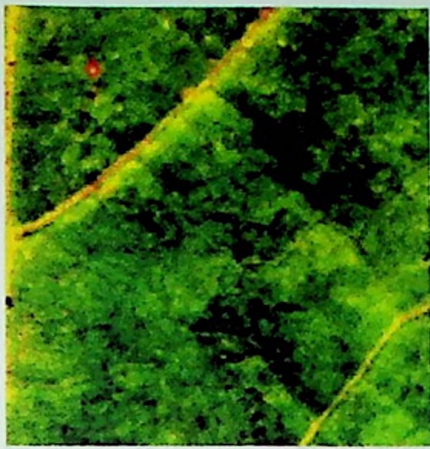


Fig. 10a Sugar Maple unchanged original scan



Fig. 10b Sugar Maple unchanged with algorithm

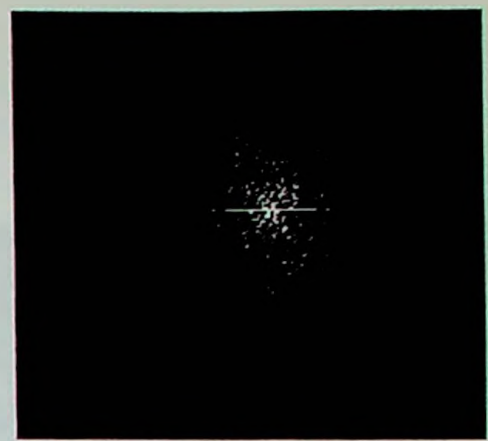


Fig. 10c Sugar Maple unchanged FFT

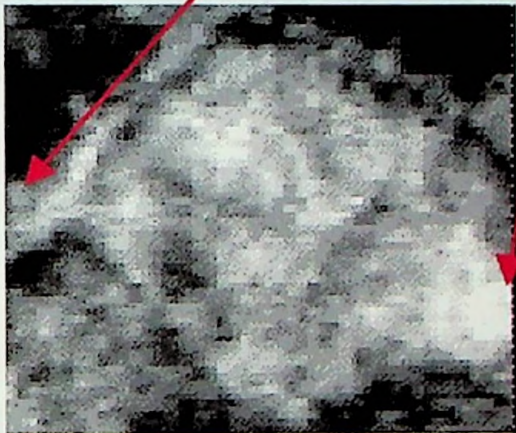


Fig. 10d Sugar Maple unchanged veinlet study area



Fig. 10e Sugar Maple unchanged veinlet FFT

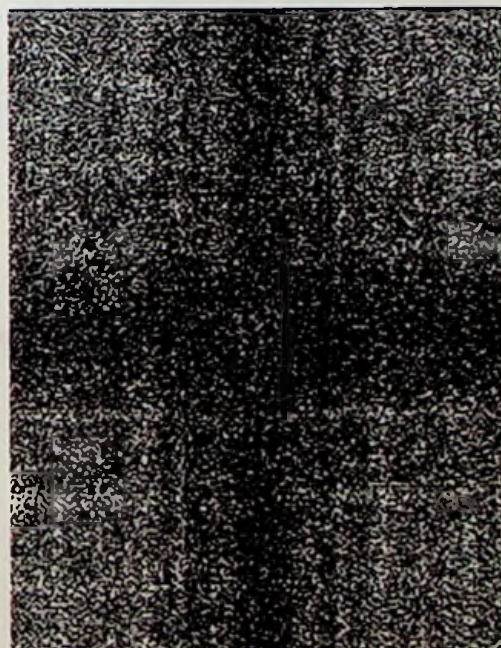


Fig. 10f Sugar Maple unchanged FFT with real and imaginary bands

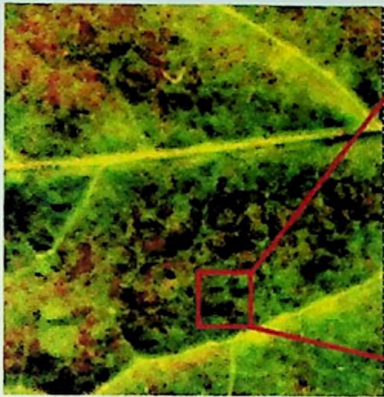


Fig. 11a Sweet Gum, green original scan



Fig. 11d Sweet Gum, green veinlet study area with algorithm

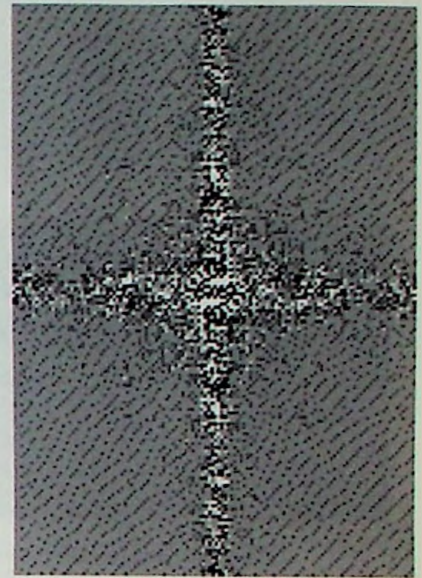


Fig. 11e Sweet Gum, green veinlet FFT

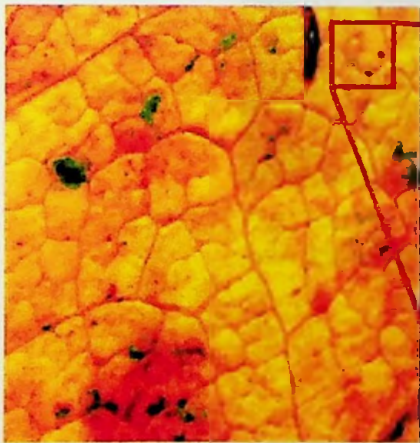


Fig. 12a Sweet Gum, yellow original scan

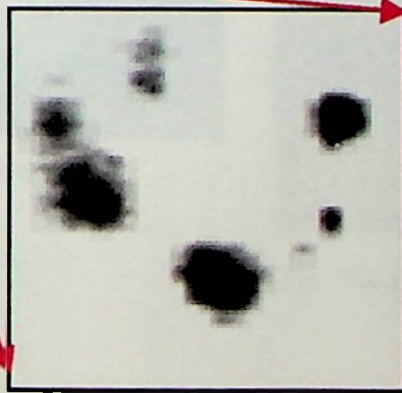


Fig. 12b Sweet Gum, yellow veinlet with algorithm

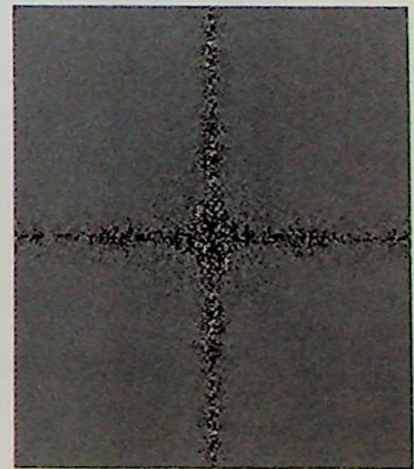


Fig. 12c Sweet Gum, yellow veinlet FFT

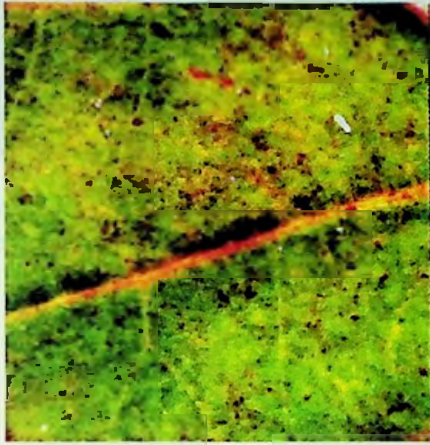


Fig. 13a Sycamore original scan



Fig. 13b Sycamore, zoomed with algorithm



Fig. 13c Sycamore FFT

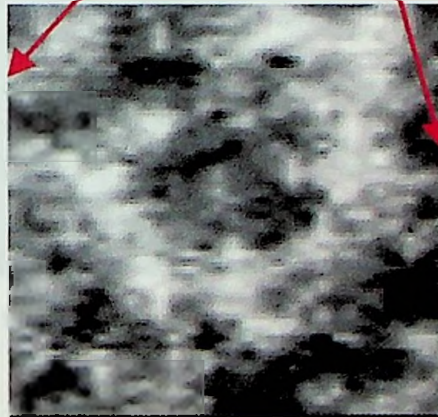


Fig. 13d Sycamore veinlet with algorithm

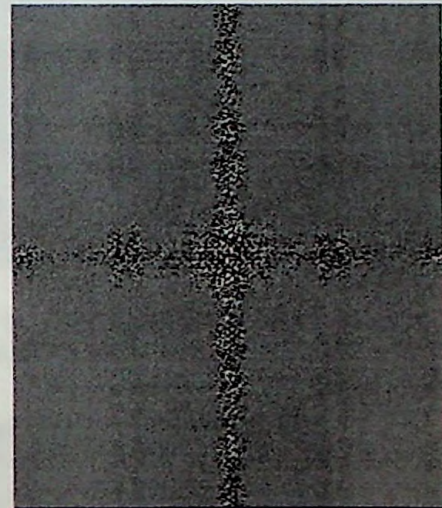


Fig. 13e Sycamore veinlet FFT



Fig. 14a Water Maple A original scan

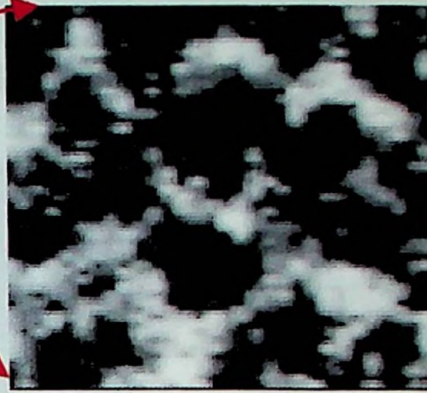


Fig. 14b Water Maple A veinlet with algorithm

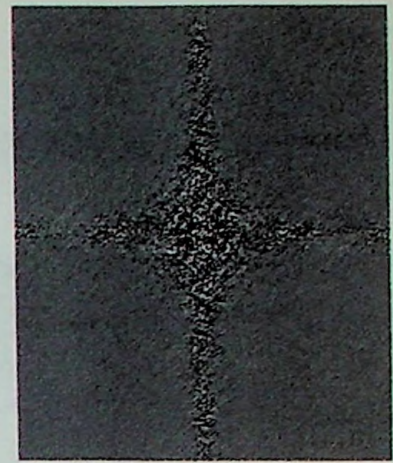


Fig. 14c Water Maple A FFT



Fig. 15a Water Maple B

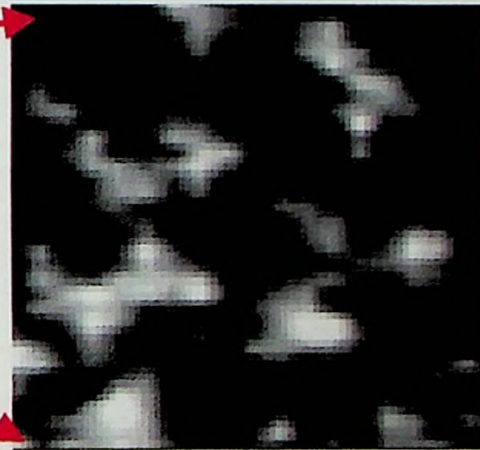


Fig. 15b Water Maple B veinlet with algorithm

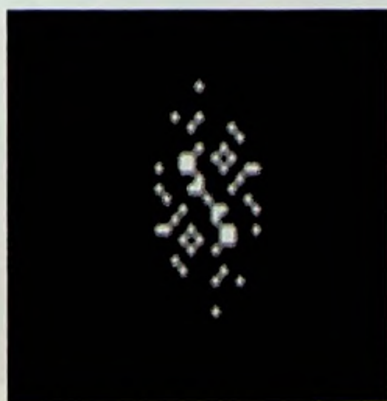


Fig. 15c Water Maple B FFT

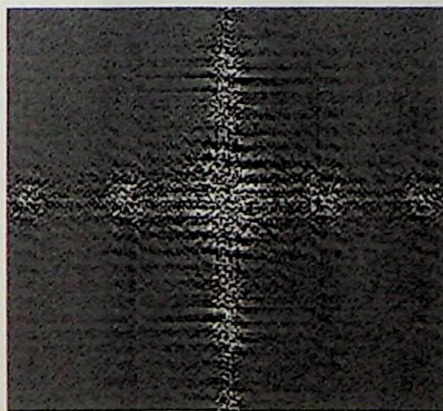


Fig. 15d Water Maple B FFT with colordrape applied

## Appendix C

### Phase Three - Verification of Research Techniques

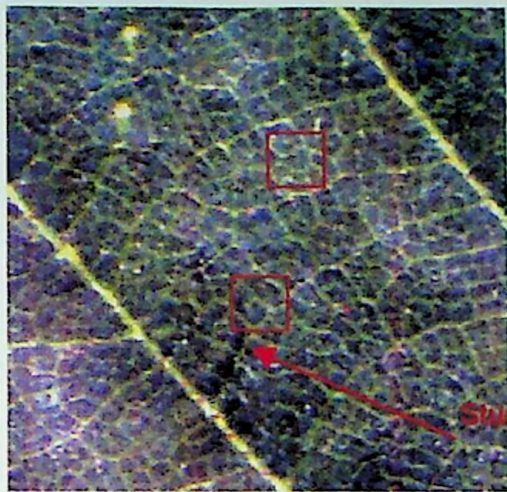


Fig. 1a Birch, original image

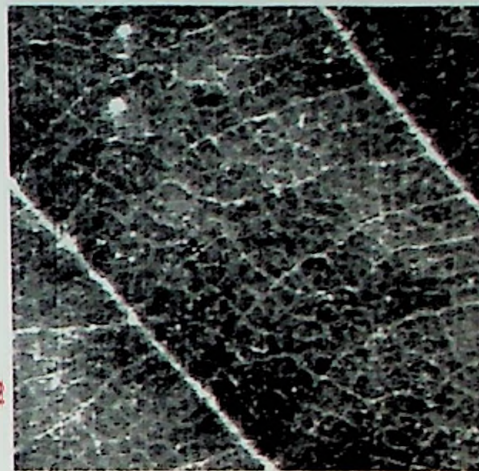


Fig. 1b Birch with algorithm

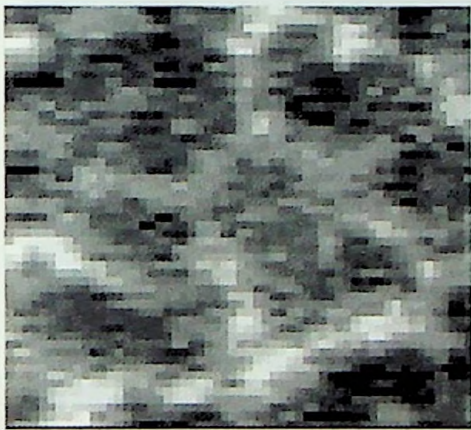


Fig. 1c Birch veinlet study area 1



Fig. 1d Birch veinlet FFT

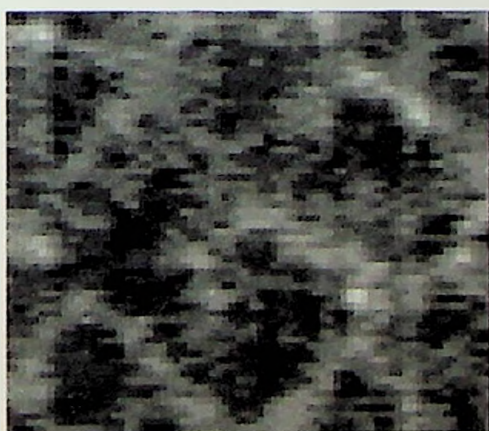


Fig. 1e Birch veinlet study area 2

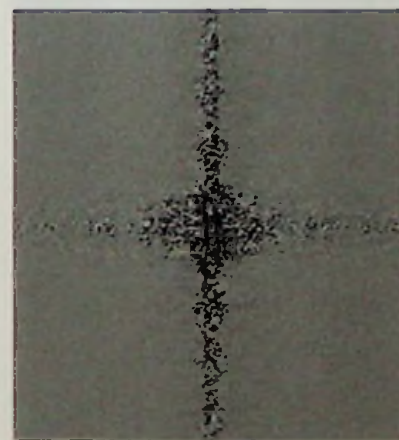


Fig. 1f Birch veinlet study area 2  
FFT

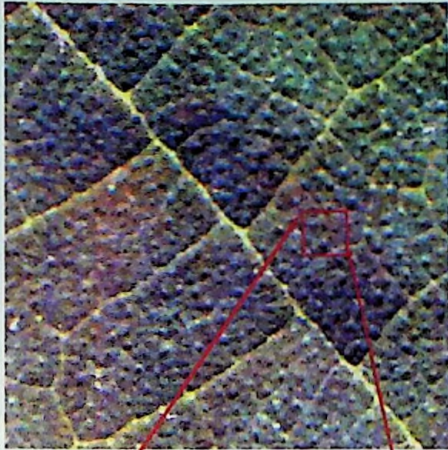


Fig. 2a Elderberry original scan

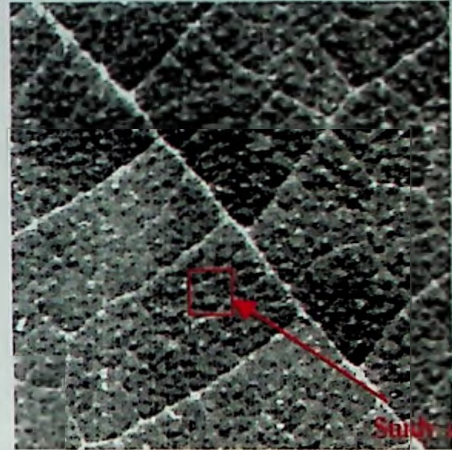


Fig. 2b Elderberry with algorithm

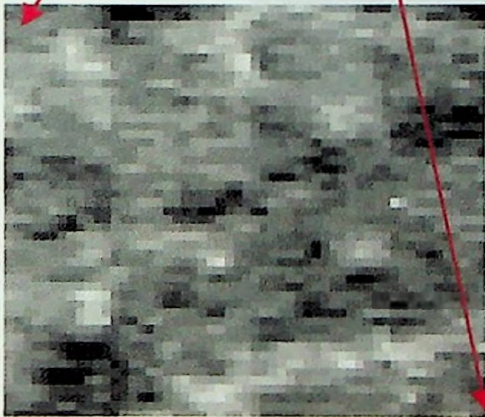


Fig. 2c Elderberry veinlet study area 1



Fig. 2d Elderberry veinlet study area 1 FFT

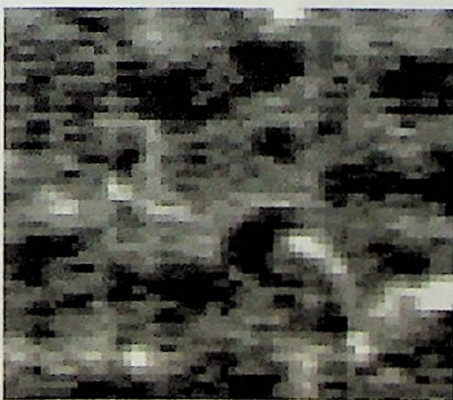


Fig. 2e Elderberry veinlet study area 2

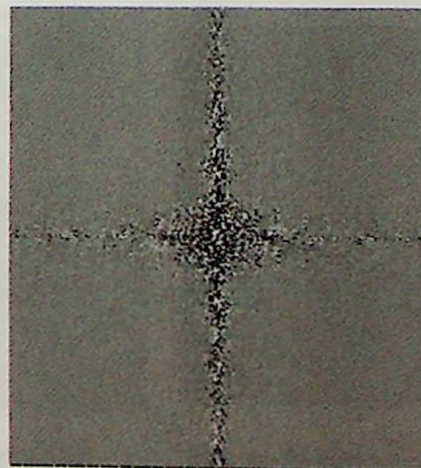


Fig. 2f Elderberry study area 2 FFT

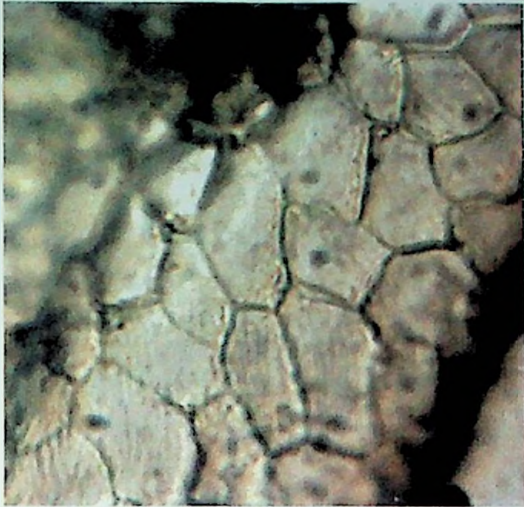


Fig. 3a Elderberry epidermis thin section 400X

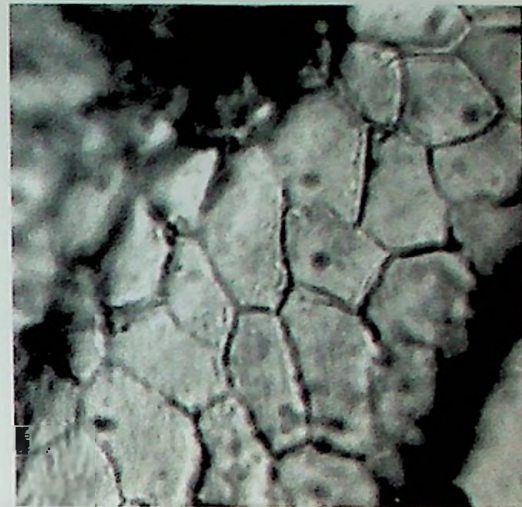


Fig. 3b Elderberry epidermis thin section 400X with algorithm



Fig. 3c Elderberry epidermis FFT

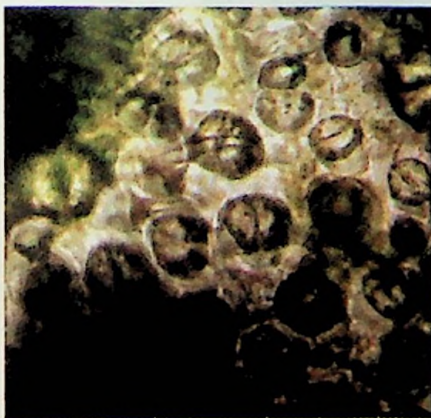


Fig. 4a Elderberry stomata 400X

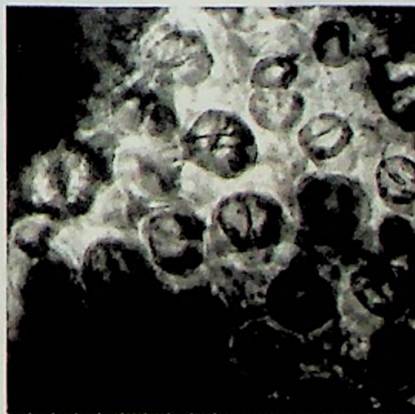


Fig. 4b Elderberry stomata 400X with algorithm



Fig. 4c Elderberry stomata FFT





Fig. 5a Elderberry striated vein at 400X

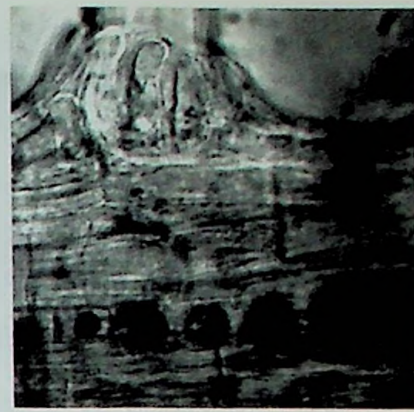


Fig. 5b Elderberry striated vein with algorithm

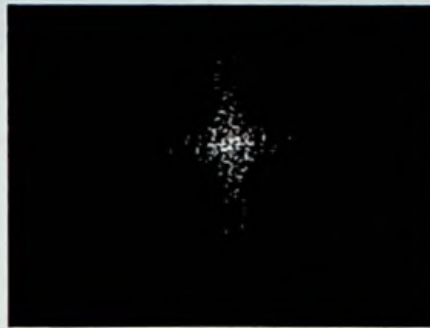


Fig. 5c Elderberry vein FFT

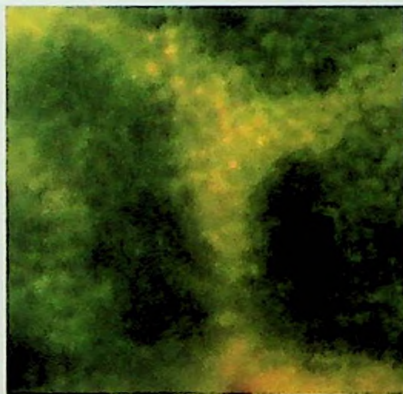


Fig. 6a Elderberry palisade layer at 400X



Fig. 6b Elderberry palisade layer with algorithm



Fig. 6c Elderberry palisade FFT

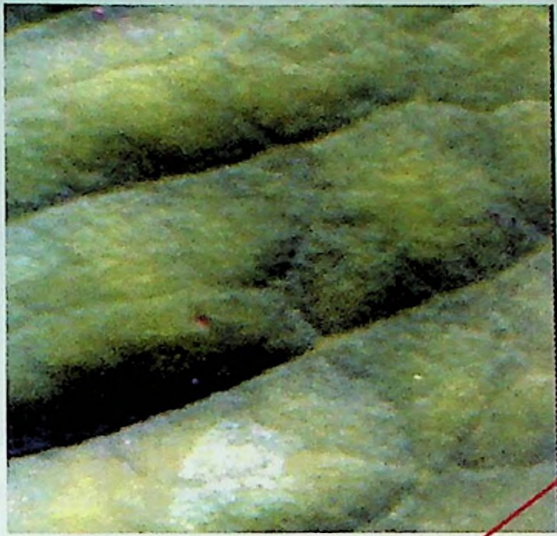


Fig. 7a Holly leaf surface

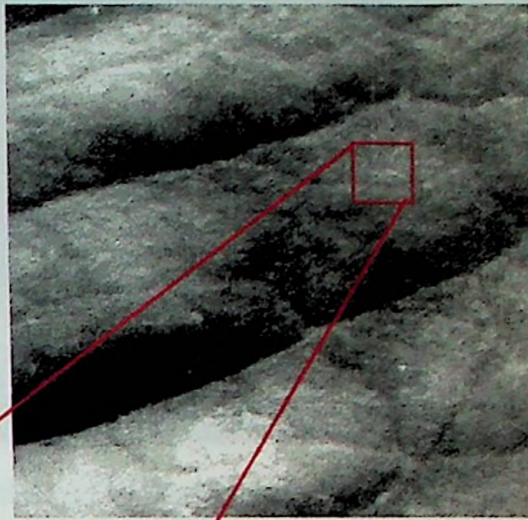


Fig. 7b Holly with algorithm



Fig. 7c Holly veinlet study area



Fig. 7d Holly veinlet FFT

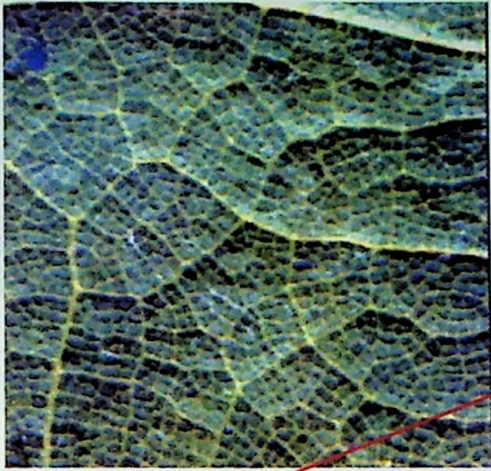


Fig. 8a Red Oak surface

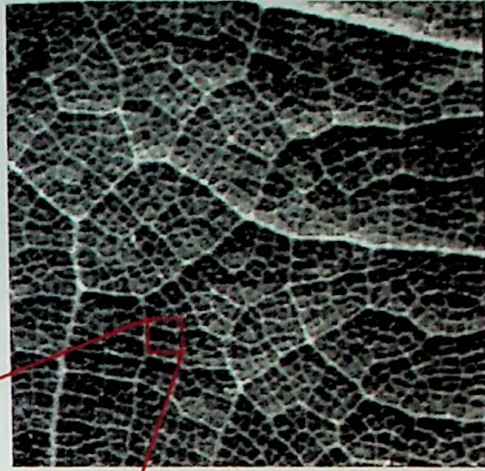


Fig. 8b Red Oak surface with algorithm

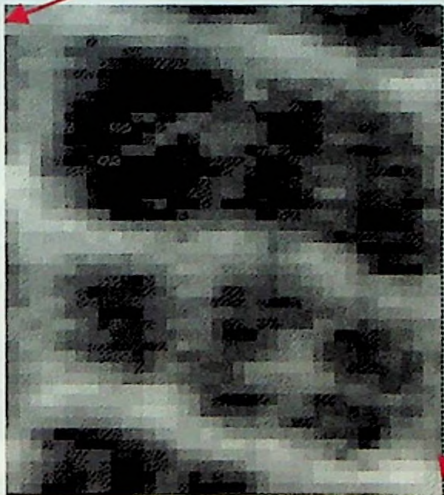


Fig. 8c Red Oak veinlet study area

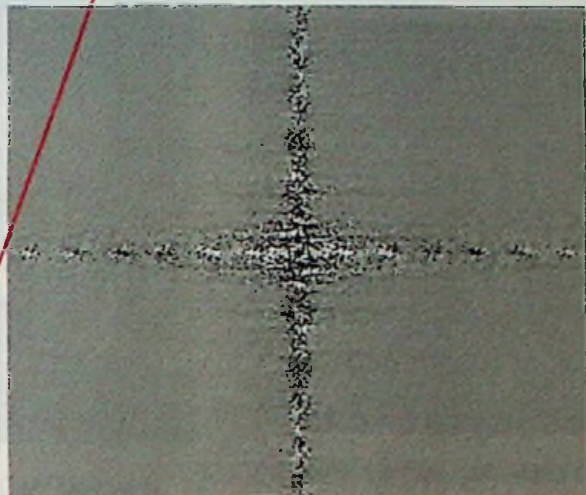


Fig. 8d Red Oak veinlet FFT



Fig.8e Red Oak palisade layer  
400X



Fig. 8f Red Oak palisade layer FFT

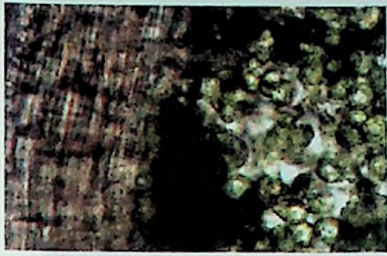


Fig. 9a Red Oak palisade cells and vein 400X

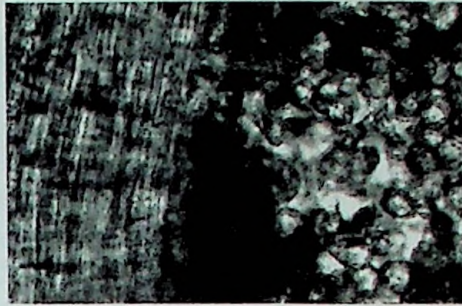


Fig. 9b Red Oak palisade cells and vein with algorithm



Fig. 9c Red Oak palisade cells and vein FFT

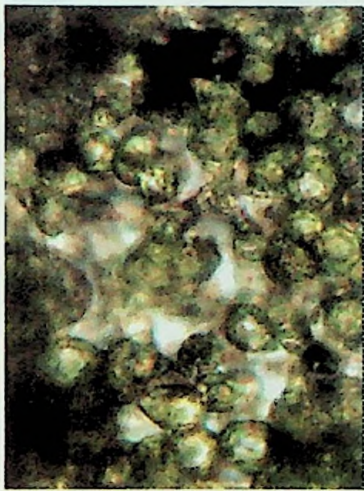


Fig. 9d Red Oak palisade cells only 400X

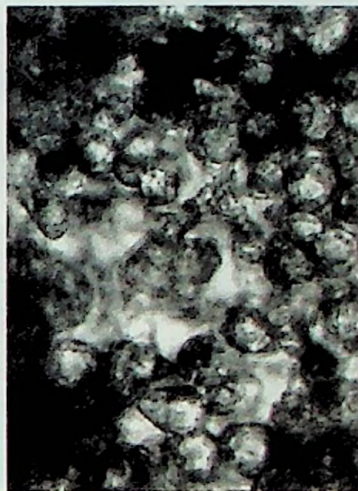


Fig. 9e Red Oak palisade cells with algorithm



Fig. 9f Red Oak palisade cells FFT

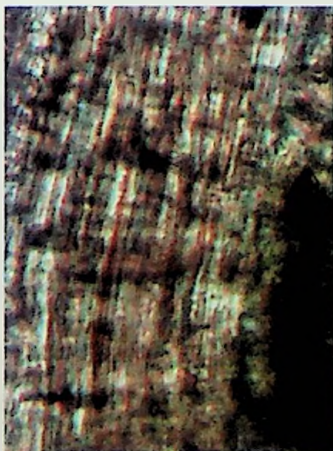


Fig. 9g Red Oak vein only 400X

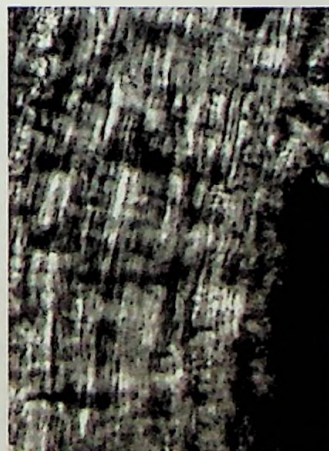


Fig. 9h Red Oak vein with algorithm



Fig. 9i Red Oak vein FFT

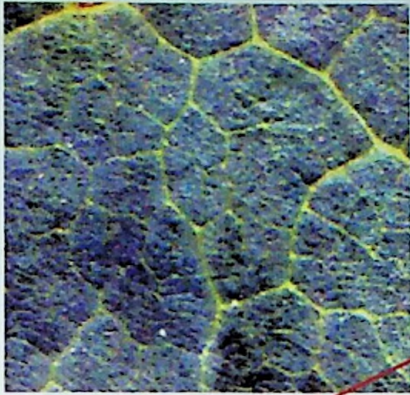


Fig. 10a Sugar Maple original scan

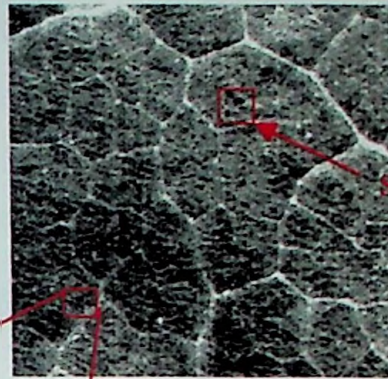


Fig. 10b Sugar Maple with algorithm

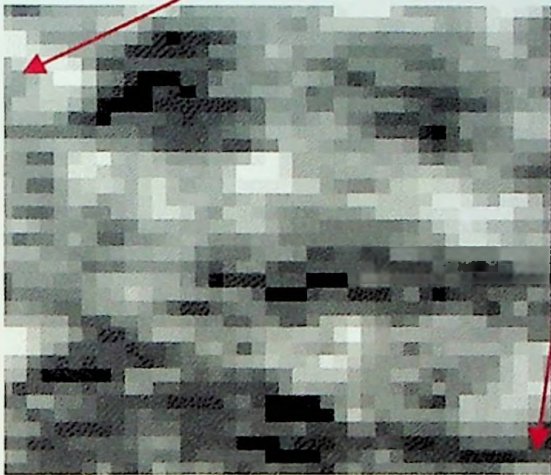


Fig. 10c Sugar Maple veinlet study area 1



Fig. 10d Sugar Maple veinlet study area 1 FFT

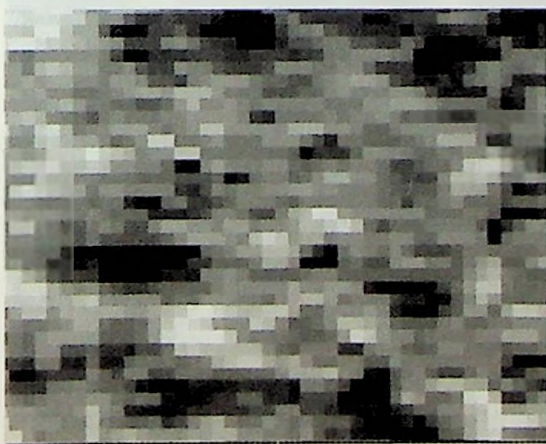


Fig. 10e Sugar Maple veinlet study area 2

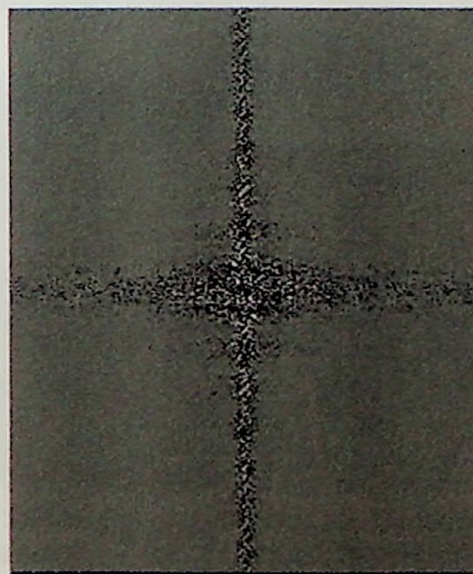


Fig. 10f Sugar Maple study area 2 FFT

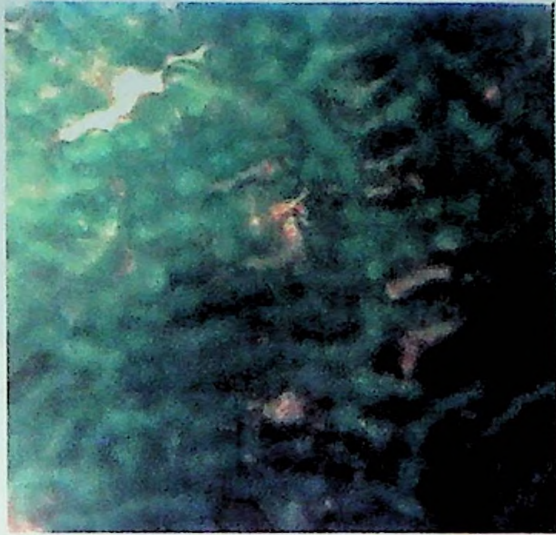


Fig. 11a Sugar Maple palisade layer 400X



Fig. 11b Sugar Maple palisade layer with algorithm

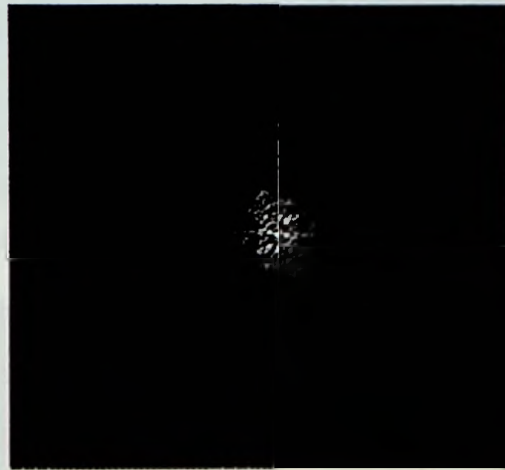


Fig. 11c Sugar Maple palisade layer FFT

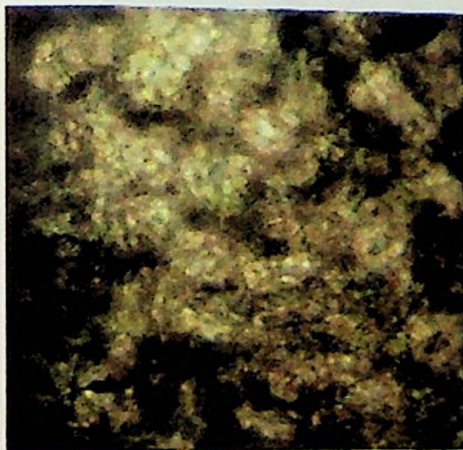


Fig. 12a Sugar Maple hexagonal matrix 400X

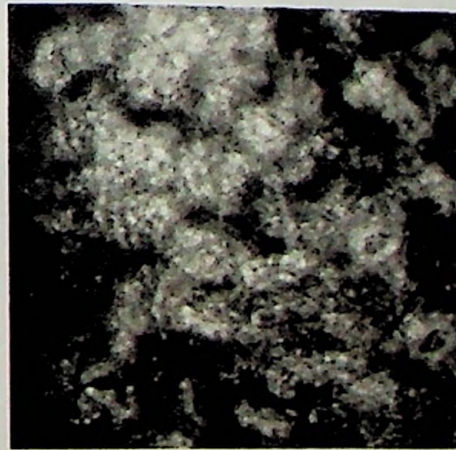


Fig. 12b Sugar Maple hexagonal matrix with algorithm



Fig. 12c Sugar Maple hexagonal matrix FFT

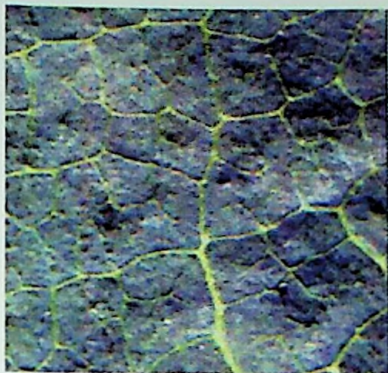


Fig. 13a Sweet Gum original scan



Fig. 13b Sweet Gum with algorithm



Fig. 13c Sweet Gum FFT with prevent wrapping



Fig. 13d Sweet Gum veinlet study area 1



Fig. 13e Sweet Gum study area 1 FFT

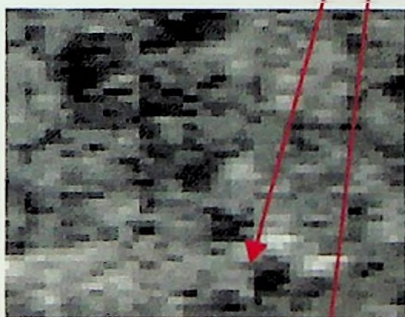


Fig. 13f Sweet Gum veinlet study area 2



Fig. 13g Sweet Gum study area 2 FFT



Fig. 13h Sweet Gum veinlet study area 3

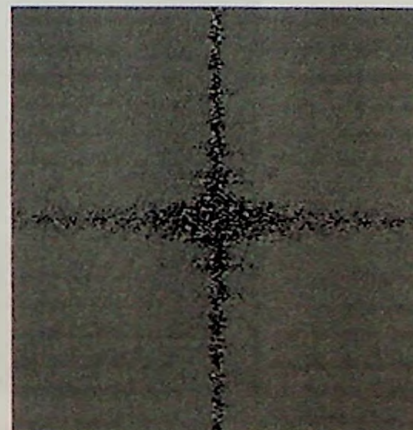


Fig. 13i Sweet Gum study area 3 FFT

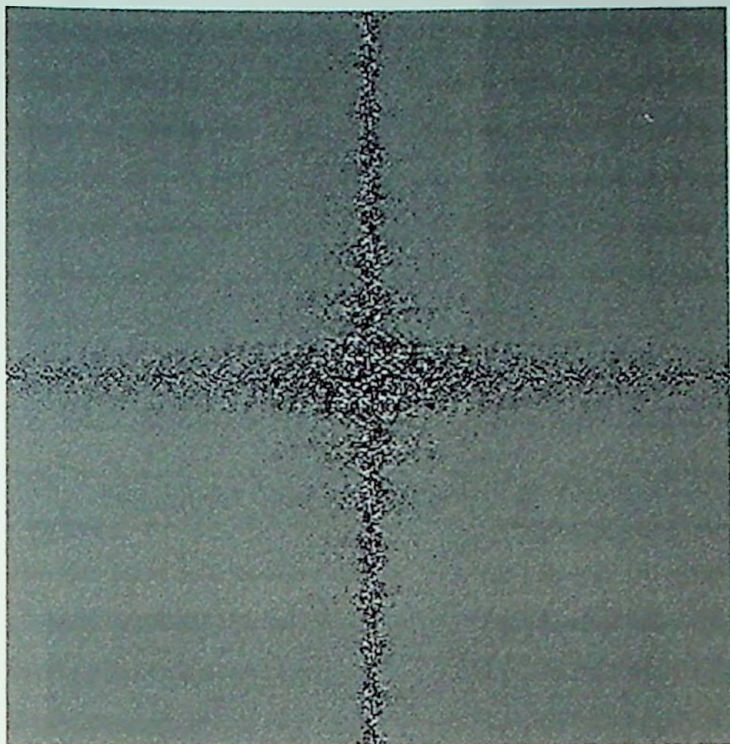


Fig. 13i Sweet Gum 3 FFT before prevent wrapping enabled

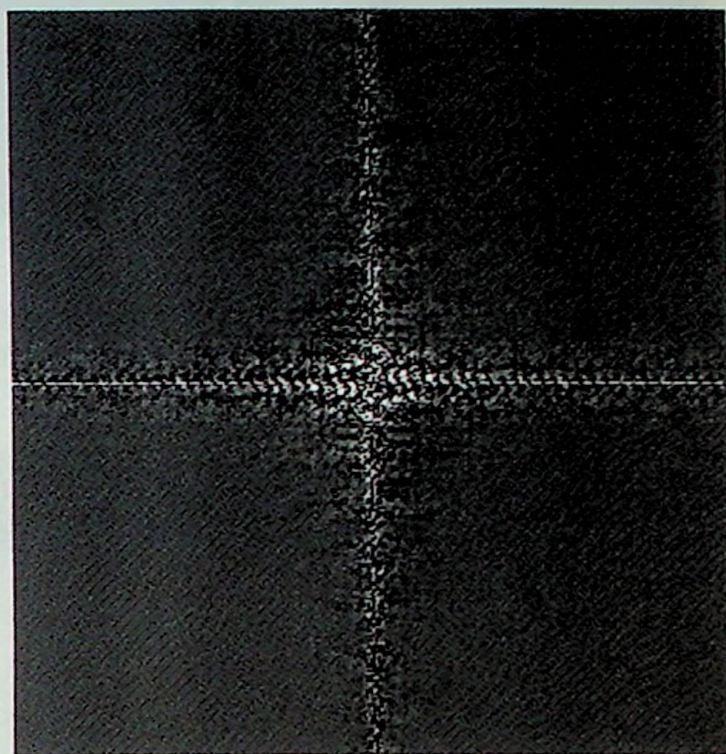


Fig. 13j Sweet Gum 3 FFT after prevent wrapping enabled

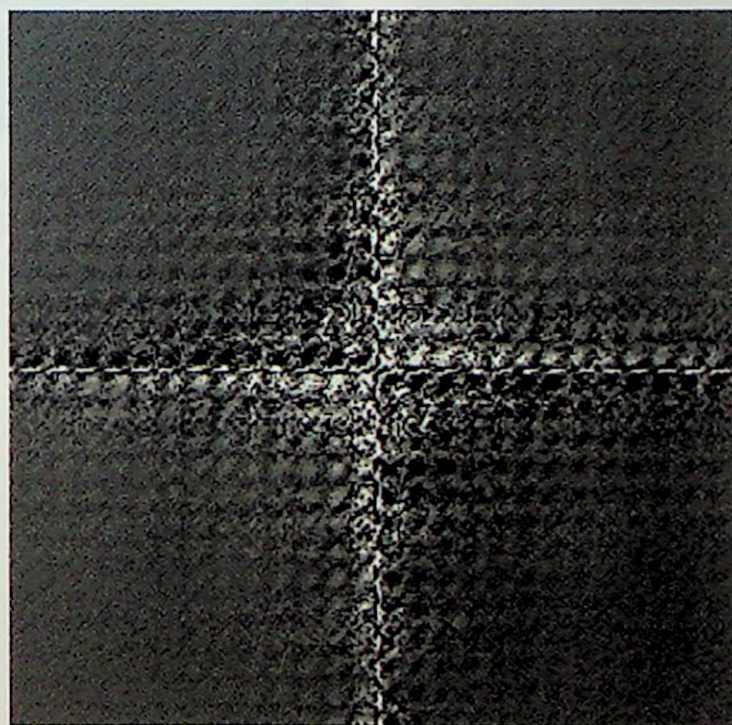


Fig. 13k Sweet Gum 3 FFT after prevent wrapping enabled, zoomed



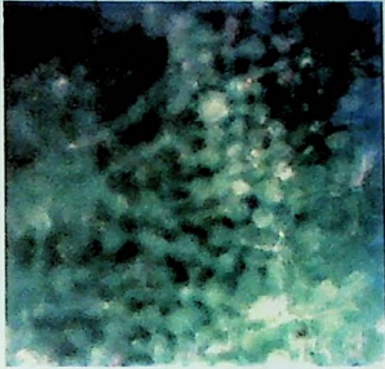


Fig. 14a Sweet Gum palisade 200X

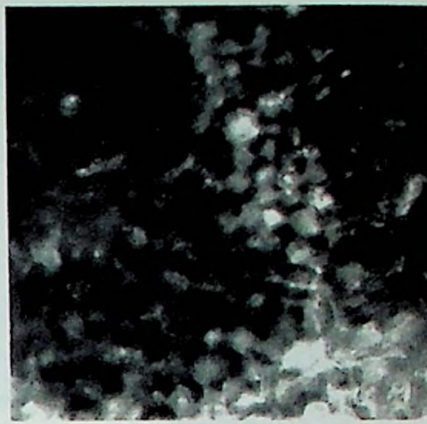


Fig. 14b Sweet Gum palisade at 200X with algorithm



Fig. 14c Sweet Gum palisade FFT

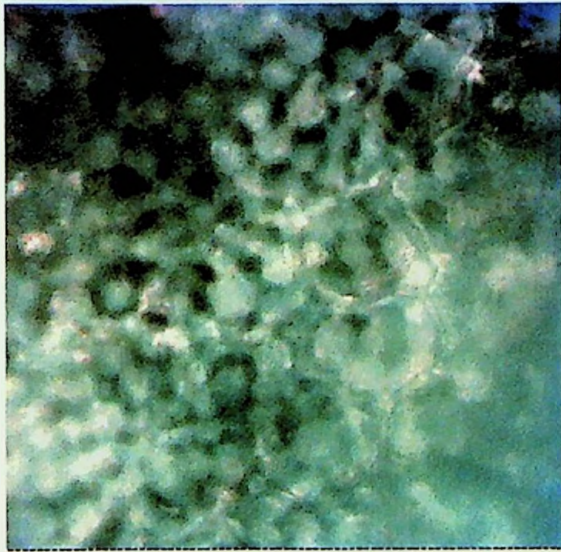


Fig. 15a Sweet Gum epidermis and palisade layer 200X

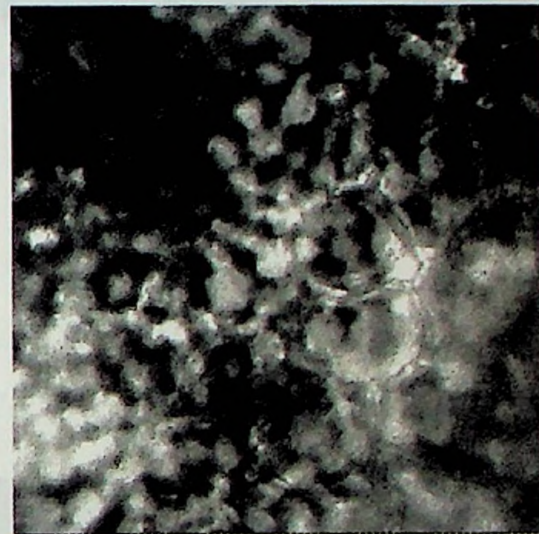


Fig. 15b Sweet Gum epidermis and palisade layer with algorithm



Fig. 15c Sweet Gum epidermis and palisade 200X FFT

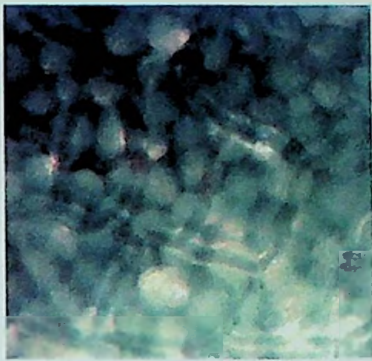


Fig. 16a Sweet Gum epidermis and palisade layer 400X

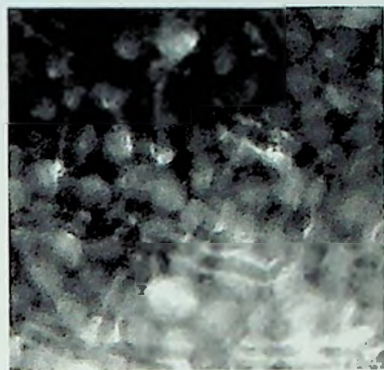


Fig. 16b Sweet Gum epidermis and palisade layer with algorithm

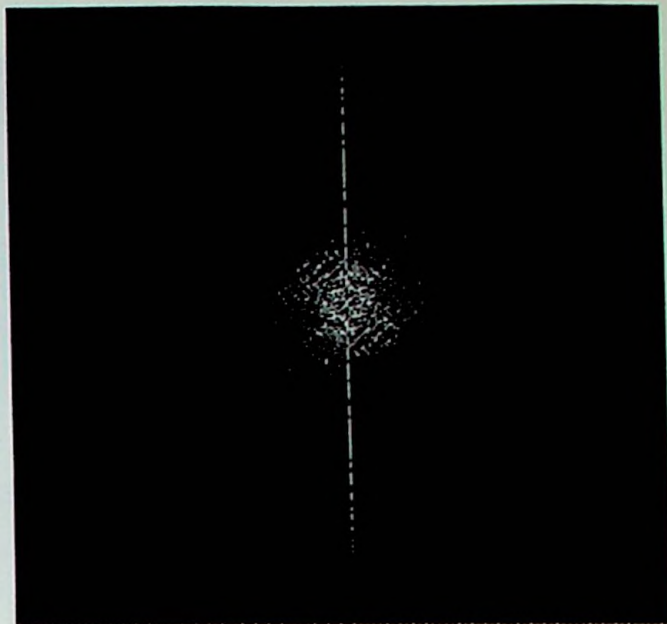


Fig. 16c Sweet Gum epidermis and palisade layer FFT



Fig. 17a Sweet Gum palisade layer 400X

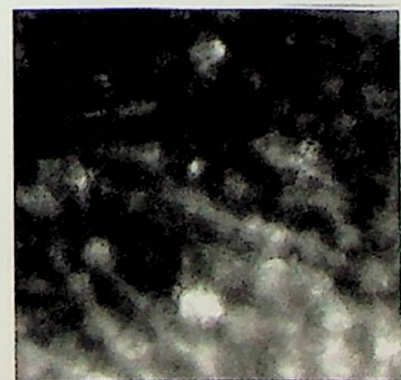


Fig. 17b Sweet Gum palisade layer with algorithm



Fig. 17c Sweet Gum palisade layer FFT

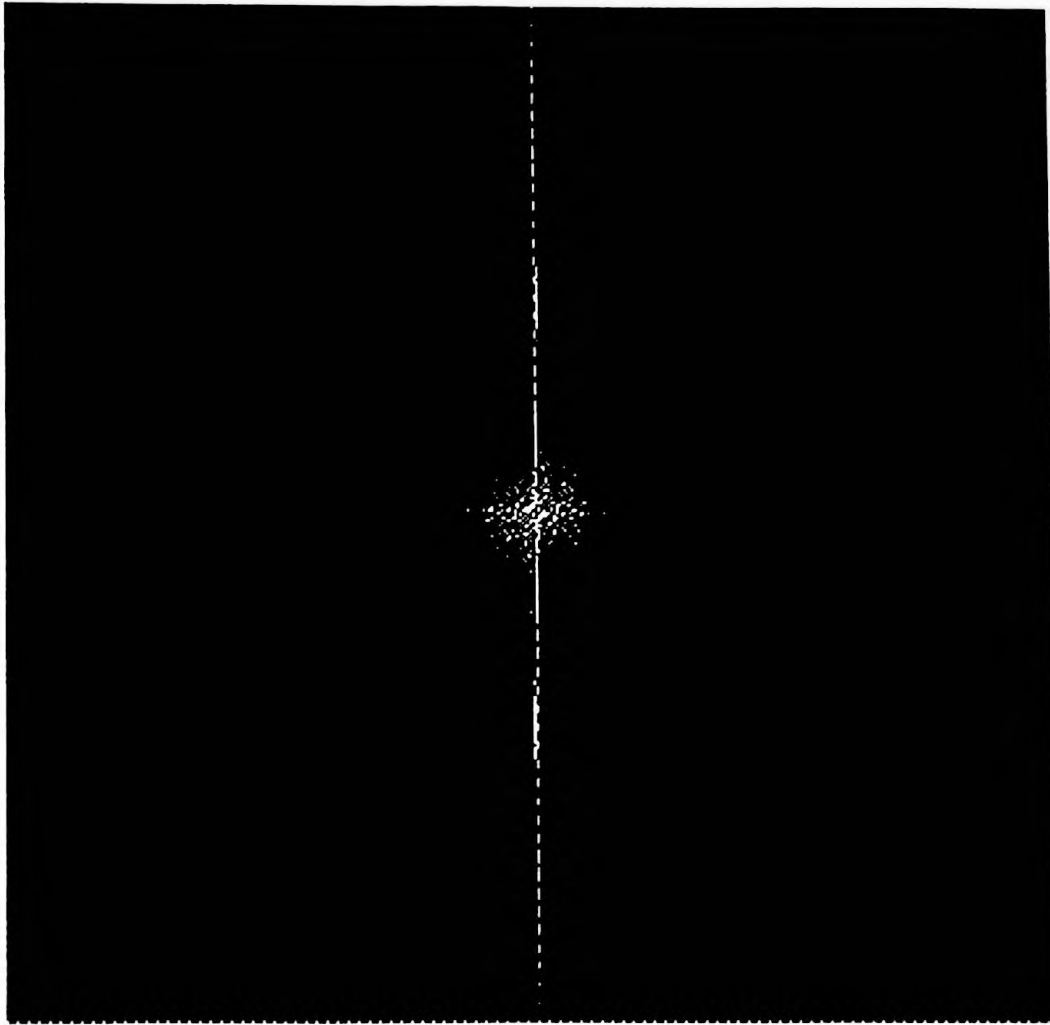


Fig. 17d Sweet Gum palisade layer FFT with prevent wrapping

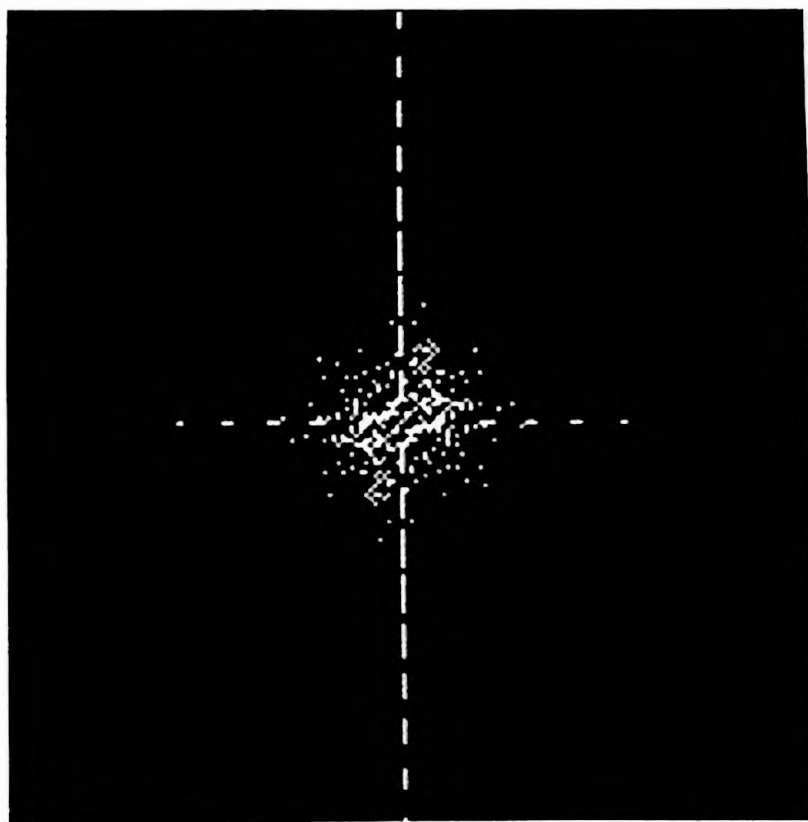


Fig. 17e Sweet Gum palisade layer FFT with prevent wrapping, zoomed central maximum

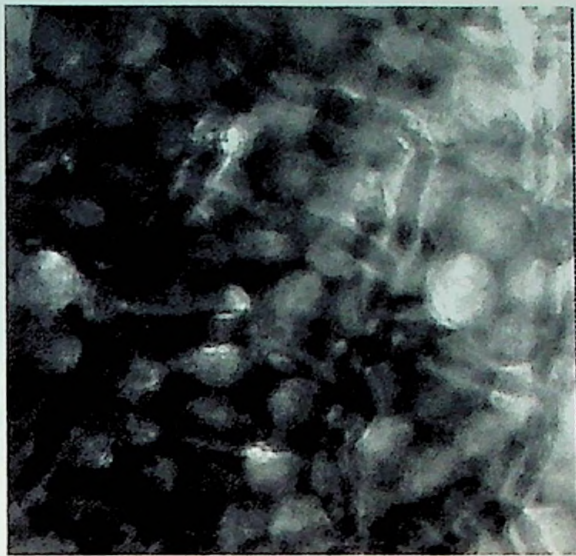


Fig. 18a Sweet Gum epidermis and palisade layer scanned at 90 degrees with algorithm



Fig. 18b Sweet Gum epidermis and palisade layer scanned at 90 degrees FFT

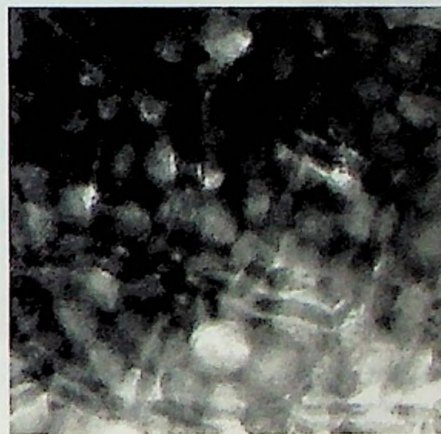


Fig. 18c Sweet Gum epidermis and palisade layer rotated back by ER Mapper rectification

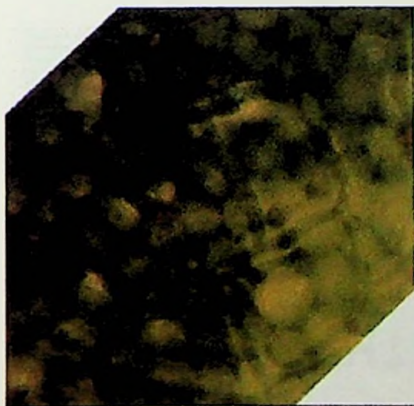


Fig. 19a Sweet Gum epidermis and palisade layer scanned at 45 degrees

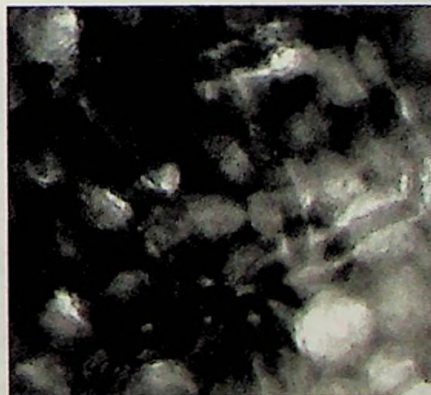


Fig. 19b Sweet Gum epidermis and palisade layer scanned at 45 degrees with algorithm



Fig. 19c Sweet Gum epidermis and palisade layer scanned at 45 degrees FFT



Fig. 20a Sycamore leaf original scan

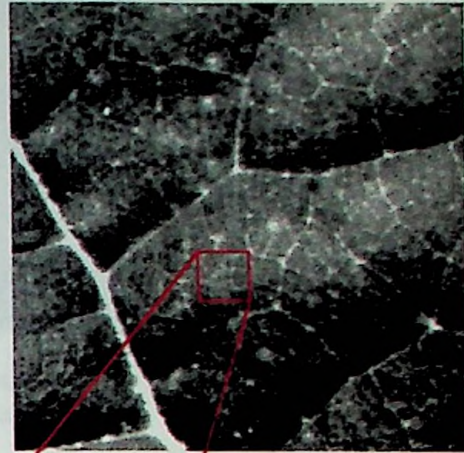


Fig. 20b Sycamore with algorithm

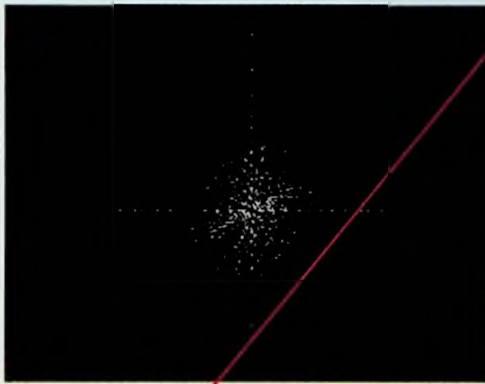


Fig. 20c Sycamore FFT with prevent wrapping enabled

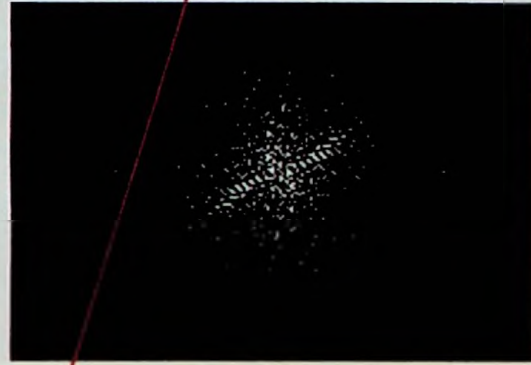


Fig. 20d Sycamore FFT without prevent wrapping

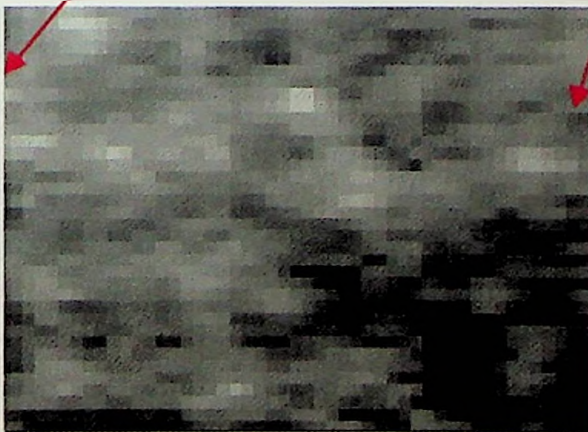


Fig. 20e Sycamore veinlet study area

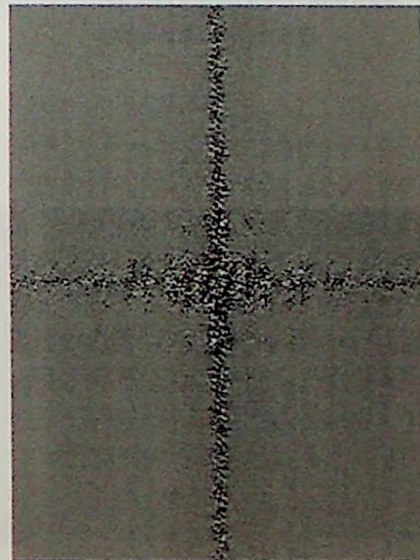


Fig. 20f Sycamore veinlet FFT

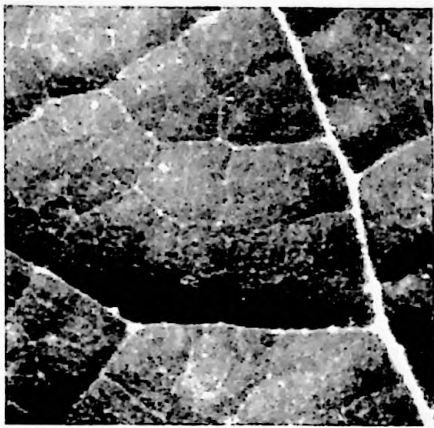


Fig. 21a Sycamore rotated by 20 degrees with algorithm

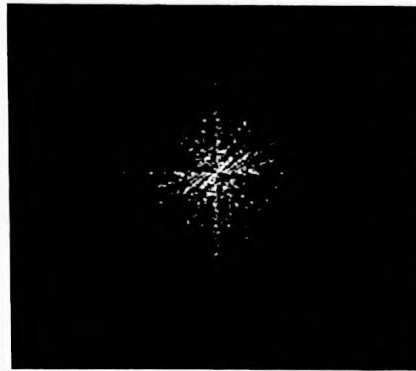


Fig. 21b Sycamore rotated by 20 degrees FFT with prevent wrapping



Fig. 21c Sycamore rotated by 20 degrees FFT without prevent wrapping



Fig. 22a Sycamore rotated by 50 degrees with algorithm



Fig. 22b Sycamore rotated by 50 degrees FFT with prevent wrapping

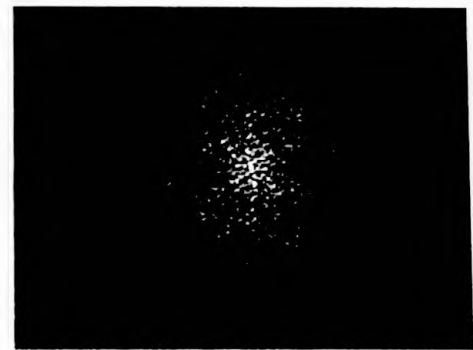


Fig. 22c Sycamore rotated by 50 degrees FFT without prevent wrapping

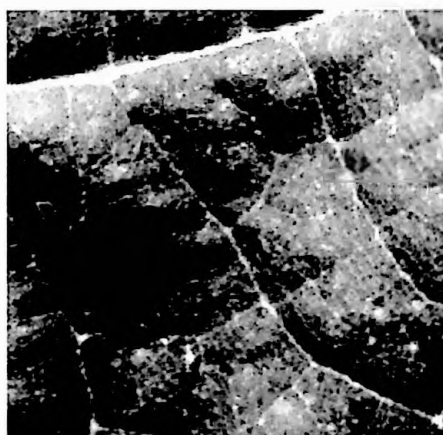


Fig. 23a Sycamore rotated by 90 degrees with algorithm

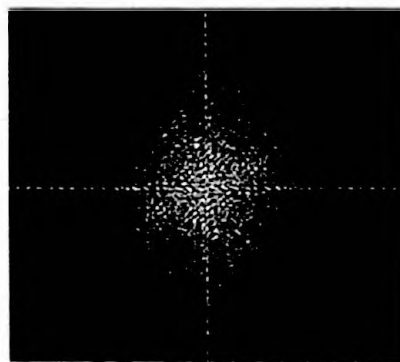


Fig. 23b Sycamore rotated by 90 degrees FFT with prevent wrapping



Fig. 23c Sycamore rotated by 90 degrees FFT without prevent wrapping



Fig. 24a Water Maple original scan

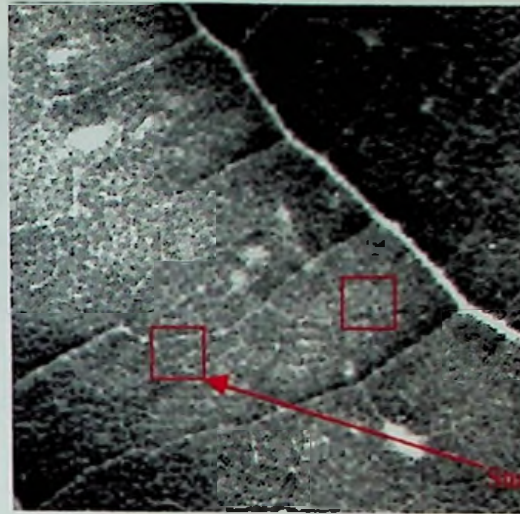


Fig. 24b Water Maple with algorithm



Fig. 24c Water Maple veinlet study area 1



Fig. 24d Water Maple study area 1 FFT



Fig. 24e Water Maple veinlet study area 2

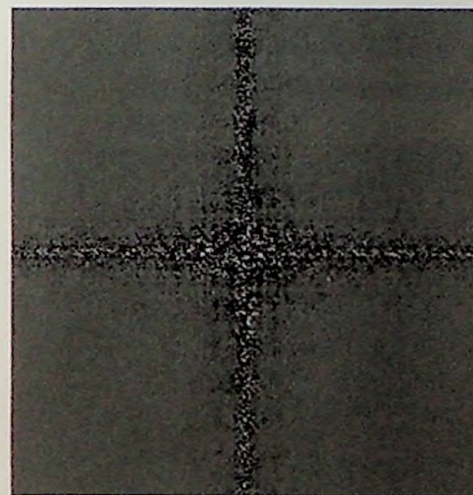


Fig. 24f Water Maple study area 2 FFT



Fig. 25a Water Maple epidermis  
400x



Fig. 25b Water Maple epidermis  
with algorithm

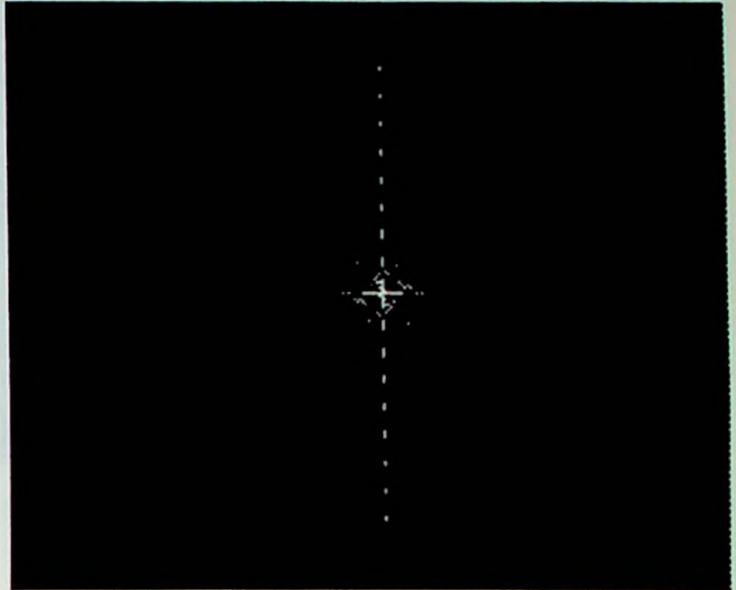


Fig. 25c Water Maple epidermis FFT



Fig. 26c Water Maple palisade layer FFT



Fig. 26a Water Maple palisade  
layer 400X



Fig. 26b Water Maple  
palisade layer with algorithm



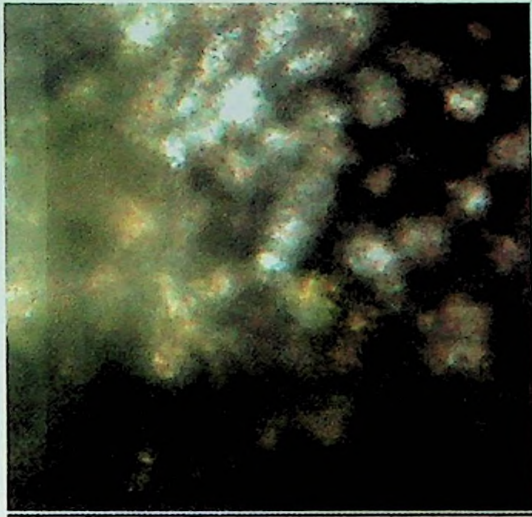


Fig. 27a Water Maple palisade layer and spongy matrix 400X

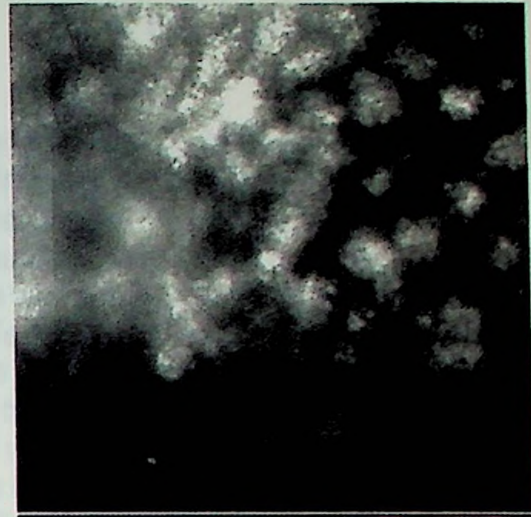


Fig. 27b Water Maple palisade layer and spongy matrix with algorithm

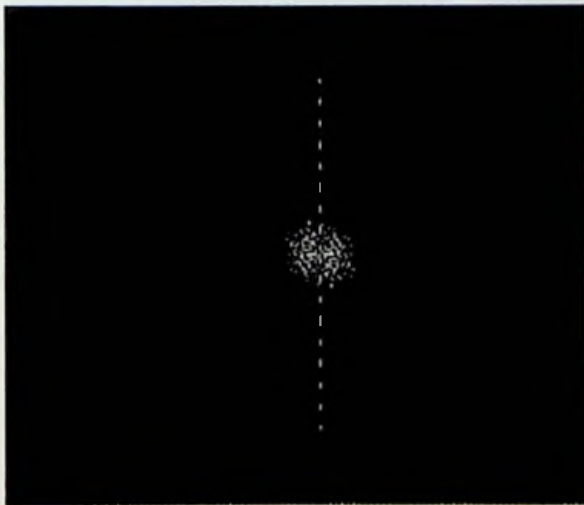


Fig. 27c Water Maple palisade/spongy matrix FFT

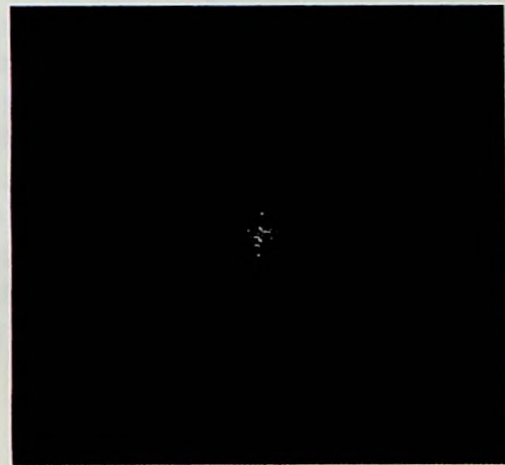


Fig. 27d Water Maple palisade/spongy matrix FFT with prevent wrapping



Fig. 27e Water Maple palisade/spongy matrix FFT with prevent wrapping, zoomed

## About the Author



*Alicia Colleen Eldridge-Spears* was born in Huntington, West Virginia, February 8, 1972 to Robert S. and Carrie W. Eldridge. After graduating summa cum laude from the Chesapeake School System in May, 1990, the author enrolled in Marshall University's honors program and the College of Education. During college, the then Miss Eldridge tutored chemistry and physics while completing student teaching at Buffalo High in Kenova, West Virginia. At

Marshall University, she received commendations by being named to the National Dean's List, 1995 Women of Marshall, and Who's Who Among American Colleges and Universities. In May of 1995, Miss Eldridge graduated cum laude with a Bachelor of Arts degree in Physics and Chemistry, 9-12.

Following graduation from 1995 to 1998, Miss Eldridge remained in the Huntington area to begin a Master's of Physical Science degree at Marshall University while teaching Physics and Chemistry and sponsoring the Quiz Bowl team at Ceredo-Kenova High. Miss Eldridge wed Gregory O. Spears in June of 1998. For the 1998-99 school year, Mrs. Eldridge-Spears moved to the new Spring Valley High and began instructing Physics 201 and 203 at Marshall University. During her teaching and graduate school career, Mrs. Eldridge-Spears has received commendations as a recipient of the 1996 regional Exemplary Teaching Techniques Award of Excellence, 1997 Outstanding Young Women of America, 1998 Who's Who Among America's Teachers, and 1997-99 National Dean's List.